Possibilities for Breakeven and Ignition of D-^{3}He Fusion Fuel in a Near Term Tokamak: Interim Report

G.A. Emmert, L.A. El-Guebaly, R. Klingelhöfer, G.L. Kulcinski, J.F. Santarius, J.E. Scharer, I.N. Sviatoslavsky, P.L. Walstrom and L.J. Wittenberg

August 1987

FPA-87-3

FUSION POWER ASSOCIATES

2 Professional Drive, Suite 248
Gaithersburg, Maryland 20879
(301) 258-0545

1500 Engineering Drive
Madison, Wisconsin 53706
(608) 263-2308

POSSIBILITIES FOR BREAKEVEN AND IGNITION OF D-^{3}He FUSION FUEL IN A NEAR TERM TOKAMAK

INTERIM REPORT

by

G.A. Emmert, L. El-Guebaly, R. Klingelhöfer,[(a)]
G.L. Kulcinski, J.F. Santarius, J.E. Scharer,
I.N. Sviatoslavsky, P.L. Walstrom, L.J. Wittenberg

August 26, 1987

FUSION POWER ASSOCIATES

(a) Kernforschungszentrum Karlsruhe

FPA-87-3

TABLE OF CONTENTS

1. INTRODUCTION

There has been a renewed worldwide interest in the advanced fusion fuels which produce relatively low levels of radioactivity.[1-4] The major emphasis of this recent research has been on the D-^{3}He cycle for which neither the fuel or reaction products are radioactive. Of course, side reactions of the deuterium fuel produce some neutrons, but the total induced radiation damage and radioactivity are reduced by 1 to 2 orders of magnitude from the DT case.

Contrary to conventional thinking of the 1970's and early 1980's, achievement of breakeven conditions for the D-^{3}He cycle by the end of this century is quite possible. The achievement of similar conditions for the DT cycle (breakeven in the early 1990's) will allow scientists to enter the 21st century with similar plasma conditions for the traditional DT cycle and the more environmentally attractive D-^{3}He cycle.

The purpose of this report is to show that such exciting near term D-^{3}He results could be obtained in a tokamak of the NET/INTOR class. This report will concentrate on the physics results as opposed to the technological advantages of this fuel cycle, some of which are covered in other papers.[1,2,5] The approach taken here is to use the present (1987) design of NET[6] as a base case to illustrate the physics results that could be obtained in a hot D-^{3}He plasma without significant activation of the vacuum vessel and diagnostics. We then proceed to examine three variations of the base case as described below.

Case	Objective	Impact on Base Cost for NET
A	No change from current NET design, use D-^{3}He fuel in place of DT	none
B	Slight inboard shield modifications of NET to achieve high Q in D-^{3}He Plasma	< 1%
C	Significant TF coil modification of NET to achieve high Q operation	< 9%
D	Major modification of NET to achieve ignition	< 11%

Cases B and C are alternative variations on the base case, A, with the objective of high Q in a driven mode of operation. Case D is an attempt to see what modifications to NET are required for ignition in a D-^{3}He plasma.

Through this study, it was assumed that the main goal of NET will continue to be the ignition of DT fuel and the demonstration of a controlled DT burn. These goals will have to be accomplished regardless of the success obtained with the D-^{3}He cycle. However, because of the difficulty in working with a radioactive device like NET, even after 1 hour of DT operation, it is assumed that the D-^{3}He tests would be conducted early in the life of NET after the initial "shakedown" phase using hydrogen or deuterium plasmas. The physics results obtained by the slowing down of the high energy proton (14.7 MeV) and helium (3.6 MeV) ions, and their impact on the plasma power balance and MHD equilibrium without significant activation of the vacuum vessel and diagnostics, is certainly an attractive bonus for the physics community.

References for Chapter 1

1. L.J. Wittenberg, J.F. Santarius and G.L. Kulcinski, Fusion Technology, 10, 167 (1986).

2. G.L. Kulcinski, J.F. Santarius and L.J. Wittenberg, "Clean Nuclear Power From the Moon," to be published in the Proceeding of the 1st Lunar Development Symposium, Atlantic City, NJ, September 1986.

3. J.F. Santarius, Nuclear Fusion, 27, 167 (1987).

4. J.F. Santarius, G.L. Kulcinski, H. Attaya, M.L. Corradini, L.A. El-Guebaly, J.W. Johnson, C.W. Maynard, M.E. Sawan, I.N. Sviatoslavsky, W.F. Vogelsang, P.L. Walstrom, L.J. Wittenberg and T.E. Luzzi, "SOAR - Space Orbiting Advanced Fusion Power Reactor," to be published, Space Nuclear Power Systems, Orbit Publishers (1987).

5. G.L. Kulcinski and H.H. Schmitt, to be published in Proceedings of 11th Int. Scientific Forum on Fueling the 21st Century, Moscow, September 1987.

6. F. Engelmann, Concept and Parameters of NET, NET Report 64, EUR-FU/XII-80/86/64, Commission of the European Communities (1986).

2. NET DT REFERENCE DESIGN

The study of D-^{3}He operation is, by necessity, based on the NET design developed for D-T operation by the NET team. Since this design continues to evolve, we present here a summary of the NET design parameters on which our study is based. These are taken from NET reports.[1,2]

The NET team has considered both single-null and double-null poloidal divertor configurations. We have adopted the parameters for the double-null configuration to use as a starting point for this study. In addition to the reference double-null case for DT operation, the NET team has studied an enhanced plasma size case with an double-null divertor. The enhanced plasma has a larger major and minor radius with a corresponding increase in the plasma current, but no change in the toroidal field at the TF magnet. The enhanced plasma case is of interest to us for D-^{3}He operation since the larger size and plasma current lead to an increased Q-value (energy multiplication). In order to distinguish between these two reference cases, we refer to the first reference case as NET-DT and the enhanced plasma size case as NET-EP. Shown in Table 2-1 are the major parameters for the NET-DT and NET-EP designs; these parameters are for D-T operation; in later sections of this report we will consider possible changes for D-^{3}He operation. The cross-section of plasma, blanket, shield, and toroidal field magnet of NET-DT is shown in Fig. 2-1.

References for Chapter 2

1. The NET Team, NET Status Report 1985, NET Report 51, Commission of the European Communities, (1985).

2. F. Engelmann, Concept and Parameters of NET, NET Report 64, EUR-FU/XII-80/86/64, Commission of the European Communities, (1986).

Table 2-1. Main Configurational and Plasma Parameters of the NET Reference Options NET-DT and NET-EP

		NET-DT	NET-EP
Plasma major radius	R (m)	5.18	5.41
Plasma minor radius	a (m)	1.35	1.68
Plasma elongation	b/a	2.18	2.17
Plasma triangularity	γ	0.65	.61
Aspect ratio	A=R/a	3.8	3.2
Plasma volume	$V_p(m^3)$	390	600
Total radial machine size	$2\,R_t$(m)	21.40	(21.40)[a]
Total machine height	H_t(m)	14.00	(14.00)
Magnetic field on axis maximum on coils	B(T) B_m(T)	5.0 10.4	4.8 (10.4)
Toroidal field ripple	δ (%)	± 1.2	± 3.4
Plasma current	I_p (MA)	10.8	14.8
Safety factor	q_I	2.1	2.2
Average burn temperature	$\bar{T}$ (KeV)	10	10
Average DT density	$\bar{n}_{DT}(10^{20}/m^3)$	1.20	1.26
Average electron density	$\bar{n}_e(10^{20}/m^3)$	1.56	1.64
Murakami parameter	$M(10^{19}/m^2T)$	16	18.5
Beta scaling factor	g	3.5	3.5
Total beta	β_{tot} (%)	5.6	6.4
DT beta	β_{DT} (%)	4.2	4.8
Poloidal beta	β_I	1.42	1.2
Fusion power	P_{fus} (MW)	600	1000
α-particle power	P_α (MW)	120	200
Fusion power density	p_{fus} (MW/m^3)	1.53	1.7
Average neutron wall loading	Q_n (MW/m^2)	1	1.4
Confinement capability	$C=P_\alpha/P_{loss}$	2.9	4.4
Confinement time during burn	τ_E(s)	2	
Burn time (minimum)	τ_b(s)	200	

(a) The items in ( ) are assumed to be the same as in NET-DT.

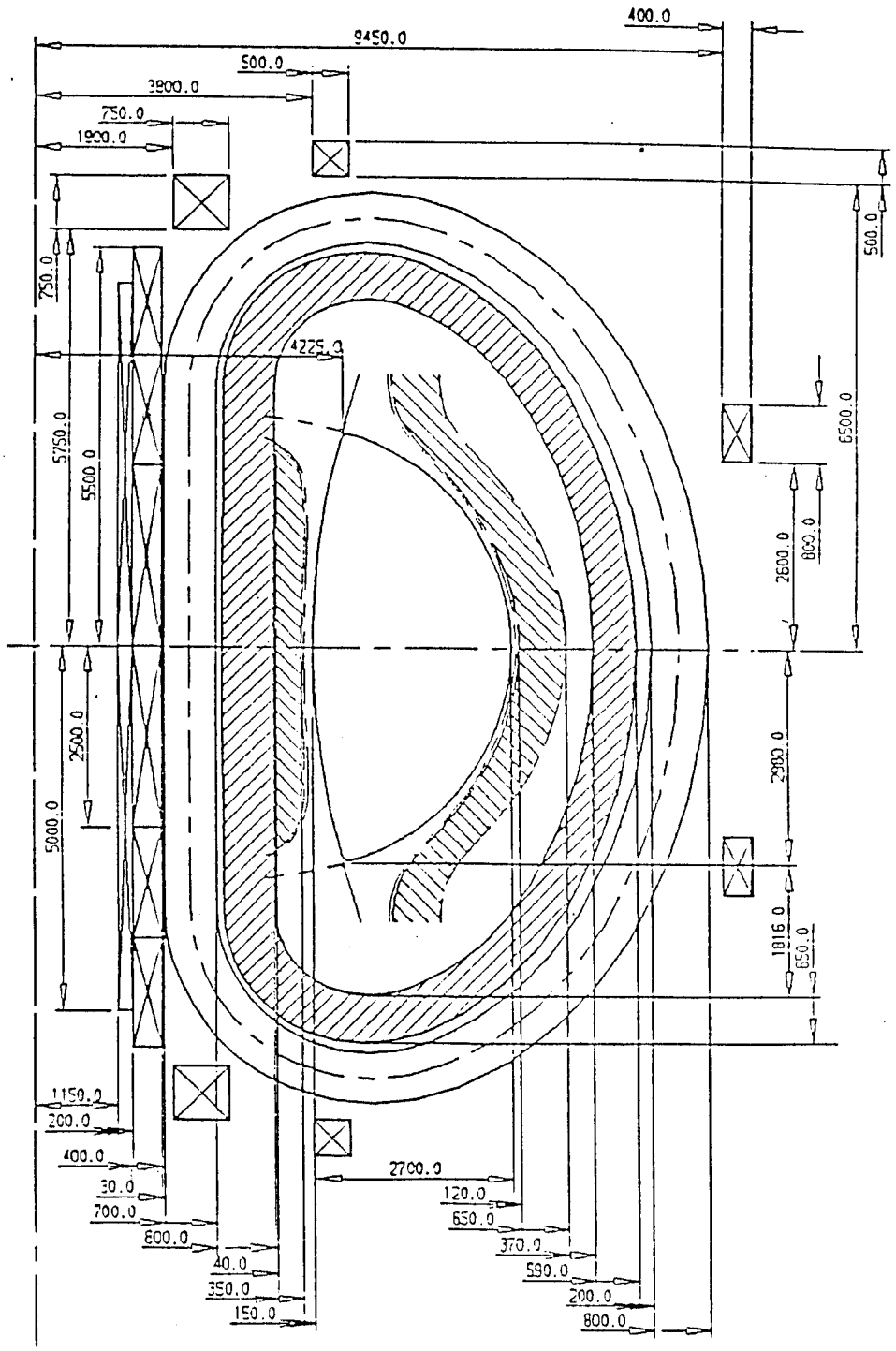

Fig. 2-1. Cross-section of the NET-DT device.

3. PLASMA PERFORMANCE MODELLING

3.1 Introduction

The performance of NET with D-^{3}He fuel can be calculated using power balance considerations to get the fusion power produced and the losses from the plasma. The fusion power produced can be calculated readily for a given plasma density and temperature profile. The loss mechanisms of concern are radiation losses by bremsstrahlung and synchrotron radiation, and transport across the confining magnetic field by conduction and convection. The plasma density and temperature that can be confined by the magnetic field is determined by MHD equilibrium and stability requirements. The plasma pressure, which is of concern for MHD, is determined not only by the fuel plasma, but also by the energetic ions generated by fusion reactions, and by the accumulation of ash and impurities. The energy of the charged particles generated by the fusion reactions also helps to maintain the energy of the reacting plasma. Folding all these effects together provides a mechanism for estimating the performance of NET using D-^{3}He fuel.

A computer code, called DHE3TOK, has been developed in order to estimate the performance of a NET-like tokamak operating with D-^{3}He. The basic physics assumptions built into this code are the same as one uses in the DT version of NET. We have built into the code the same level of conservatism or optimism as is implied in the analysis of NET by the NET design team. In particular, the following assumptions are made:

1. The beta, ratio of plasma pressure to magnetic pressure, is determined by the Troyon formula, which is an empirical fit to numerical MHD calculations.
2. The energy confinement time is given by empirical scalings. The NET team uses the so-called ASDEX H-mode scaling law which is based on H-mode confinement in ASDEX. The Kaye-Goldston scaling law is used in the U.S. TIBER study. It is based on a larger set of data from a variety of tokamaks and was developed for so-called L-mode operation. The effect of H-mode operation is generally included by multiplying the confinement time by a factor which represents the improved confinement of the H-mode.

The code is basically a zero-dimensional power balance code which calculates the ignition margin, M,

$$M = \frac{\text{Fusion Power}}{\text{Total Losses}}$$

and the energy multiplication, Q,

$$Q = \frac{\text{Fusion Power}}{\text{Injected Power}} = \frac{M}{1-M}$$

for a given set of plasma conditions. The injected power is the power required to sustain the plasma conditions. At ignition, the injected power is zero, $Q = \infty$ and $M = 1$. At scientific breakeven $Q = 1$; the fusion power produced is equal to the injected power. Note that $Q = 1$ in a D-^{3}He plasma is a stronger condition than $Q = 1$ in D-T because in the D-T case 80% of the power produced is in the form of neutron energy. The $Q = .2$ case in D-^{3}He is equivalent to $Q = 1$ in D-T from the impact on the plasma power balance and the study of burn physics.

In the following sections we present in detail the various effects included in the code. We then present a series of parametric calculations in order to determine how the various parameters influence the performance. From these one can determine the machine parameters which lead to an optimum ignition margin for a given set of constraints. Finally, we present possibilities for D-^{3}He breakeven ($Q = 1$) and ignition in NET.

3.2 Plasma Power Balance Model

Shown in Fig. 3.2-1 is a schematic of the plasma; the major radius is R, the horizontal half-width is a and the half-height is b and the elongation $K = b/a$. The plasma cross-section is assumed to be elliptical; triangularity is required for maximum beta, but the effect of triangularity on the plasma volume is neglected in this analysis. The magnetic field strength is B_0 at the magnetic axis and B_c at the toroidal field coil (peak field point); the separation point between the toroidal field winding pack on the inboard side and the plasma edge is Δ; this distance includes the cryostat, neutron shield, and plasma scrape-off layer. Because of the 1/r variation of the toroidal field, B_0 and B_c are related by

$$B_0 = B_c \left(\frac{R-a-\Delta}{R}\right) . \qquad (3.2\text{-}1)$$

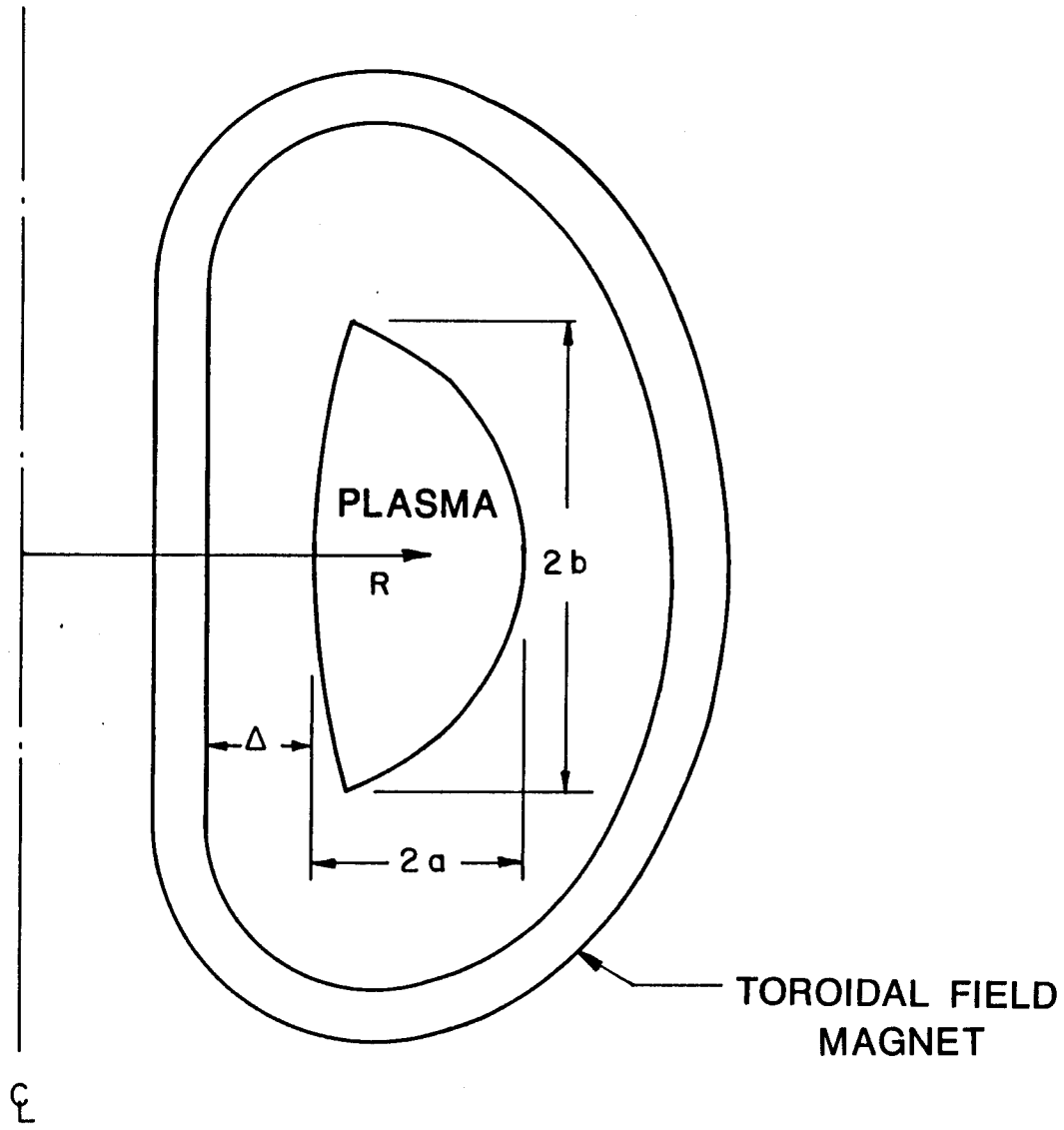

Fig. 3.2-1. Schematic of the plasma and toroidal field magnets defining the dimensions.

The plasma contains two fuel ion species (deuterium and ^{3}He) and three "ash" ion species (protons, alphas, and tritium). Protons and alphas are produced primarily by the ^{3}He(d,p)^{4}He reaction. The D(d,p)T side reaction produces tritium which is important for evaluating the generation of 14 MeV neutrons. We denote these 5 ionic species by the subscripts 1, 2, 3, 4, and 5, respectively. Thus, for example, $n_1(r)$ is the density profile for the deuterium. Here r is the distance of a flux surface from the magnetic axis in the midplane. The density profile of each charged particle species is taken to be of the form

$$n_j(r) = n_j(o)\ (1 - r^2/a^2)^{\alpha_N} \tag{3.2-2}$$

and the electron and ion temperature profile is

$$T(r) = T(o)\ (1 - r^2/a^2)^{\alpha_T} \tag{3.2-3}$$

where the exponents α_N and α_T are input data. For the calculations presented here, the values $\alpha_N = 1.$ and $\alpha_T = 1.5$ have been used. These functional forms have the advantage that the volume average of n^p is given by

$$\langle n^p \rangle = \frac{[n(o)]^p}{1 + p\ \alpha_N} \tag{3.2-4}$$

where p is an arbitrary exponent. An exception to this rule is that <T> is defined as a density weighted average,

$$\langle T \rangle = \frac{\int nT\ dV}{\int ndV} = \frac{\langle nT \rangle}{\langle n \rangle} = [T(o)]\ \frac{(1 + \alpha_N)}{1 + \alpha_N + \alpha_T}\ .$$

The fusion power, P_f, is given by integrating the local fusion power density over the plasma,

$$P_F = 2\pi\ R\ K \int_o^a n_1(r)\ n_2(r)\ \langle \sigma v \rangle_f\ 2\pi r dr\ Q_f\ . \tag{3.2-5}$$

Here, $\langle \sigma v \rangle_f$ is the Maxwellian-averaged fusion cross-section and depends on r through its dependence on the ion temperature. Note that $\langle \sigma v \rangle_f$ assumes the two ion species are Maxwellian at the same temperature. For sub-ignited operation, higher Q can be obtained by using ICRF to generate an enhanced tail in one species; this increases the

fusion power produced for a given injection power. This is not considered in the DHE3TOK code, but is discussed in Chapter 7. Equation (3.2-5) is written for a single nuclear reaction with yield Q_f; the code includes the contributions from all possible reactions, including D-D and D-T, but the power from the D-^{3}He reactions dominates.

We define f_d to be the fraction of the total fuel ion density which is deuterium; the helium fraction is then $1 - f_d$. We also consider the accumulation of fusion produced ash (protons, tritons, and alpha particles); the ash density is determined by the balance of the production rate and the loss rate. For example, the proton density is determined by

$$\int n_1 n_2 \langle \sigma v \rangle_f \, dV = \frac{1}{\tau_p} \int n_3 dV \ . \tag{3.2-6}$$

The particle confinement time, τ_p, is taken to be the same for all species. The electron density, n_e, is determined by quasi-neutrality. The total fuel ion density is n_f,

$$n_f = n_1 + n_2,$$

where $$n_1 = f_d n_f$$

and $$n_2 = (1 - f_d) n_f \ .$$

The volume averaged plasma beta is given by the Troyon formula,[1]

$$\langle \beta \rangle = \frac{C \ I_p \ (MA)}{a(m) \ B_0(T)} \tag{3.2-7}$$

where I_p is the plasma current. This equation requires that the quantities be entered in the units indicated. The NET team uses the value C = .035; we use the same value for this study. The volume-averaged plasma pressure is then given by

$$\langle p \rangle = \langle \beta \rangle \frac{B_0^{\,2}}{2 \ \mu_0} \ . \tag{3.2-8}$$

Included in the pressure are the effect of the various ion species, all of which are assumed to have the same ion temperature, the electrons, which have temperature $T_e(r)$, and also the pressure of the hot ions generated by fusion reactions. The distribution function of the hot ions is calculated using the slowing down approximation to the

Fokker-Planck equation, and the pressure is evaluated as a moment of the distribution function. This analysis, which is given in Ref. 2, gives the local hot ion pressure. As an example, Fig. 3.2-2 shows the ratio of the fast ion pressure to the pressure of the background plasma for a 50:50 mixture of deuterium and ^{3}He. The resulting fast ion pressure is then averaged over the plasma volume to give the contribution to the volume-averaged plasma pressure. The total volume-averaged pressure is then

$$\langle p \rangle = \{[n_1(o) + n_2(o) + n_3(o) + n_4(o) + n_5(o)]\, T_i(o) + n_e(o)\, T_e(o)\}/(1 + \alpha_N + \alpha_T) + \langle p_{fast} \rangle \cdot \tag{3.2-9}$$

Using Eq. (3.2-8) and (3.2-9) coupled with the particle balance equations, Eq. (3.2-6), for each ash species to determine the densities, n_3, n_4, and n_5, we then get the allowed fuel ion densities, n_1 and n_2. The total ion density is then

$$n_i = \sum_i n_i \quad .$$

To determine the injected power required to sustain the plasma at a specified operating temperature, it is necessary to account for the various mechanisms by which the plasma loses energy. Bremsstrahlung radiation from the electrons is given by[3]

$$P_B = \frac{5.31 \times 10^{-3}\, n_e^2(o)\, \sqrt{T_e}\, V}{1 + 2\,\alpha_N + .5\,\alpha_T} (Z_e(1 + .0155\, T_e + 7.15 \times 10^{-6}\, T_e^2) + .071\, Z_T/\sqrt{T_e} + .00414\, T_e) \quad (MW) \tag{3.2-10}$$

where

$$Z_e = \sum_j n_j Z_j^2/n_e \tag{3.2-11}$$

$$Z_T = \sum_j n_j Z_j^3/n_e$$

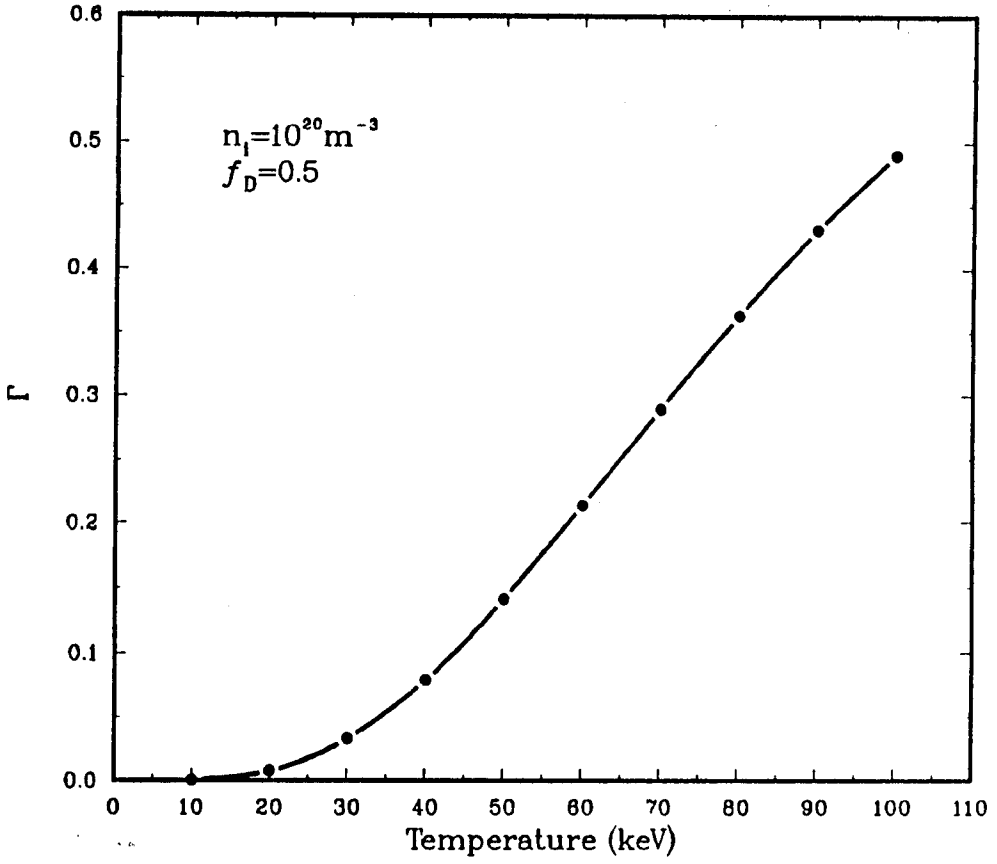

Fig. 3.2-2. Ratio of the fast ion pressure to the background plasma pressure in a D-He^3 plasma versus electron temperature.

and V is the plasma volume. In Eq. (3.2-11) the sums are over the various ionic species in the plasma. Eq. (3.2-10) and following equations are written in units where the temperature is in keV, the magnetic field is in Tesla, the density is in units of 10^{20} $m^{-3}s$, the volume is in m^3, dimensions are in meters, the plasma current is in MA, and the power is in megawatts.

Synchrotron radiation from the electrons is another form of radiation loss. While this is a classical process and is in principle calculable, it is a difficult radiation transport problem because the plasma is both a strong emitter and absorber of synchrotron radiation. We use a "universal formula" developed by Trubnikov[4] to estimate the synchrotron power loss,

$$P_s = P_0 \Phi$$

$$P_0 = 6.24 \times 10^{-3} \, n_e \, B^2 \, T_e \quad \left(\frac{MW}{m^3}\right) .$$

P_0 is the radiation emitted not considering re-absorption and $1 - \Phi$ is the fraction re-absorbed. Trubnikov suggests a reasonable approximation for Φ is

$$\Phi = 60 \left(\frac{T_e}{m_e c^2}\right)^{1.5} \frac{1}{\sqrt{p_a}}$$

$$p_a = \frac{a}{1 - R_e} \left(\frac{1}{1 + \chi}\right) \frac{\omega_{pe}^2}{c \, \omega_{ce}}$$

where R_e is the reflectivity of the walls, ω_{pa} is the electron plasma frequency, ω_{ce} is the electron cyclotron frequency, and χ contains the effect of the torus,

$$\chi = \frac{2 a}{R} \sqrt{\frac{2\pi \, T_e}{m_e c^2}} .$$

In the code we evaluate the electron cyclotron frequency at the magnetic axis, use the volume-averaged temperature in the computation of χ, and volume-average the remaining density and temperature dependences in P_0 and Φ to get the result

$$P_S = \frac{4.2 \times 10^{-7} \sqrt{n_e}\, B_0^{2.5} \sqrt{1 - R_e}\, \sqrt{1 + \chi}\, T_e^{2.5}\, V}{\sqrt{a_p}\,(1 - .5\,\alpha_N + 1.5\,\alpha_T)} (1 + \alpha_N + \alpha_T)\ (MW). \qquad (3.2\text{-}12)$$

This volume-averaging is not rigorous because photons emitted from the center of the plasma, where the emission is high, pass through a cooler and less dense plasma where they can be re-absorbed before escaping. It is not evident that this volume-averaging procedure includes this effect correctly, but there is no real alternative at the present state of development of this subject.

The reflectivity of the first wall is a concern. IPP Garching provided steel plates which had been exposed to plasma in the ASDEX divertor chamber. The JET team provided graphite tiles which were exposed to plasma in the JET tokamak. The reflectivity of the steel plates and graphite tiles was measured by G. Hochschild and H. Stickel of KfK. This yielded an average reflectivity of .95. It was assumed that 20% of the first wall surface is holes. Consequently, an effective reflectivity of .77 for synchrotron radiation was used in this study.

The remaining energy loss process is transport across the magnetic field by conduction and convection. This is treated using empirical energy confinement times. The NET team has used the ASDEX H-mode confinement time[5],

$$\tau_H = .1\ I_p\ (MA)\ R\ (m) \qquad (sec) \qquad (3.2\text{-}13)$$

which is based on H-mode operation in the ASDEX tokamak. There are a variety of alternative "scaling laws" for energy confinement (probably as many as there are scientists analysing energy confinement); the scaling law currently in favor in the U.S. is the Kaye-Goldston[6] scaling law

$$\tau_{KG} \propto I_p^{1.24}\ P_{ext}^{-.58}\ R^{1.65}\ a^{-.49}\ K^{.28}\ n_e^{.26}\ A_i^{.5}\ B_0^{-.09}\ f_H \qquad (sec)$$

where A_i is the atomic mass number of the ions. This scaling law is determined empirically from a larger set of data covering many tokamaks operating in the L-mode regime with sufficient auxiliary heating. To account for the improved confinement in the H-mode regime, the factor f_H is introduced. One normally takes f_H to be 2. The ASDEX H-mode scaling law is based on H-mode behavior in the ASDEX tokamak, which does not

show degradation of the energy confinement time with increasing neutral beam power. Recent experiments with Doublet III-D[7] substantiate this result at an injection power up to 6 MW. The Doublet III-D results are quantitatively consistent with ASDEX H-mode scaling law. The JET tokamak, however, shows degradation of the energy confinement time with neutral beam power and follows the Kaye-Goldston scaling law with a H-mode factor, f_H, of about 2.

The use of either of these scaling laws represents a considerable extrapolation from the data on which they are based when applied to either D-T or D-^{3}He operation. A rather strong assumption in the Kaye-Goldston scaling law is that charged particle heating by fusion reactions is no different than any other form of auxiliary heating. Since the fusion power achieved to date is negligible in comparison with the external heating power, there is no experimental evidence for, or against, this hypothesis. This assumption is made in the U.S. in order to introduce some conservatism in the analysis. It is possible, however, that drift-type instabilities can become worse at fusion plasma conditions and lead to even worse confinement. The lack of a good energy confinement scaling law is the biggest source of uncertainty in our analysis.

In the parametric studies we consider both the ASDEX H-mode and Kaye-Goldston scaling laws. In the Kaye-Goldston law the heating power, P_{ext}, can be eliminated by the self-consistency relation,

$$P_{ext} = P_t = \frac{3}{2}\frac{1}{\tau_E}\int (n_i T_i + n_e T_e)\, dV \qquad (3.2\text{-}14)$$

With this relation, the Kaye-Goldston law can be rewritten in the form,

$$\tau_{KG} = \frac{.003\, R^{2.55} I_p^{2.95} A_i^{1.19} n_e^{.62} f_H^{2.38}}{a^{3.93} B^{.21} K^{.71} (n_i T_i + n_e T_e)^{1.38}} \quad \text{(sec)} \qquad (3.2\text{-}15)$$

If the auxiliary heating power is small compared with the ohmic heating power, the empirically determined energy confinement time is[8]

$$\tau_\Omega = .071\, n_e\, a^{1.04} R^{2.14} \sqrt{q} \qquad (3.2\text{-}16)$$

Goldston suggests that the two scaling laws can be combined in the form

$$\frac{1}{\tau_E^2} = \frac{1}{\tau_\Omega^2} + \frac{1}{\tau_{KG}^2} \tag{3.2-17}$$

to get a single result covering both ohmic and external heating. In our analysis we use Eq. (3.2-15) in conjunction with (3.2-16) to get the overall energy confinement time.

The transport energy loss is then given by Eq. (3.2-14) and is primarily due to the electrons in present experiments. The ion energy transport appears to be within a factor of 2 or 3 of the neoclassical energy transport. At the conditions appropriate for D-^{3}He the neoclassical energy confinement time for the ions is very long in comparison with the empirical energy confinement times given above.

The energy flow for the system is as follows: The fast ions produced by fusion reactions slow down in the plasma and transfer their energy to the background ions and electrons; the electrons get the larger share in a D-^{3}He plasma (about 80%). The fuel ions are also heated by the external heating system, if present, and lose energy to the electrons by Coulomb collisions. Because the energy flow has to be from the ions to the electrons, the ions are hotter than the electrons. The electrons radiate some of the power to the walls and transport the rest by thermal conduction across the magnetic field. Some of the external heating power may also be coupled to the electrons depending on the heating mechanism chosen. In this report, we assume that with suitable design of an ICRF system the power can be coupled only to the ions and neglect any coupling to the electrons. If the plasma is ignited ($M > 1$) then the external heating power is zero and the radiation power must be increased to maintain a power balance.

The overall injection power, P_{inj}, required to sustain the plasma is determined by a power balance on the entire plasma.

$$P_B + P_s + P_t = P_F + P_{inj} \tag{3.2-18}$$

The temperature difference between the electrons and the ions is determined by a power balance on the electrons if the plasma is not ignited, or on the ions if the plasma is ignited. For electron-ion energy transfer due to Coulomb collisions we use the Spitzer[9] formula. The equation for power balance on the electrons, for example, is

$$P_B + P_s + P_t = P_F\,(1 - f_i) + P_{ie} \tag{3.2-19}$$

where P_{ie} is the power flow from the ions to the electrons due to Coulomb collisions and f_i is the fraction[2] of the fusion power transferred to the ions. When the plasma is subignited the code finds a self-consistent solution to the above equations for a given ion temperature and calculates the injected power required to sustain that set of plasma conditions. If the plasma is ignited, the "injected" power is negative; in this case the equation for the ion power balance is solved and the code calculates the increased radiation power loss required to maintain a power balance on the plasma.

In the next section we present a series of parametric calculations to determine the influence of various effects on the ignition margin, or energy multiplication. From these calculations we can determine the "optimum" conditions to achieve breakeven or ignition in a D-^{3}He tokamak.

References for Section 3.2

1. F. Troyon, et. al. Plasma Physics Cont. Fusion 5, 261 (1980).

2. B.Q. Deng and G.A. Emmert, "Fast Ion Pressure in Fusion Plasmas", University of Wisconsin Fusion Technology Institute UWFDM-718, Jan. 1987.

3. J. Rand McNally, Nuclear Fusion/Technology, 2, 9 (1982).

4. B.A. Trubnikov, "Universal Coefficients for Synchrotron Emission from Plasma Configurations", Reviews of Plasma Physics, vol. 7 Plenum Press (1979) 345.

5. The NET team, NET Status Report 1985, NET Report 51, Commission of the European Communities, (1985).

6. S.M. Kaye and R.J. Goldston, Nuclear Fusion 25, 65 (1985).

7. K.H. Burrell, S. Ejima, et al., Phys. Rev. Lett. 59, 1432 (1987).

8. R.J. Goldston, Plasma Physics Cont. Fusion 26, 87 (1984).

9. L. Spitzer, Jr., "Physics of Fully Ionized Gases," Interscience Publishers (1962) p. 135.

3.3 Parametric Studies

The plasma physics model described in Sec. 3.2 forms the basis for estimating the performance of NET, and variations of it, using D-^{3}He as the fuel. In this section we present the results of parametric studies using this model. A summary of the various regimes investigated is given in Table 3.3-1.

We first consider the NET-DT and NET-EP tokamak (see Section 2) with no changes in the dimensions or magnetic field, but change only the fuel composition from D-T to D-^{3}He and change the operating temperature to that required for D-^{3}He, with a corresponding change in the injected power because of the higher operating temperature. The objective here is to investigate the physics of ions slowing down in a hot plasma and the approach to Q = 1 for the NET-EP configuration. This is case A in Table 3.3-1.

In regime B we investigated a possible variation on the NET parameters to take advantage of the fact that tritium breeding is not required and less space for neutron shielding is needed with D-^{3}He (the details are in Chapter 4.) This means that the plasma major radius can be reduced. The reduced major radius increases the plasma current if the MHD safety factor, q, is held constant; the magnetic field at the plasma is also increased by the inward displacement. However, the magnetic field at the TF coil remains unchanged. These adjustments improve both the fusion power density and the confinement of the plasma.

The third regime, (C), we considered was to increase the toroidal field at the TF magnet while retaining the original plasma and machine dimensions. This gives a more modest increase in the plasma current, at constant q, but increases the fusion power density, while also raising the Q-value.

Finally in regime D, we considered the effect of both reducing the major radius and increasing the toroidal field and/or the plasma elongation in order to see what parameters are required to achieve ignition with D-^{3}He in a modified version of NET.

3.3.1 D-^{3}He in the Reference NET-DT and NET-EP Designs (Case A)

Shown in Fig. 3.3-1 is the Q-value that can be obtained in the reference NET-DT tokamak (NET-DT described in Chapter 2) for the two scaling laws, Kaye-Goldston and ASDEX H-mode, versus the average ion temperature. We see that the optimum ion temperature (all temperatures quoted in this section are density weighted and averaged over the plasma volume) is about 45 keV. The higher temperature required for D-^{3}He

Table 3.3-1. Regimes Studied for the Burning of D-^{3}He Fuel in a NET Class Tokamak

Regime		Objective	B_{max} at Coil	Inboard Shield Thickness	Plasma Radius R_p	Plasma Current I_p	Plasma Elongation K
A	NET-DT	Physics of Fast Ions	Ref	Ref	Ref	Ref	Ref
	NET-EP	Breakeven	Ref	Ref	Ref	Ref	Ref
B	NET-EP	High Q Operation	Ref	Thinner	Smaller	Higher	Ref
C	NET-EP	High Q Operation	Higher	Ref	Ref	Higher	Ref
D	NET-EP	Ignition	Higher	Thinner	Smaller	Higher	Larger

*Ref means as designed by the NET team for either the NET-DT or NET-EP configurations and reported in Chapter 2.

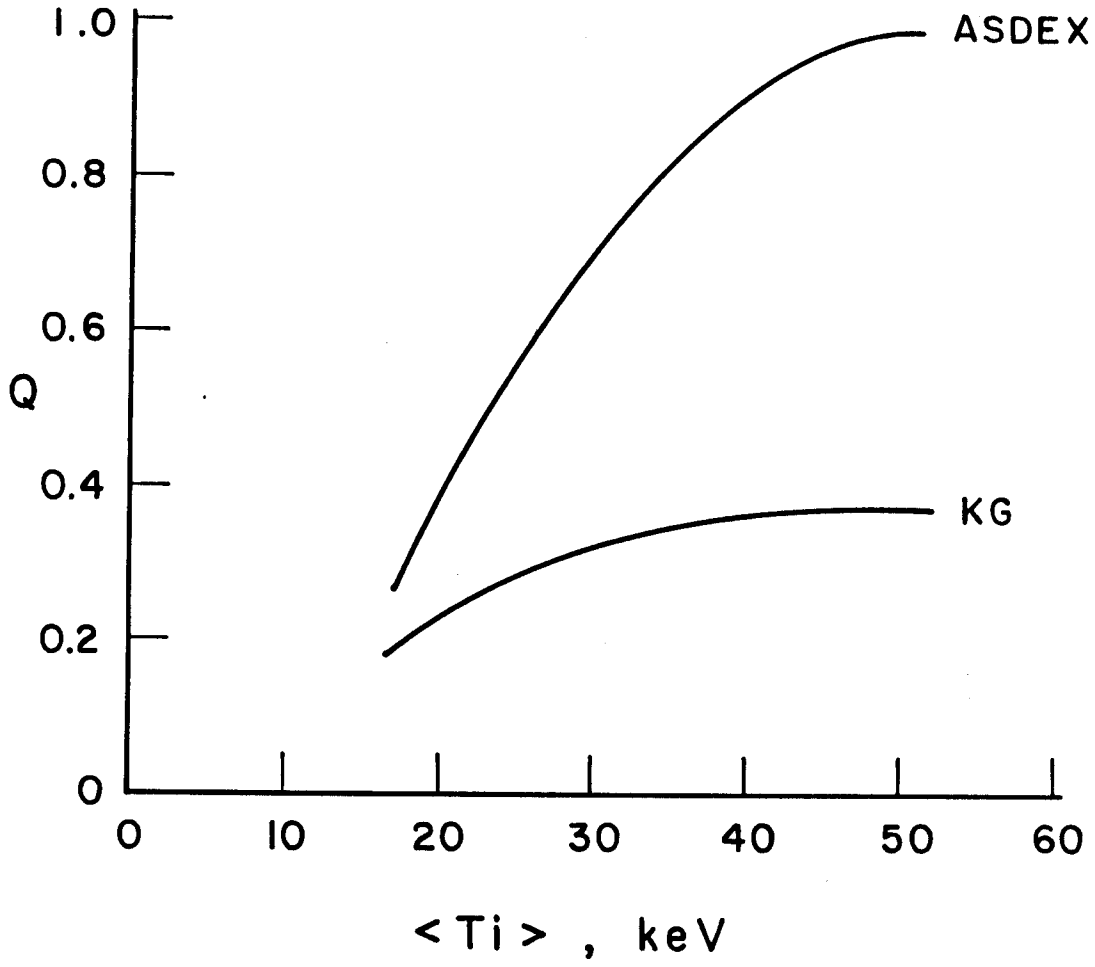

Fig. 3.3-1. Energy multiplication, Q, versus average ion temperature for D-^{3}He operation in NET-DT for both ASDEX H-mode and Kaye-Goldston energy confinement scaling.

arises from the fact that $\langle\sigma v\rangle_f/T^2$ peaks at 55 keV for D-^{3}He versus 13 keV for D-T, as shown in Fig. 3.3-2; an average temperature of 45 keV corresponds to a central temperature of about 80 keV for the profiles used in this analysis. It is obvious from Fig. 3.3-1 that the plasma performance is much more favorable for ASDEX scaling than for Kaye Goldston. It is gratifying to note that $Q \tilde{=} 1$ could be achieved in the NET device as it is presently designed with essentially no modifications (or added cost)!

Shown in Fig. 3.3-3 is the injected power required to maintain the plasma at the operating temperature and the resulting fusion power; the injected power decreases with increasing ion temperature for ASDEX H-mode scaling since the beta is kept constant at the Troyon limit. Hence density is decreasing as the temperature is raised in Fig. 3.3-1 and 3.3-3. The power levels required are excessive if the confinement is Kaye-Goldston, but within the present NET limits if the confinement is ASDEX H-mode. Note that this power is the power coupled to the plasma since the details of the heating mechanism, and hence the coupling efficiency are beyond the scope of this study. (The NET design calls for 50 MW of coupled power for plasma startup and heating to ignition.)

Shown also in Fig. 3.3-3 is the fusion power released versus ion temperature. Here the fusion power is defined as the total power released in charged particles due to fusion reactions. The power in the neutrons produced is not included. Almost all the fusion power is due to D-^{3}He reactions, although there is a small amount of D-D power also. The fusion power is slightly higher in the Kaye-Goldston scaling; this is because the electrons run colder because of the poorer confinement. This reduces the electron pressure and allows a slightly higher ion density for a given beta. The relatively low fusion power obtained in regime A is of concern since the fusion power density is low in the plasma. Consequently, the plasma will be sensitive to impurity accumulation which, in turn, affects the fusion power and the Q-values. This effect needs further study but is beyond the scope of this work.

Shown in Fig. 3.3-4 is the Q-value obtained with the NET-EP (see Chapter 2) configuration. The injected power and the fusion power versus ion temperature are shown in Fig. 3.3-5. We see that with ASDEX H-mode scaling a Q value of 1.45 is obtainable with an injection power of slightly less than 40 MW. With Kaye-Goldston scaling the maximum Q-value is less than .5 and the required injection power is almost 170 MW. Consequently, if the ASDEX H-mode scaling law holds, one can achieve breakeven in NET-EP with no change in the basic machine parameters except for the fuel composition

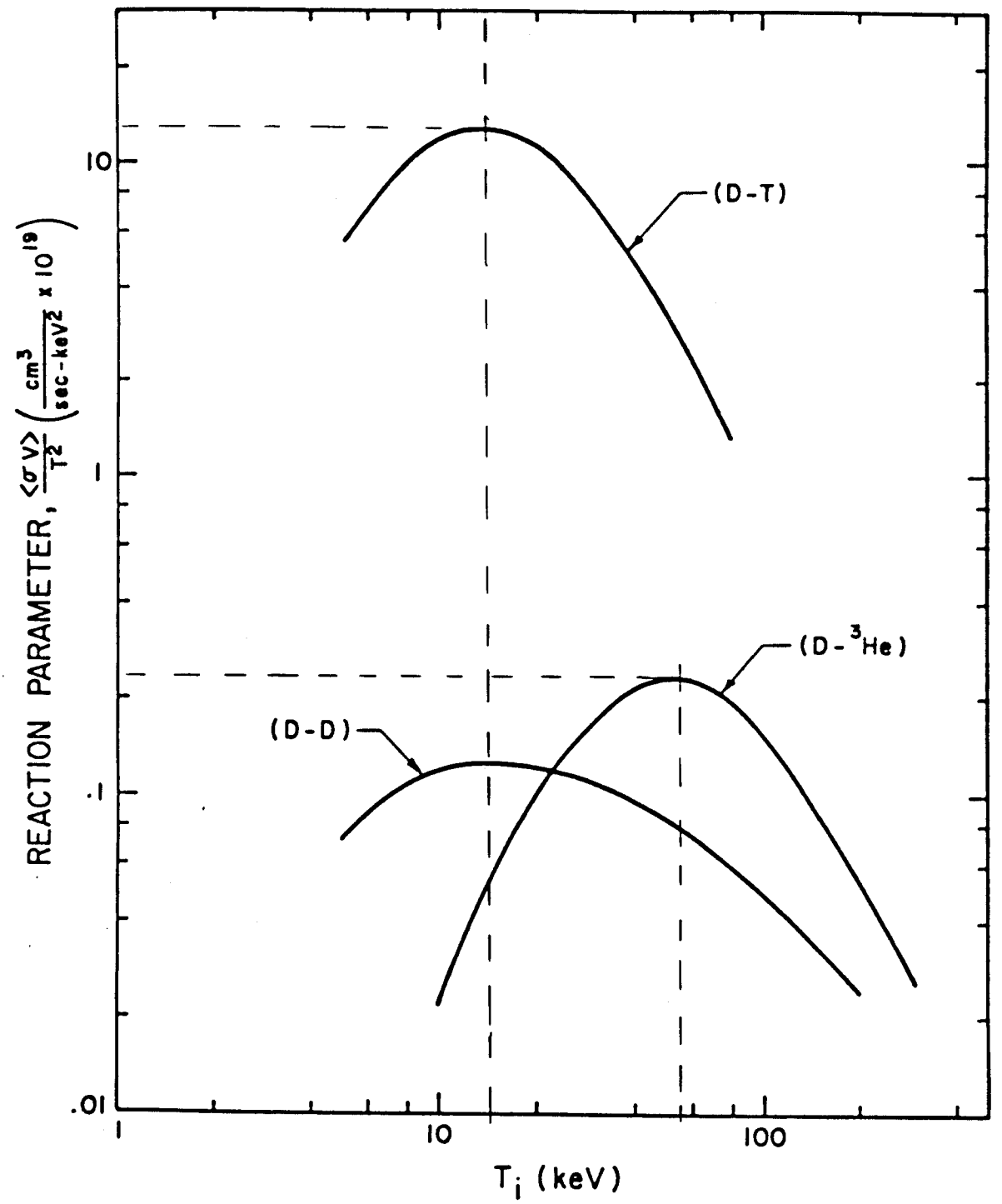

Fig. 3.3-2. The Maxwellian averaged reaction rate parameter, $\langle\sigma v\rangle$, as a function of ion temperature for several fusion fuel cycles.

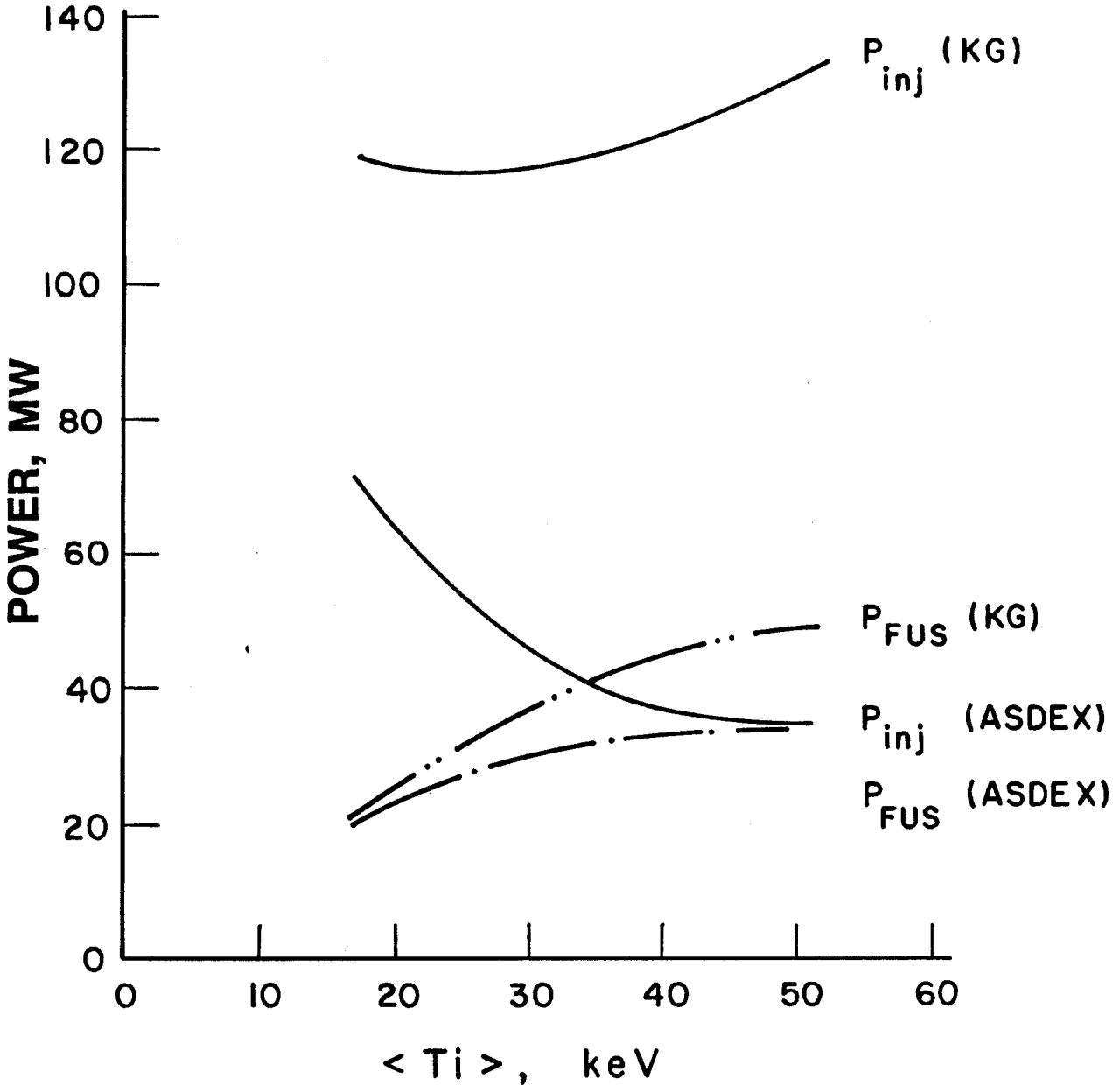

Fig. 3.3-3. Injection power and fusion power versus average ion temperature for NET-DT for both ASDEX H-mode and Kaye-Goldston energy confinement scaling.

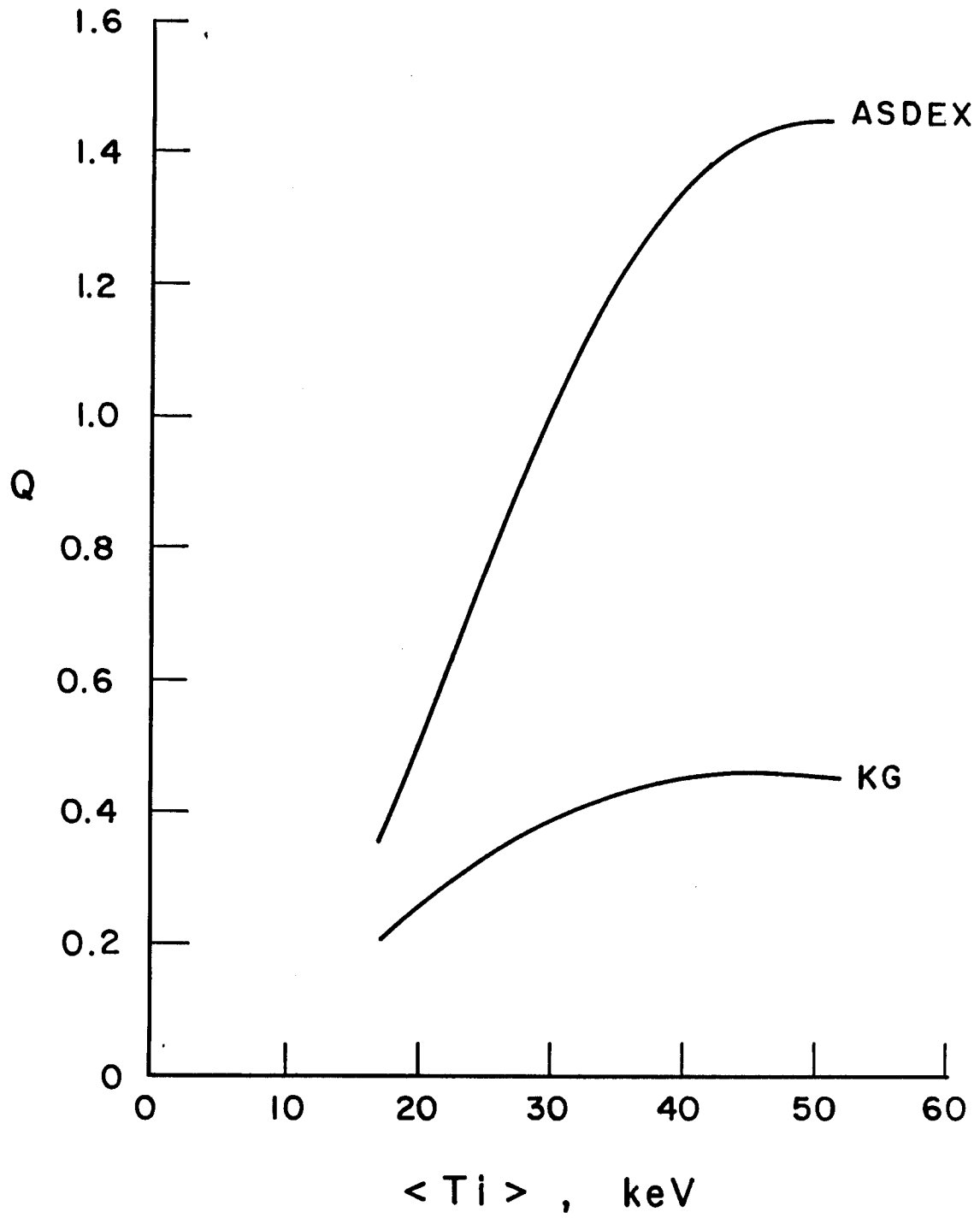

Fig. 3.3-4. Energy multiplication, Q, versus average ion temperature for NET-EP for both ASDEX H-mode and Kaye Goldston energy confinement scaling.

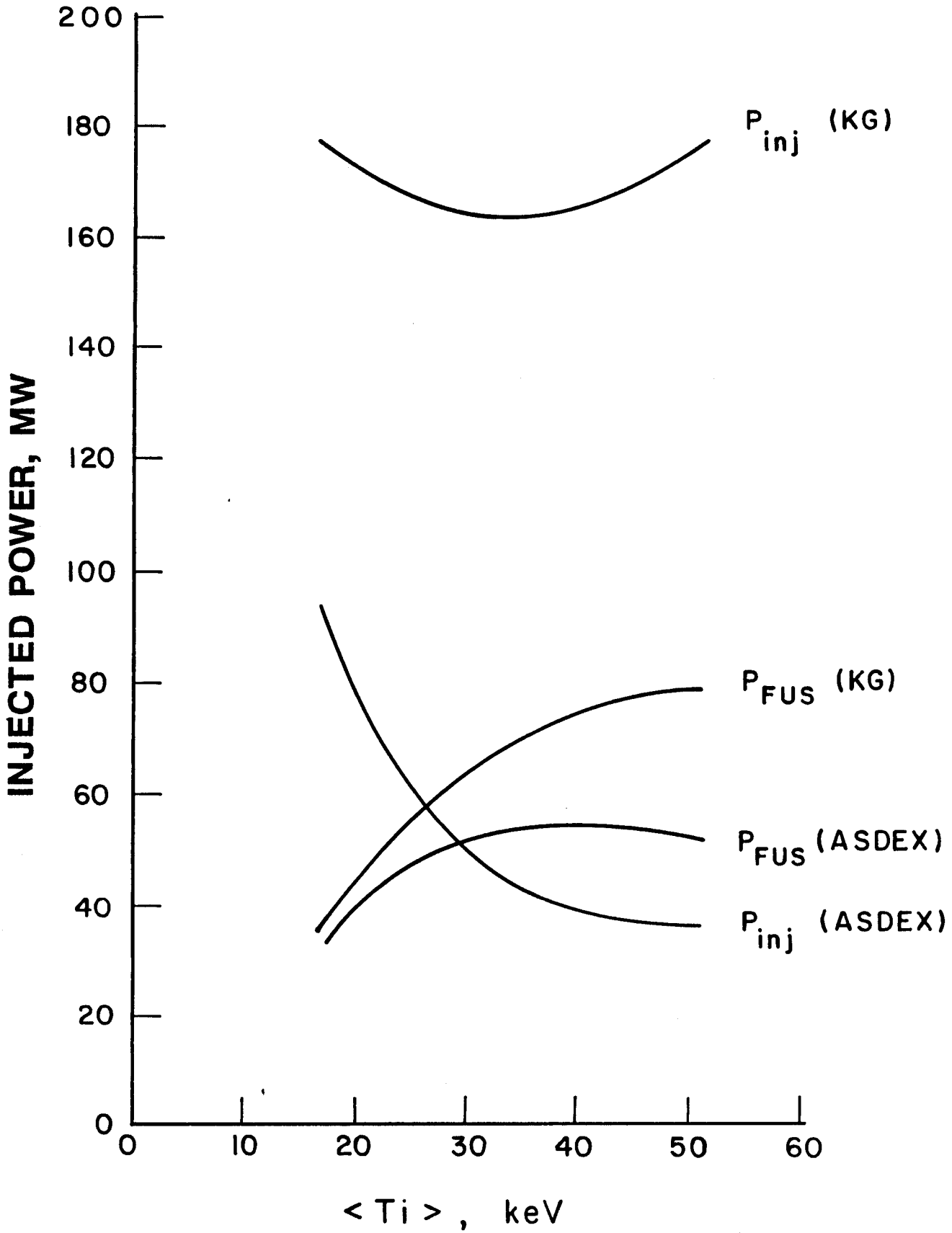

Fig. 3.3-5. Injection power and fusion power versus average ion temperature for NET-EP for both ASDEX H-mode and Kaye-Goldston energy confinement scaling.

and the operating temperature. There will need to be some modifications to the auxiliary heating system because of the change in fuel and operation temperature.

3.3.2 Reduced Major Radius Variations of NET-EP (Regime B)

The NET-DT and NET-EP reference designs have a large region for a thick tritium breeding blanket and shield between the plasma and the TF magnet. This is not needed for D-^{3}He operation. The blanket can be removed and the shield replaced by a thinner shield optimized for the D-^{3}He neutron spectrum (see Chapter 4). Consequently, the plasma major radius can be reduced; this leads to a lower plasma aspect ratio, higher beta, and higher plasma current if the MHD safety factor is held constant. The higher plasma current increases the energy confinement time. In addition, the reduced major radius of the plasma increases the magnetic field at the plasma and increases the fusion power output. All this is accomplished with the original TF coil design and operating conditions.

Shown in Fig. 3.3-6 is the effect of reducing the major plasma radius on the Q-value and the plasma current. In this figure, f_d is 0.65, and the average ion temperature is kept constant at 37 keV. The Q-value reaches a value of about 2.9 for ASDEX H-mode scaling and the plasma current increases from 14.8 to 20 MA when the plasma radius is reduced from 5.41 m to 4.61 m. The required injection power decreases slightly from 40 MW to 35 MW. For Kaye-Goldston scaling, the ignition margin increases to .74 and the injection power to 180 MW when the major radius is reduced to 4.61 m.

At a major radius of 4.61 m, the space available for the shield, cryostat, and inboard scrape-off layer has been reduced to a total of 45 cm. Because of the greatly reduced neutron wall loading (0.019 MW/m^2), the magnet can still be protected adequately against nuclear heating and radiation damage effects. This is discussed further in Chapter 4. The production rate of neutrons can be reduced even further by changing the fuel mixture. The value f_d = .65 used so far has been chosen to optimize the Q-value. Reducing the percentage of deuterium in the fuel will reduce the D-D reactions and the production of tritium. Shown in Fig. 3.3-7 is the effect of f_d on the Q-value and the amount of power in D-T and D-D neutrons. This graph corresponds to the R = 4.61 m point in Fig. 3.3-6. We see that f_d = .65 is about the optimum fuel mixture and Q drops sharply as the deuterium fraction is increased or reduced. The reason for f_d = .65 being the optimum, and not f_d = .5 as in D-T, is that helium ions have Z = 2. Consequently,

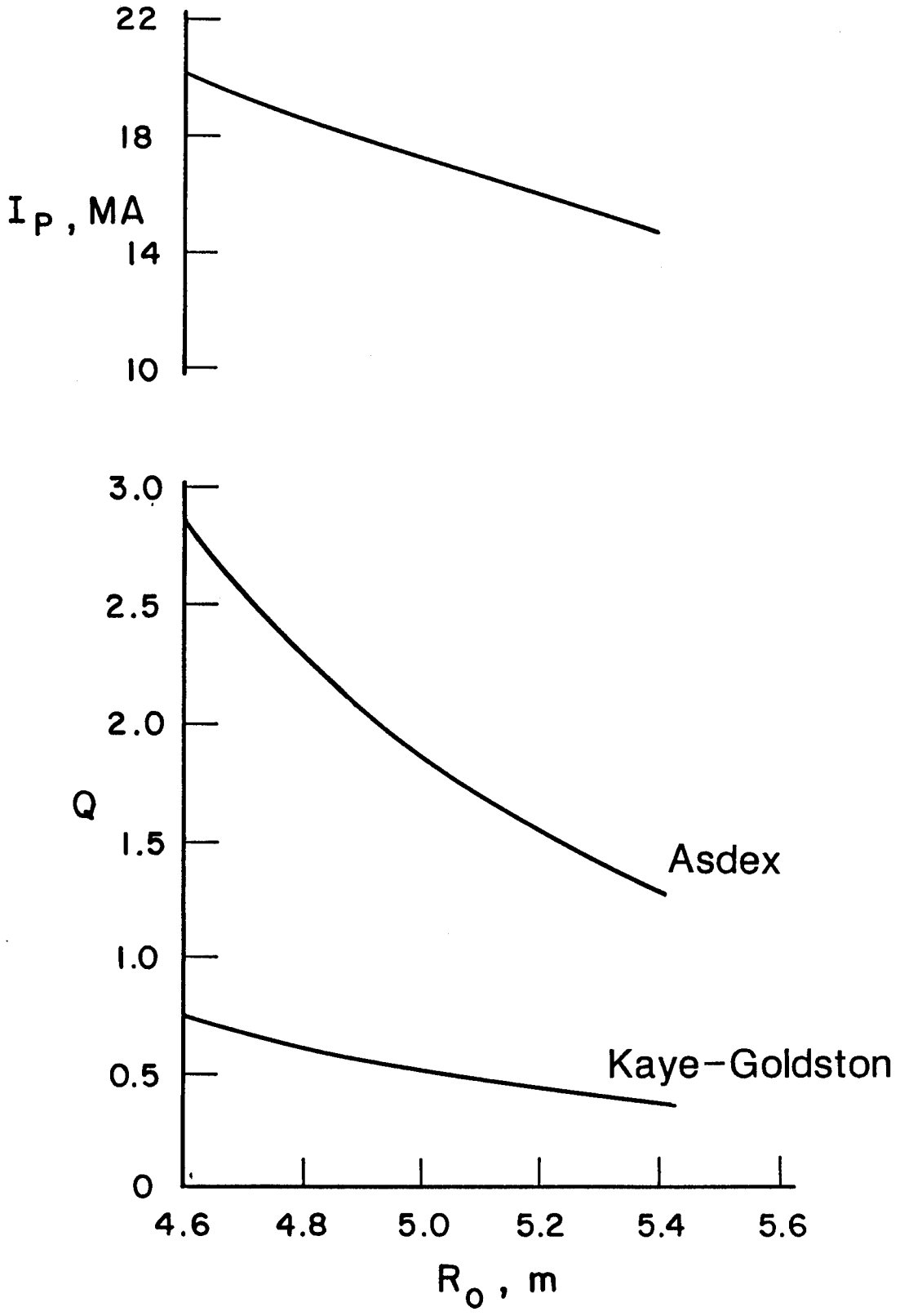

Fig. 3.3-6. Q and plasma current versus major radius; a = 1.69 m, B_c = 10.4 T, K = 2.17, $\langle T_1 \rangle$ = 37 keV.

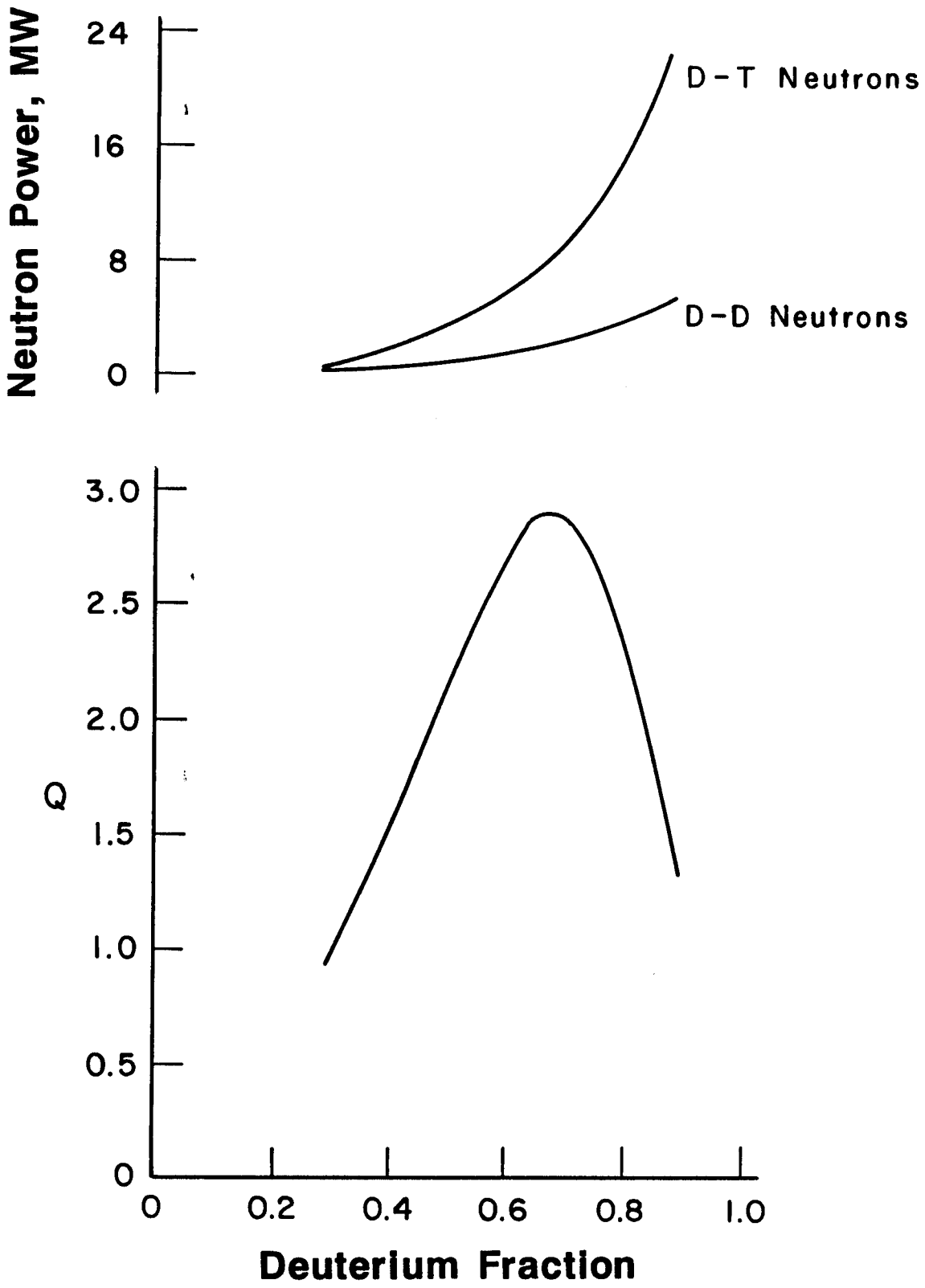

Fig. 3.3-7. Effect of changing fuel mixture on the energy multiplication, Q, and neutron power. R = 4.61 m, B_c = 10.4 T, $\langle T_i \rangle$ = 37 keV, ASDEX H-mode scaling.

increasing the deuterium fraction (starting from .5, for example) decreases the electron density and the electron pressure. Consequently, the total ion density can be increased to maintain constant beta. This more than compensates for the reduced helium fraction in the fuel. Of course, if the helium fraction is too low, then the increased ion density is not sufficient and the fusion power drops as f_d is increased further. In addition, reducing the electron density reduces the bremsstrahlung and synchrotron radiation losses and improves Q.

The above analysis assumes the fuel is not spin polarized. It seems to be well accepted that using spin polarized d and ^{3}He increases the reaction rate of the process $d(^3He,p)^4He$ by a factor of 1.5.[1] The same authors claim a reduction of the cross section for the reaction channel $d(d,n)^3He$ of about 0.6 at 75 keV if polarized dueterons are used; this is based on calculations of the corresponding matrix elements.

Another group predicts an even stronger reduction of the spin polarized $d(d,n)^3He$ reaction by more than a factor of ten.[2] Thus, although the results are still controversial, taking the more pessimistic result into account it should be possible to decrease the ratios of neutron power to total ion power in a d-^{3}He mixture by at least a factor of 2/3 for the 14.1 MeV neutrons and by a factor of about 3 for the 2.5 MeV neutrons. Questions concerning the production of polarized fuel as well as the expected lifetime of the particles in the polarized state are discussed in Reference 3.

It is worthwhile to consider the relative magnitude of the various loss terms to see the sensitivity of a possible operating point to uncertainty in the various loss terms. Shown in Fig. 3.3-8 is the power in the various loss mechanisms normalized to the fusion power versus ion temperature. This curve is for the R = 4.61 m, f_d = .65 case. We see that in the temperature range where Q is largest ($\langle T_i \rangle$ = 35 to 50 keV) transport is the largest single loss; synchrotron is next and bremsstrahlung is close behind. We see that bremsstrahlung dominates at low T_i, but drops rapidly as T_i increases; this is because the density is high when the temperature is low. Consequently, the Q-values given in this report are rather sensitive to uncertainties in the energy confinement time scaling laws.

The above calculations are based on the ASDEX H-mode scaling law for energy confinement. We now consider what H-mode factor is necessary to achieve breakeven (Q = 1) in a reduced major radius version of NET-EP. We fix the major plasma radius at 4.61 m and the average ion temperature at 37 keV. Shown in Fig. 3.3-9 is the Q-value obtained versus the H-mode factor. Recall that the H-mode factor is defined as the

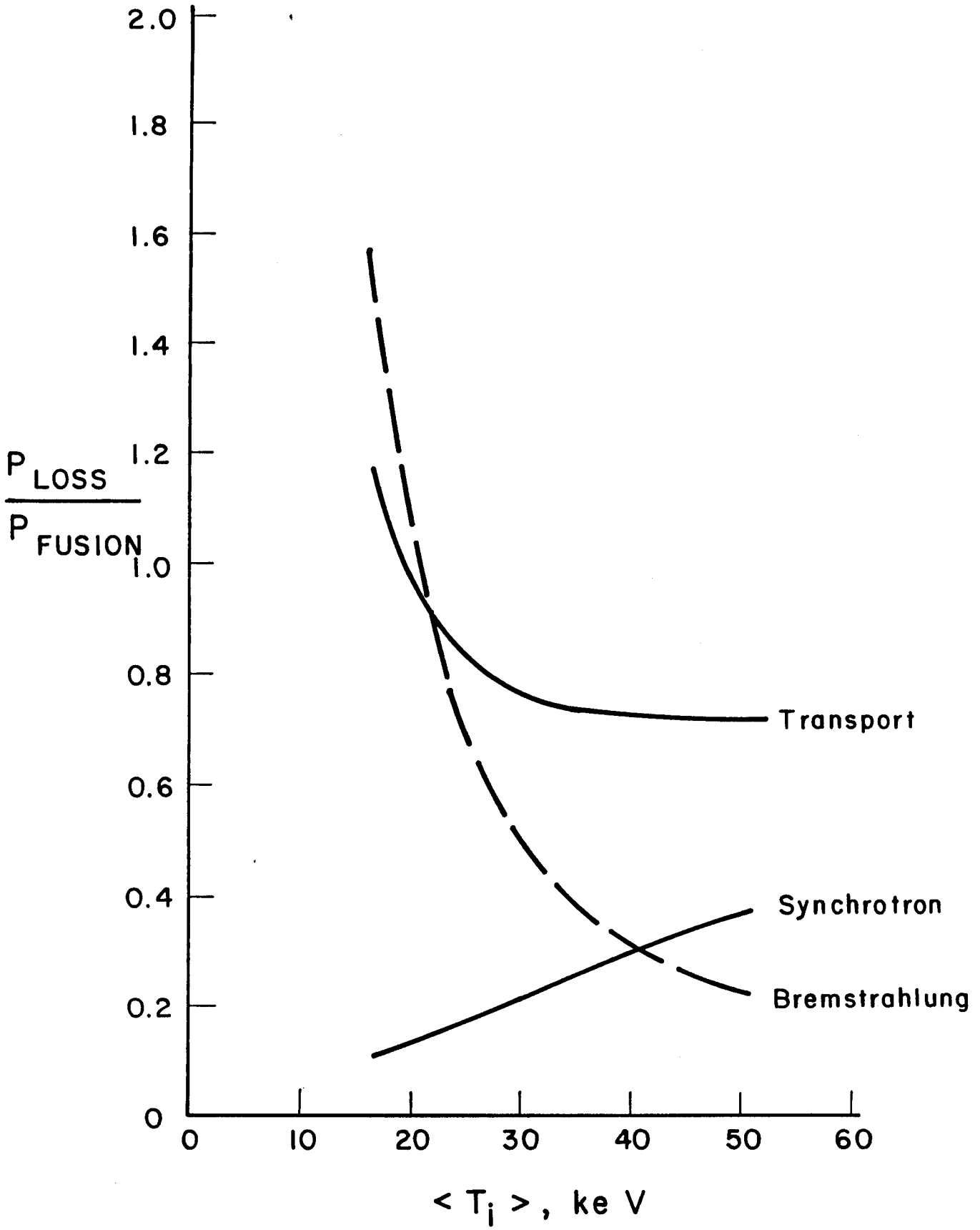

Fig. 3.3-8. Distribution of power loss versus average ion temperature. R = 4.61 m, B_c = 10.4 T, f_d = .65, ASDEX H-mode scaling.

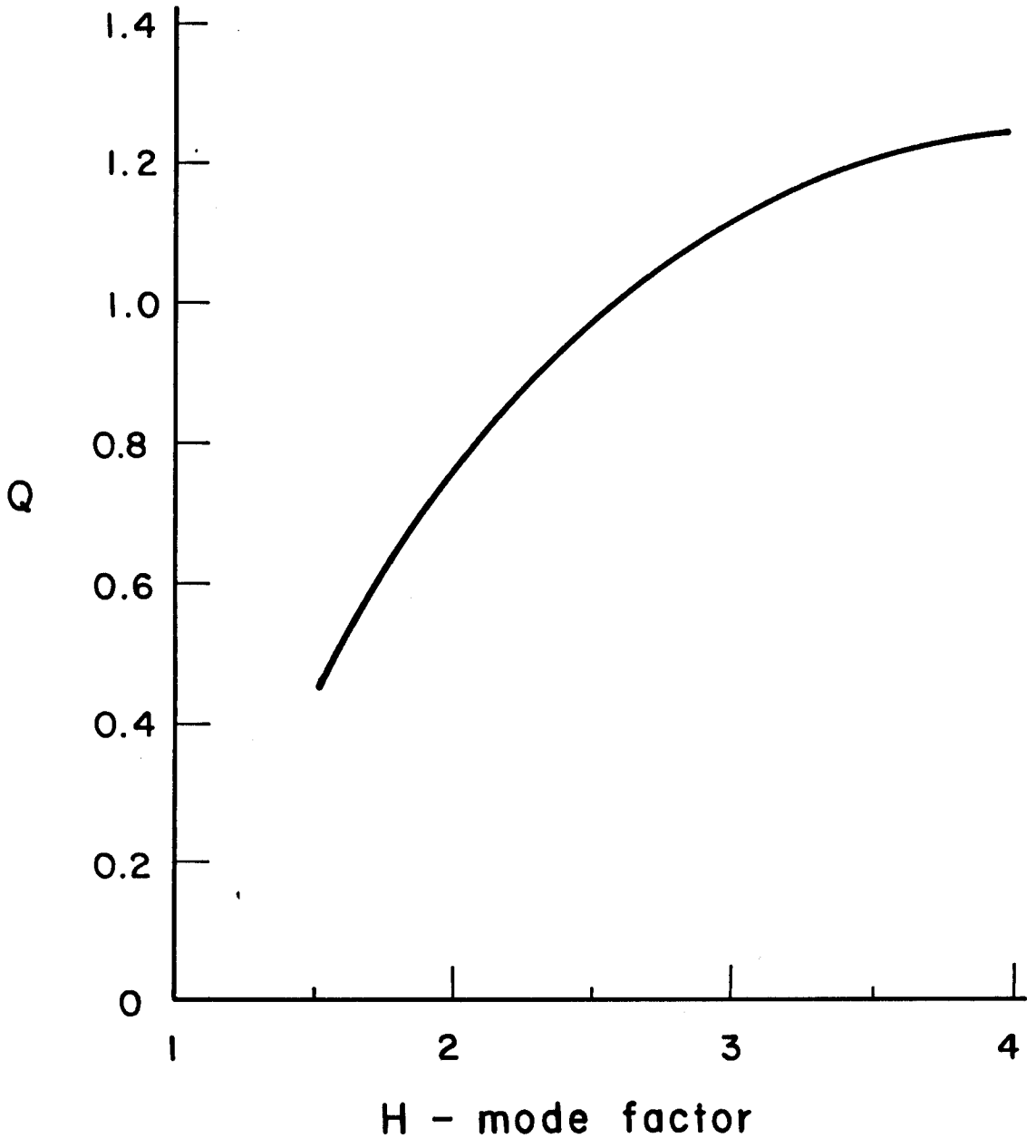

Fig. 3.3-9. Effect of the Kaye-Goldston H-mode factor on the energy multiplication, Q. R = 4.61 m, B_c = 10.4 T, f_d - .65, $\langle T_i \rangle$ = 37 keV.

improvement in energy confinement over the L-mode scaling law due to the H-mode. Consequently, an H-mode factor of 1 means no H-mode at all. Typical values achieved experimentally are about 2 to 3. We see that an H-mode factor of about 2.5 is necessary to obtain breakeven in this device. Further increases in the H-mode factor do not lead to significant increses in Q because of the saturation effect of the ohmic confinement term in Eq. (3.2-17). The required injection power at an H-mode factor of 2.5 is about 130 MW; this is a rather large amount of power in comparison with the 50 MW planned for NET and would require 100-200 million dollars in heating equipment.

3.3.3 Increased Magnetic Field Variations of NET-EP (Regime C)

A second option for improving the performance of NET-EP with D-^{3}He is to increase the magnetic field strength without changing the plasma dimensions. This regime does not benefit from the reduced aspect ratio obtained with the reduction of major plasma radius, but it has a lesser impact on the poloidal field magnet system since the plasma position is not changed. Shown in Fig. 3.3-10 is the Q-value and the plasma current versus maximum magnetic field strength at the TF magnet. This figure uses ASDEX H-mode scaling with the mean ion temperature held at 50 keV. As expected, we see that increases in the magnetic field strength also increase Q and the current. Comparing Figs. 3.3-6 and 3.3-10, we see that increasing B_c gives more increase in Q for the same increase in plasma current than reducing the plasma radius. Consequently, if the increased plasma current is a major concern, it may be better to get to high Q by increasing B_c at constant R, rather than reducing R at constant B_c. Of course, raising B_c does increase costs and we have not considered the exact amount within the context of this study. However, it appears that it should be less than 10% of the total cost of NET.

3.3.4 Ignition in NET with D-^{3}He (Regime D)

Finally, we consider the possibility of achieving ignition in a D-^{3}He plasma. To achieve ignition with ASDEX H-mode scaling, it appears necessary to both reduce the major radius and aspect ratio, and to increase the magnetic field at the TF coil. In addition, one can consider raising the plasma elongation; this affects both the beta and the confinement since it raises the plasma current. Shown in Fig. 3.3-11 is the elongation required for ignition versus magnetic field strength at the TF magnet. The major

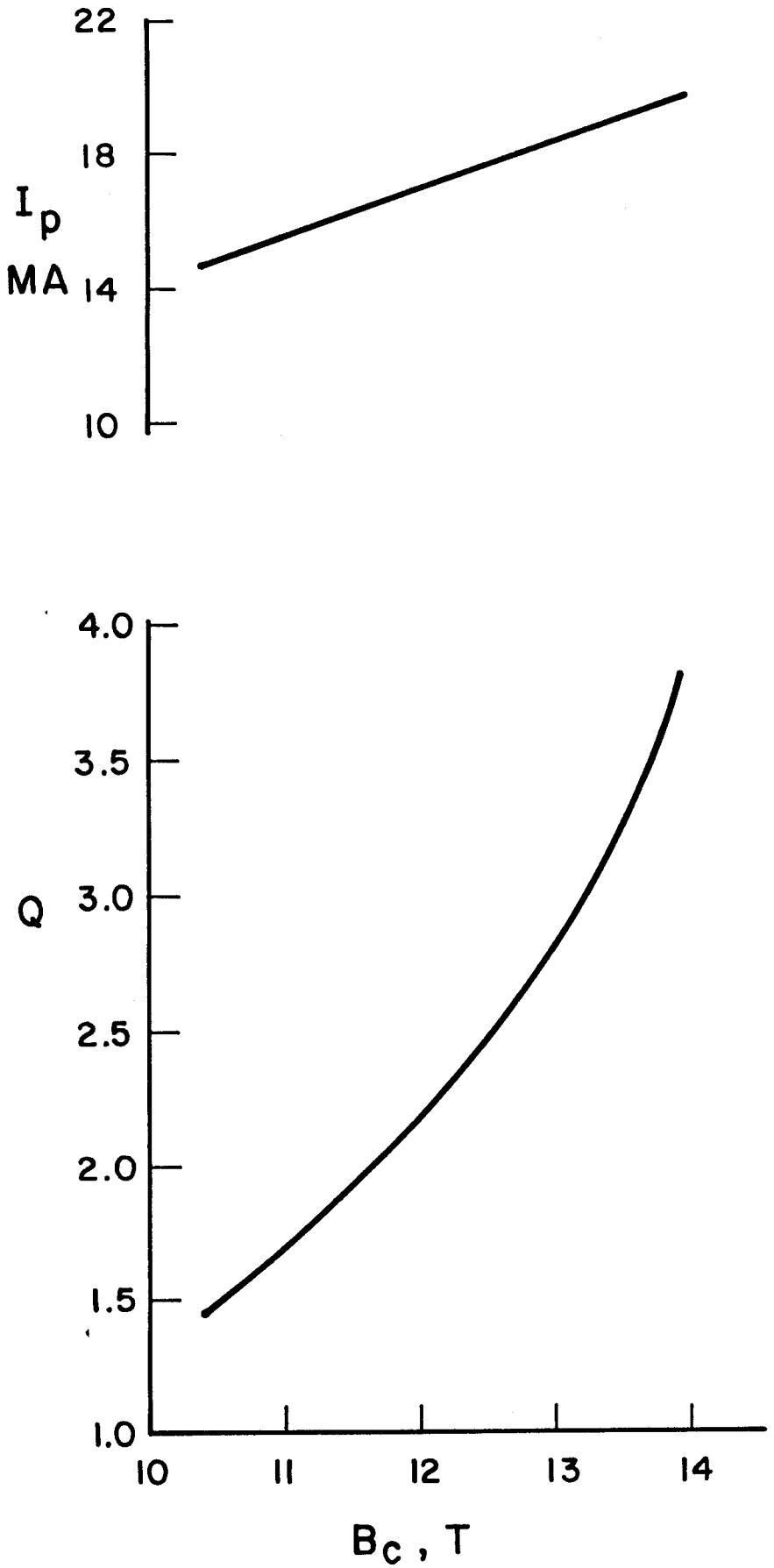

Fig. 3.3-10. The effect of raising the toroidal field at the magnet on the energy multiplication, Q, and the plasma current, I_p. R = 5.41 m, f_d = .65, $\langle T_i \rangle$ = 50 keV.

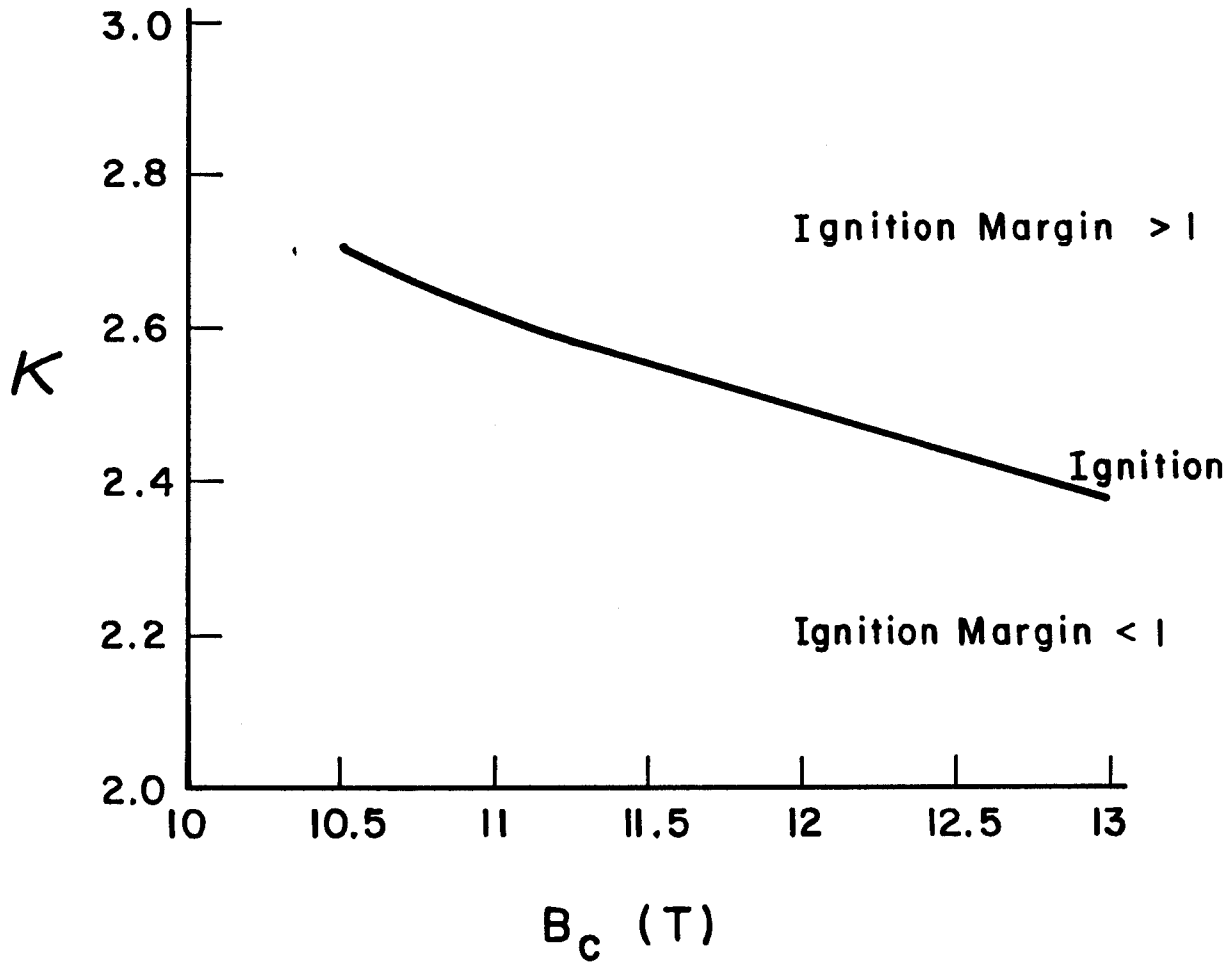

Fig. 3.3-11. The elongation required to achieve ignition versus toroidal magnetic field at the magnet. Points above the curve have ignition margin above 1; points below are sub-ignited. R = 4.61m, a = 1.69 m, $\langle T_i \rangle$ = 37 keV, ASDEX H-mode scaling.

plasma radius is held constant at 4.61 m and the plasma half-width is 1.69 m. We see that one can trade elongation for magnetic field and still achieve ignition. It is somewhat surprising that the plasma current is essentially constant at about 29 MA along the curve in Fig. 3.3-11. This is probably due to strong coupling between plasma current, energy confinement, and beta. The range of plasma elongations shown in Fig. 3.3-11 are higher than the value used in the NET design (2.17) but are comparable to that used in the TIBER study (2.4) at the higher magnetic field strength. Such values (2.4) can be accommodated within the present NET divertor design.

References for Section 3.3

1. H.M. Hofmann and D. Fick, "Fusion of Polarized Deuterons," Phys. Rev. Letters 52, 2038 (1984).

2. J.S. Zhang, K.F. Liu and G.W. Shuy, "Fusion Reactions of Polarized Deuterons," Phys. Rev. Letters 57, 1410 (1986).

3. W. Herringa, "Polarization of Solid Deuterium-Tritium Fuel for Nuclear Fusion," KfK 4168 (1986).

3.4 Summary

We have developed a physics model which allows one to calculate the plasma performance for given dimensions, fuel composition, magnetic field, etc. The model is zero-dimensional, but uses specified profiles for the electron and ion temperatures and densities. The beta is assumed to be limited by the Troyon formula. The energy confinement is assumed to be given by an empirical scaling law; we have focussed on the ASDEX H-mode and Kaye-Goldston scaling laws in this report. With this model one can calculate the ignition margin and energy multiplication, injection power, and plasma parameters for specified plasma dimensions, toroidal magnetic field, and MHD safety factor.

This plasma model has been used in a parametric survey of D-^{3}He operation in NET, and variations of it. From this parametric survey, the following general conclusions may be drawn.

Breakeven (Q = 1) may be obtained in the present NET-DT design if ASDEX H-mode scaling is applicable. In addition, the required injection power is less than that planned for startup in NET-DT. If Kaye-Goldston scaling continues to plague tokamaks,

then the Q-values obtained are much lower (Q = .4) and the injection power is much higher (P_{inj} = 120 MW). The enhanced plasma size NET case (NET-EP) can achieve a Q-value of about 1.4 using ASDEX H-mode scaling with no changes in the machine parameters except for the fuel and the operating temperature.

The Q-value can be increased in many ways in NET because of the low neutron production with D-^{3}He fuel. Reduction of the major plasma radius to 4.61 m increases the Q-value to about 3. This improvement in Q is due to the increase in magnetic field at the plasma and to the reduced aspect ratio which leads to higher plasma current, energy confinement times, and beta. The reduction in major radius can be achieved by removing the inboard blanket designed for DT operation and using much thinner shield designed for the low DD and DT neutron exposure.

An alternative approach is to increase the magnetic field at the toroidal field magnets without changing the plasma dimensions from the NET-EP case. Q values of about 2.5 - 3 can be obtained by a 20% increase in the magnetic field strength at the TF coil.

Ignition with D-^{3}He in NET is feasible if the plasma major radius is reduced in conjunction with an increase in the toroidal field and in the plasma elongation. The required elongation for ignition is about 2.4 at B_c = 13 T and 2.7 at B_c = 10.5 T. (B_c is the toroidal field at the TF magnet.)

The major parameters for possible operating points in these variation regimes are given in Table 3.4-1. Case A-1 is the reference NET-DT design and case A-2 is NET-EP. Cases B-1 and B-2 are reduced major radius cases with different fuel composition. Case C-1 is the same size as A-2, but with increased toroidal field. Cases D-1 and D-2 represent possible ignition cases.

The above predictions are obtained using the ASDEX H-mode scaling law. Break-even in NET is possible with the Kaye-Goldston scaling law for an H-mode factor of about 2.5, but the required injection power is about 120 MW. This assumes the major radius of the plasma has been reduced to 4.61 m and the toroidal field at the magnet remains at the NET value of 10.4 T.

From these results we see that significant energy multiplication in a mildly revised form of NET can be obtained if nature is not too perverse. Significant energy multiplication means that the fusion reactions are as important as the external heating power in determining the power balance of the plasma. Consequently, important questions regarding burn physics and the effects of a significant number of fast fusion produced ions in

Table 3.4-1. Summary of D-^{3}He NET Optimum Operating Parameters for Regimes A-D Using ASDEX H-Mode Scaling

	Case						
	A-1	A-2	B-1	B-2	C-1	D-1	D-2
Major Plasma Radius, m	5.18	5.41	4.61	4.61	5.41	4.61	4.61
B at magnet, T	10.4	10.4	10.4	10.4	13	10.5	13
B at plasma, T	4.96	4.75	5.57	5.57	5.93	5.63	6.97
Q	.96	1.4	3.06	.95	2.8	∞	∞
P_{inj}, MW	35	37	32	84	38	0	0
Plasma Current, MA	10.8	14.8	20.2	20.2	18.3	29.6	29.5
Elongation	2.17	2.17	2.17	2.17	2.17	2.7	2.38
Deuterium Fraction	.65	.65	.65	.34	.65	.65	.65
$\langle n \rangle$, 10^{13} cm^{-3}	3.6	3.5	4.7	6.0	4.6	8.8	10.7
$\langle T_i \rangle$, keV	45	45	51	37	51	37	37
$\langle T_e \rangle$, keV	28	31	37	30	37	34	34
$\langle \beta \rangle$	.056	.064	.075	.075	.064	.11	.088
Energy Confinement Time, sec	5.6	7.9	9.3	9.3	9.9	13.6	13.6
Inboard Shield, cm	116	100	29	29	100	29	29
<Neutron Wall Load>, MW/m^2	.004	.006	.016	.002	.016	.055	.08
Photon Heat Flux to Wall, W/cm^2	4.5	5.9	14.5	20.9	15	31	50
Fusion Power, MW	34	53	98	79	108	240	286
Neutron Power, MW	0.9	1.9	4.9	0.67	5.7	21.9	28.6
Power to Divertor, MW	53	62	71	79	76	94	103

the plasma can be studied with such a machine. In addition, the much reduced neutron production makes the environment more hospitable to performing physics experiments on burning plasmas than is the case with DT fuel.

4. NEUTRONICS

The goal of the neutronics analysis is to estimate the thickness of the thinnest possible inboard (i/b) shield that protects the inner legs of the TF coils and satisfies the limits and constraints for the NET-D^{3}He reactor. This work is applicable to regimes B and D of the parametric studies in Chapter 3. The primary shield design requirement is to limit the TF coil nuclear heating to that allowed by the NET coil designers, presently estimated to be 20 kW. The engineering constraints are that the geometry of the TF coils and the dimensions of specific regions (such as the cryostat, gaps, and scrape-off) remain the same as that of the NET-DT design. Additional requirements include physics items such as the desirability of a high D:^{3}He ratio and small Δ (inboard distance between plasma edge and winding pack) in order to achieve the highest Q value possible.

The relation between Q, Δ, and f_D (deuterium fraction in the D-^{3}He mixture) is illustrated in Fig. 4-1. This figure uses the parameters of case B-1 except that f_D is changing. As f_D increases, the required shield thickness to protect the magnet increases since more neutrons are produced in the plasma. Note that high f_D could be used when $Q \gg 1$. For the same f_D, designing an efficient i/b shield will reduce the Δ and thus increase the Q. Furthermore, for the same Δ, the efficient shield will help the Q by allowing for the use of higher f_D value.

The NET-D^{3}He is a low fluence machine. It is expected to be designed for 1000 shots with a shot duration of 200 seconds. A machine lifetime of 2×10^5 s is anticipated and that is equivalent to 2.32 full power days (FPD).

Figures 4-2a and 4-2b shows cross sections through the upper halves of the NET-DT and NET-D^{3}He reactors. In the NET-D^{3}He design, the breeding blanket was removed, the outboard (o/b) permanent shield was left in place, and the i/b shield was thinned to accommodate the larger plasma size. In Section 4.1, the poloidal variation of the neutron wall loading for both NET-DT and NET-D^{3}He designs is presented. The radiation limits for the TF coils are covered in Section 4.2. An optimized shield design for the i/b region is described in Section 4.3. Section 4.4 presents the magnet radiation effects for different f_D values and shows the sensitivity of the results to the scrape-off zone thickness.

4.1 Neutron Wall Loading Distribution

In tokamak reactors, the neutron wall loading (r_n) exhibits a poloidal variation that can deviate considerably from the average value of the neutron wall loading, defined as

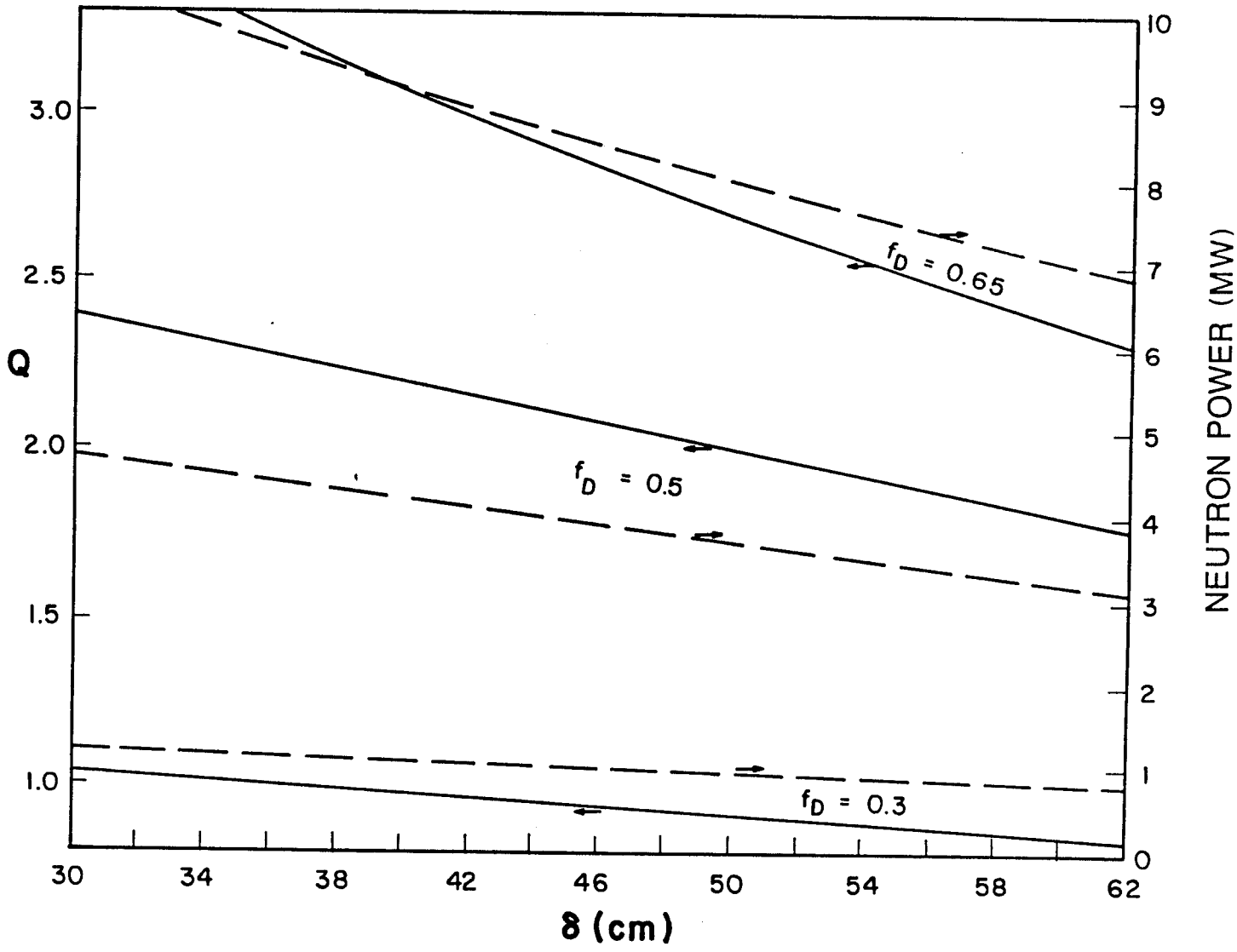

Fig. 4-1. Q and P_n vs. Δ in NET-D^{3}He reactor.

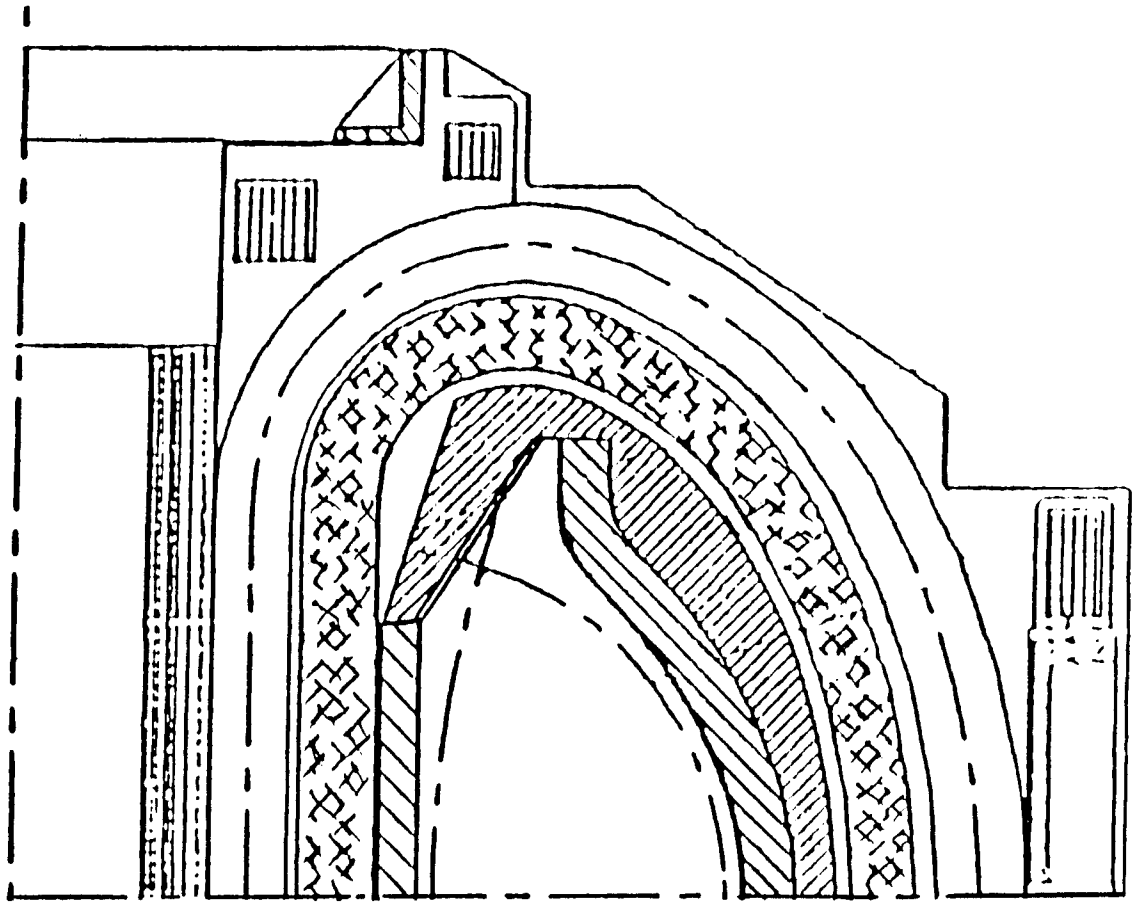

Fig. 4-2a. Cross section through the TF coil of NET-DT reactor.

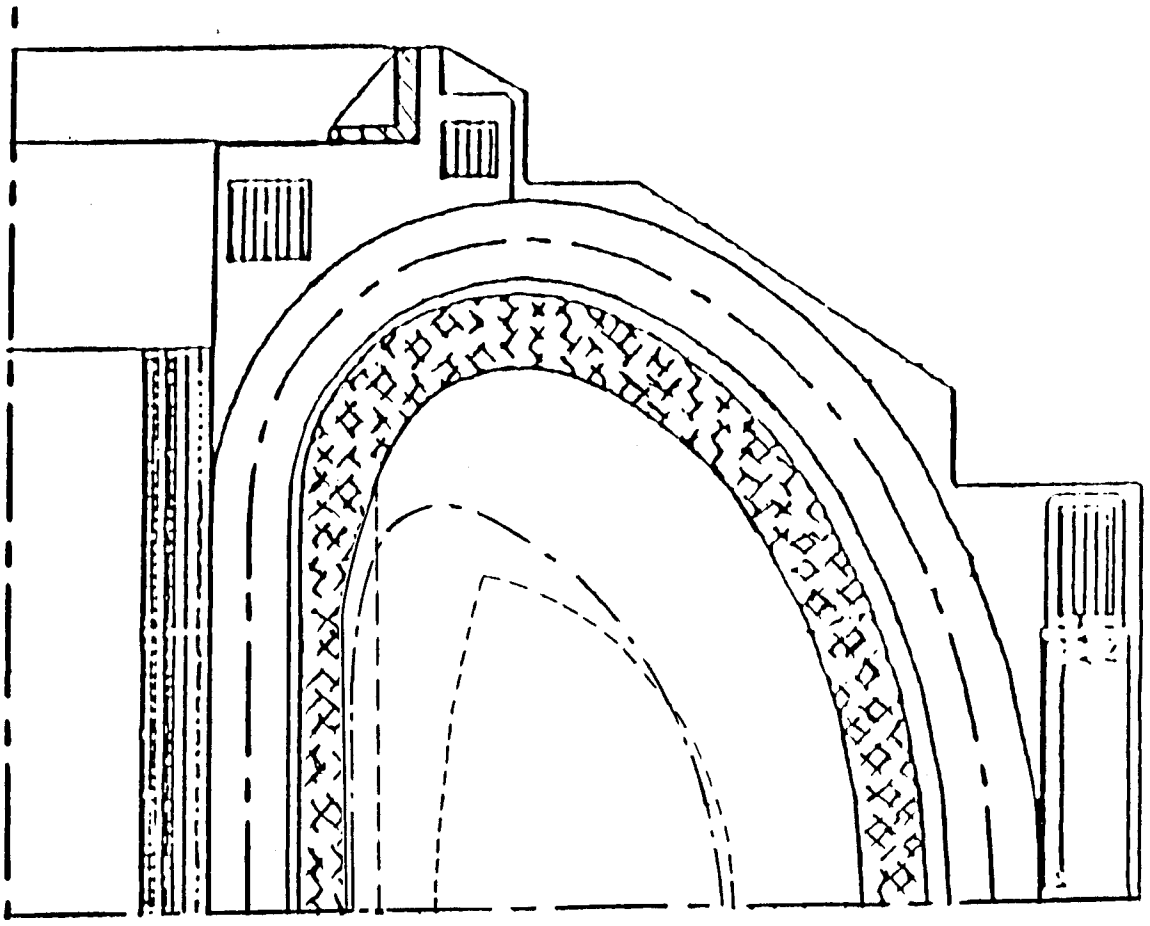

Fig. 4-2b. Cross section through the TF coil of NET-D^{3}He reactor (dashed lines indicate the NET-DT permanent shield and plasma boundaries).

the neutron power divided by the first wall area. The poloidal distribution of Γ_n is important in identifying the locations of the peaks so that enough shield is placed therein to protect the magnets and avoid hot spots. The distribution depends on the plasma shape, the neutron source distribution in the plasma, and the first wall shape. The NEWLIT code[1] was used to determine the poloidal variation of the neutron wall loading for both the NET-DT and NET-D^{3}He designs. The source distribution within the plasma is taken into account by properly representing the different magnetic flux surfaces. The D-shaped plasma outer boundary was represented by the parametric equations

$$r_p = R_p + a_p \cos (t + C_p \sin t) , \qquad (4.1\text{-}1)$$

and

$$z_p = \kappa_p a_p \sin t , \qquad (4.1\text{-}2)$$

with the NET plasma parameters listed in Table 4.1-1. The parameter t varies from 0 to π. The neutron source profile within the plasma was considered to vary from the magnetic axis to the outer boundary as $\{1 - (a/a_p)^2\}^4$, where a is the minor radius of any magnetic flux surface in the plasma. The results were normalized to the neutron power given in Table 4.1-1.

The results of the calculations are given in Figs. 4.1-1 and 4.1-2 for NET-DT and NET-D^{3}He (case B-1), respectively. The first wall and plasma shapes are shown, as are the magnetic flux surfaces. The wall loading distribution in each segment is indicated and the dashed line represents the average neutron wall loading. Figure 4.1-2 is generated for an i/b scrape-off thickness of 6 cm and a deuterium fraction of 0.65. A comparison between the wall loading values for the different cases is given in Table 4.1-2. As noticed, 2-3 orders of magnitude reduction in the wall loading is achieved by using the D-^{3}He as a fuel. This translates into a reduction of several tens of centimeters in the thickness of the i/b shield, as will be shown later. Other advantages related to the low neutron production of the D-^{3}He fuel are the low activation level, afterheat, and radioactive waste rating of the shield.

4.2 Radiation Limits

The thickness, composition, and geometric configuration of the shield strongly depend on the allowable radiation limits for the TF magnets. The magnet components

Table 4.1-1. Major NET Parameters Needed for the NEWLIT Code

	NET-DT	NET-D^3He
Plasma Major Radius (R_p)	5.18 m	4.61 m
Plasma Minor Radius (a_p)	1.35 m	1.69 m
Elogation (κ_p)	2.18	2.17
Triangularity (C_p)	0.65	(0.65)
Magnetic Shift	16.2 cm	(16.2) cm
Neutron Power (P_n)	480 MW	8.5 MW
Fusion Power (P_F)	600 MW	97 MW
Deuterium Fraction (f_D)	--	0.65

Items in ( ) are assumed to be same as in NET-DT.

Table 4.1-2. Comparison of Key Neutronic Parameters for Various NET Designs

	NET-DT	NET-D^{3}He		
f_D	---	0.65	0.5	0.3
Neutron Power (MW)	480	8.53	3.96	1.0
r_n (MW/m^2):				
Average	1.0	0.0114	0.0053	0.0013
i/b peak	1.13	0.0193	0.00896	0.0023
o/b peak	1.5	0.0144	0.0067	0.0017

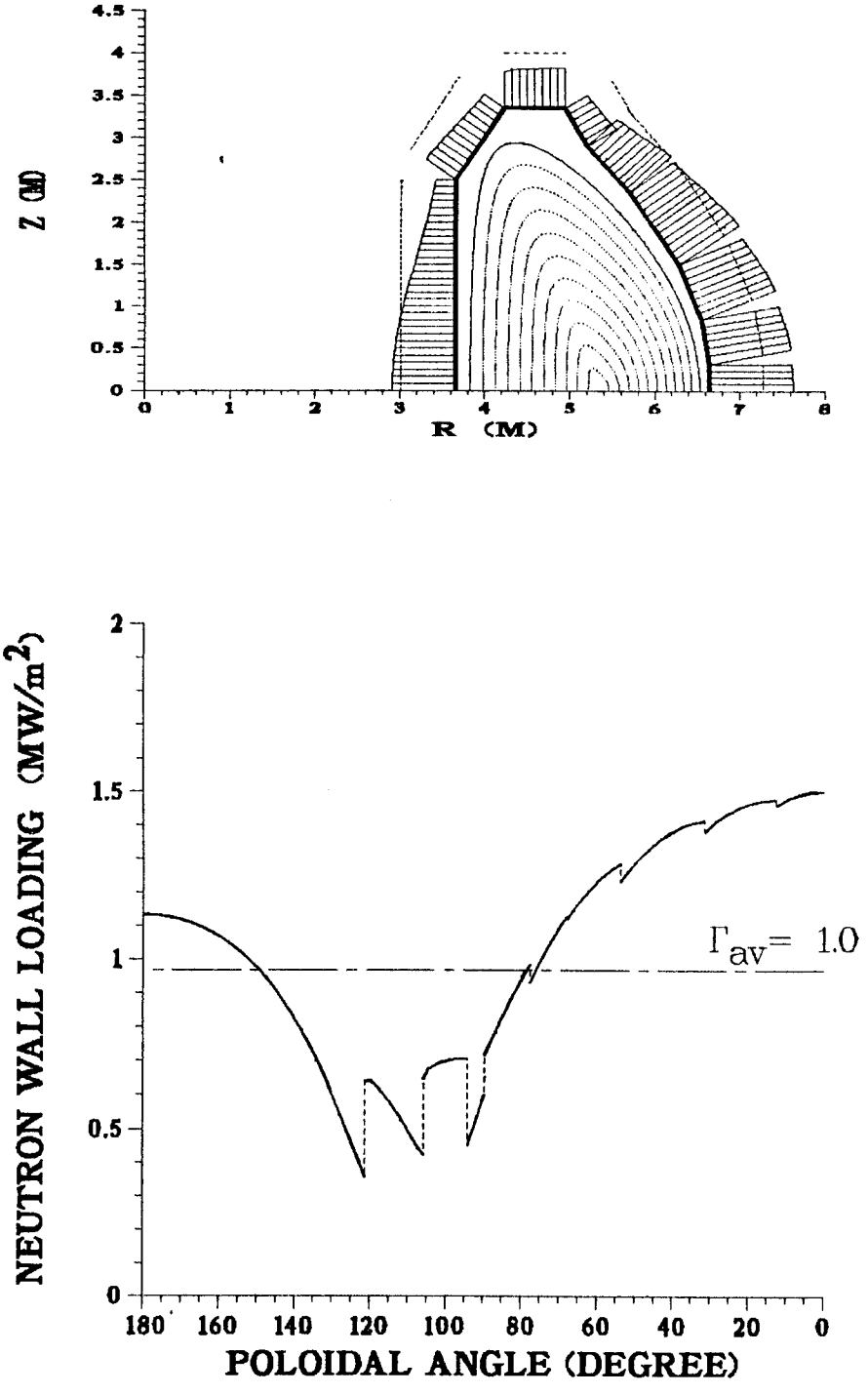

Fig. 4.1-1. Poloidal variation of the neutron wall loading in NET-DT reactor.

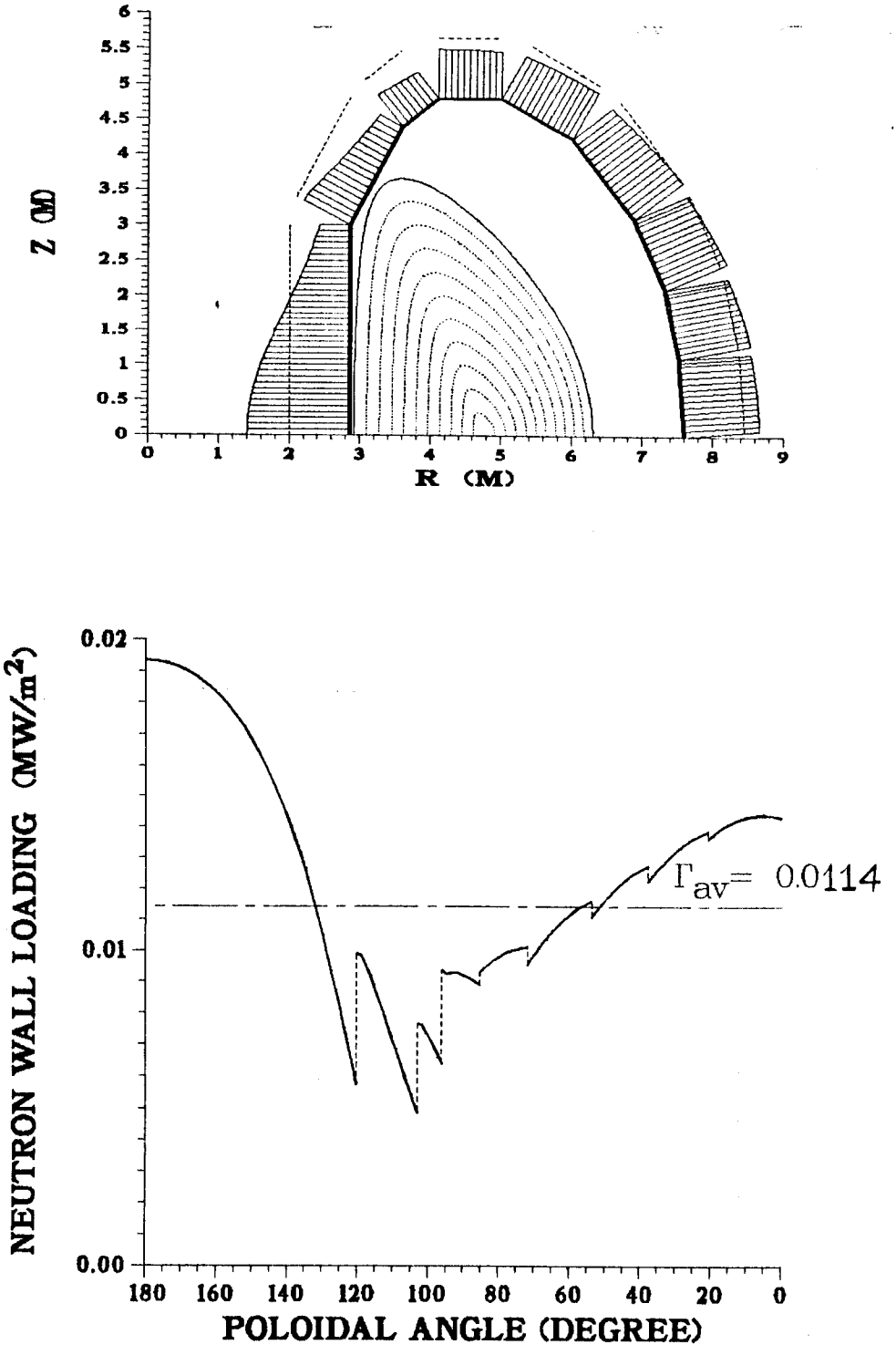

Fig. 4.1-2. Poloidal variation of the neutron wall loading in NET-D^{3}He reactor.

most sensitive to radiation damage are the electrical insulator (GFF epoxy), Cu stabilizer, Nb_3Sn superconductor filaments, and thermal insulator (mylar). The nuclear heating in the magnet affects the winding pack temperature and the economic performance of the reactor through the refrigeration cost.

The total nuclear heating in the 16 TF coils is currently limited to 20 kW. This heating can be accomodated by the He refrigeration plant without much impact on the refrigeration cost.[2] The limits on the dose to the GFF epoxy and fast neutron fluence (E_n > 0.1 MeV) were set by the NET team[3] to be 5 x 10^8 rads and 5 x 10^{17} n/cm^2, respectively.

4.3 Shield Composition

The highest damage in the inner legs of the TF coils occurs at the midplane of the reactor where the neutron wall loading has its peak value. A schematic of the i/b shield and the inner leg of the TF magnet at the midplane of the reactor is shown in Fig. 4.3-1 for Δ = 45 cm. The 3 cm thick coil case is cooled with 5 v/o liquid nitrogen and the winding pack composition is taken as 34.5 v/o 304 SS, 33.4 v/o Cu, 3 v/o Ni, 6.6 v/o Nb_3Sn, 11.7 w/o GFF epoxy, and 10.8 v/o liquid helium. The details of the 5.5 cm thick cryostat are shown in the figure and there is a 1.5 cm gap between the cryostat and the back of the shield. If we leave 2 cm for the first wall graphite tiles, then the space available for the shield (Δ_s) is 29 cm thick. The scrape-off thickness (S) is considered to be 6 cm and the effect of having thicker scrape-off is discussed in the next section.

An optimization study was performed to determine the optimum shield composition that minimizes the nuclear heating in the magnets. Tungsten alloy is used as the main i/b shielding material to provide adequate protection for the inner leg of the magnet. The coolant is borated water (5 g boric acid/100 cm^3 of H_2O) and the structure is PCA. Two additional shielding materials were considered as a backup to the W-shield. These are B_4C (at 90% density factor and 90% ^{10}B in B) and Pb. The o/b shield was taken as 90 w/o PCA and 10 v/o coolant. The problem was modeled as an infinite toroidal cylinder and the calculations are performed using the one-dimensional code ONEDANT[4] with the MATXS5 data library based on ENDF/B-V in 30 neutron and 12 gamma groups, and the P_3-S_8 approximation.

The shield consists of alternate layers with a thick W-shield followed by a B_4C-shield and, then, a Pb-shield. In all layers, we considered 10 v/o structure and 5 v/o

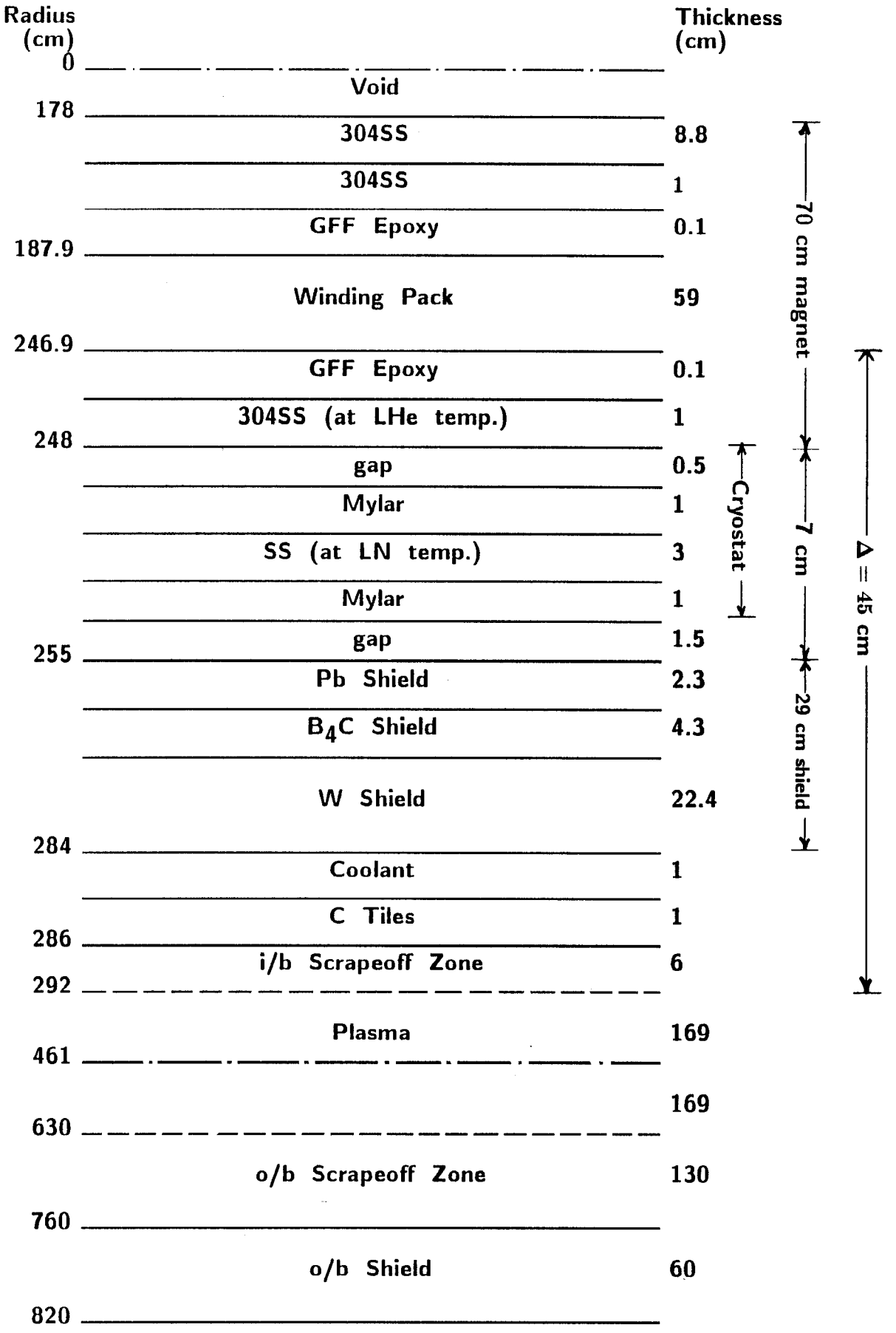

Fig. 4.3-1. Schematic of the i/b shield and inner leg of the TF coil.

coolant. In the optimization study, the three layers were varied in thickness to reduce the nuclear heating in the magnets. The optimum shield was found to consist of 77.3% W-shield, 14.7% B_4C-shield, and 8% Pb-shield by thickness.

4.4 Magnet Heating and Damage

The radiation effects at the TF coil are given in Table 4.4-1 for the three f_D values. The same Δ of 45 cm, Δ_s of 29 cm, and S of 6 cm were considered for the sake of comparison. As anticipated, the lower the f_D, the lower the radiation effects at the magnet are. The dose to the GFF epoxy and the fast neutron fluence are much below the design limits. In addition, the end-of-life radiation-induced resistivity[5] in the stabilizer is less than ~ 1% of the unirradiated stabilizer resistivity at the operating field. In all cases, the nuclear heating in the TF coils is less than the 20 kW limit. This suggests that the shield can be made thinner in order to meet the heating limit.

A set of curves was generated to illustrate the variation of the heating in the magnets as a function of the shield thickness. Figure 4.4-1 shows this variation for the different f_D values. It should be mentioned that the drop in the neutron power, and thus the neutron wall loading, as Δ increases (see Fig. 4-1) was taken into account. In the calculations, the inner scrape-off thickness was varied (by moving the plasma out) to determine the sensitivity of the total nuclear heating in the magnets. The scrape-off thickness was increased to 10 cm and the NET-DT reference value of 15 cm. The figure indicates that the heating drops as the scrape-off thickness increases. This is due to the lower neutron wall loading as a result of the farther plasma location and the less neutron power (see Fig. 4-1). The variation also shows that the total heating increases by a factor of 2 for each ~ 4 cm decrease in the shield thickness. Therefore, to meet the heating limit, the i/b shield can be as thin as 27, 23, and 16 cm for f_D of 0.65, 0.5, and 0.3, respectively.

As mentioned earlier, one of the reasons for designing a thin i/b shield is to achieve a high plasma Q value. The items which have significant impact on the Q value are the i/b scrape-off, deuterium fraction, and the allowable heating limit of the magnet. Some questions, thus, arise as to how the Q, S, f_D, and magnet heating are related and what values are preferable to achieve a Q of at least 1. To answer these questions, Fig. 4.4-2 was generated to give the relation between the Q and the heating by combining Figs. 4-1 and 4.4-1 and parametrizing S and f_D. The figure reveals that the Q increases as the

Table 4.4-1. Comparison Between the Radiation Effects at the TF Coils for Three Different Values of f_D

f_D	0.65	0.5	0.3
Q	2.87	2.1	0.95
$r_{i/b}$ (MW/m^2)	0.0193	0.00896	0.0023
Total Nuclear Heating in 16 TF Coils (kW)	13.3	6.2	1.65
Dose in GFF epoxy (rad @ 2.32 FPD)	0.1×10^8	0.05×10^8	0.013×10^8
Peak Nuclear Heating in Winding Pack (mW/cm^3)	1.2	0.57	0.15
Peak dpa in Cu Stabilizer (dpa @ 2.32 FPD)	1.1×10^{-5}	5×10^{-6}	1.3×10^{-6}
End-of-Life Radiation Induced Resistivity (nΩm)	7.9×10^{-3}	3.6×10^{-3}	9.4×10^{-4}
Peak Fast Neutron Fluence (n/cm^2 @ 2.32 FPD)	1.7×10^{16}	7.8×10^{15}	2.1×10^{15}

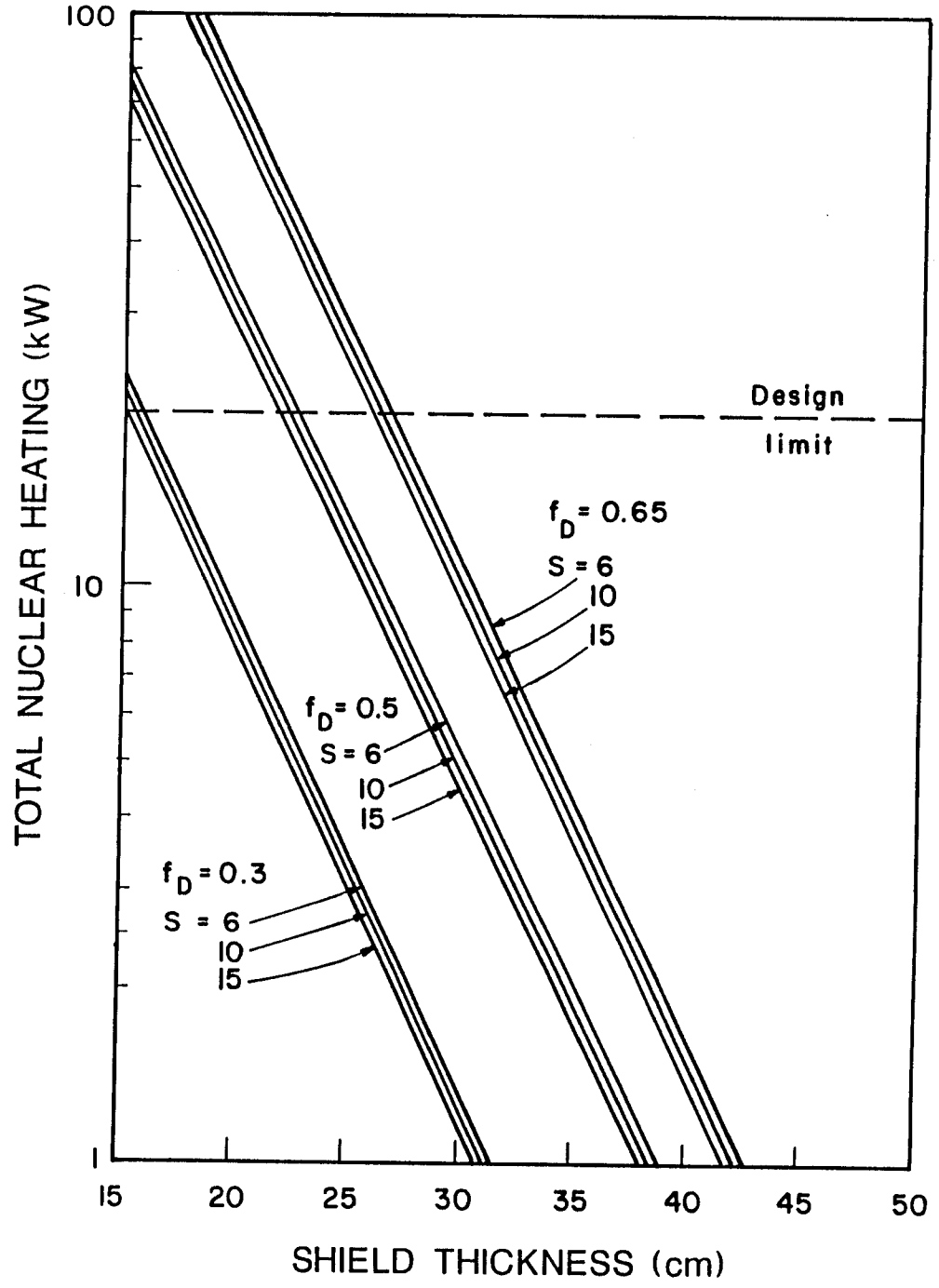

Fig. 4.4-1. Variation of the total nuclear heating in the 16 TF coils with the i/b shield thickness.

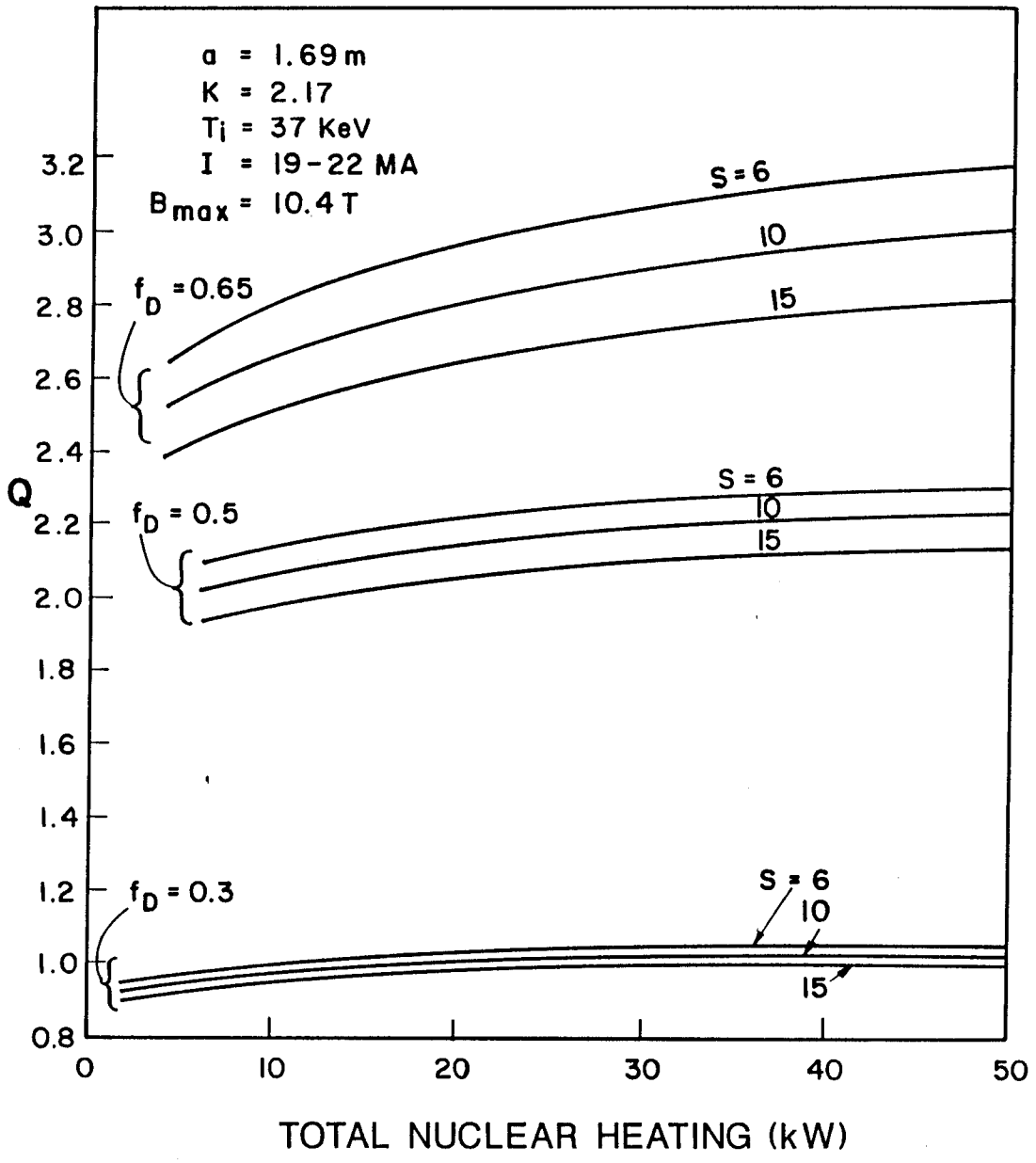

Fig. 4.4-2. Q vs. total nuclear heating in the 16 TF coil.

i/b scrape-off decreases and/or more heating is allowed in the magnet. Also, the minimum f_D and maximum S values to achieve Q of 1 are 0.3 and 10 cm, respectively, for a nuclear heating of 20 kW. Thicker scrape-off layers, e.g. 10 or 15 cm, can be obtained without a serious less of Q.

References for Chapter 4

1. H. Attaya and M. Sawan, "NEWLIT - A General Code for Neutron Wall Loading Distribution in Toroidal Reactors," Fusion Technology 8/1, 608, (1985).

2. E. Salpietro, KfK, Germany, Private Communication, June 1987.

3. The NET Team, "NEXT European Torus-Status Report #51," Max-Plank-Institut fur Plasmaphysik, Garching, West Germany (December 1985).

4. R.D. O'Dell et al., "User's Manual for ONEDANT: A Code Package for One-Dimensional, Diffusion-Accelerated, Neutral Particle Transport," LA-9184-M, Los Alamos National Laboratory (February 1982).

5. M. Sawan,"Charts for Specifying Limits on Copper Stabilizer Damage Rate," J. Nucl. Mat. 122&123, 1376 (1984).

5. FAST ION EFFECTS

This section will address the status of alpha particle loss modelling for D-T tokamaks and the extrapolation to alpha particles and protons in a D-^{3}He tokamak. Two factors make D-^{3}He fusion reactors more susceptible to fusion-product losses than D-T reactors:

- Five times as much energy is produced in charged particles, and
- The gyroradius of the 14.7 MeV proton, which carries 80% of the fusion energy, is twice that of the 3.67 MeV alpha particle.

The alpha-particle part of the problem should be essentially the same for both D-^{3}He and D-T tokamaks, with appropriate modifications for plasma operating parameters. The larger total energy and gyroradius of the proton, however, will lead to larger prompt losses and, possibly, larger losses as the protons thermalize. Section 5.1 will give an overview of alpha particle loss modelling in D-T tokamaks. Prompt loss of fusion products for D-^{3}He operation of NET will be treated in Section 5.2, and ripple-loss will be examined in Section 5.3. Finally, Section 5.4 will provide a summary, conclusions, and suggestions for further research.

5.1 Status of Alpha Particle Loss Modeling in D-T Tokamaks

There are five main fast-particle loss mechanisms in a tokamak (Goldston and Towner 1981):

- Prompt loss, due to banana orbits intersecting the chamber walls;
- Direct ripple loss due to the birth of fast ions in the ripple loss cone;
- Collisional ripple diffusion, whereby collisions with fuel ions cause fast ions to become ripple-trapped;
- Collisionless ripple diffusion, in which finite orbit effects lead to ripple-trapping; and
- Banana-drift diffusion, where ripple modifies the banana orbits and causes a net radial drift.

Only the first of these, for which a method based on constants of the motion applies (Rome and Peng 1979, Rome et al. 1981, Hively et al. 1981), can be said to have a well-established theory. This is, perhaps, not surprising, because even the correctness

of Maxwellian-plasma tokamak transport theory (Hinton and Hazeltine 1976) remains unverified, with discrepancies from experiment of over a factor of ten for electrons and of about a factor of three for ions. The present explanation of these discrepancies is that microscopic fluctuations lead to this anomalous transport, although there is considerable controversy about the detailed mechanisms (Ross et al. 1987). This situation results primarily from the difficulty of analyzing plasmas in the complicated magnetic field geometry of the tokamak.

Fortunately, the fusion-product problem simplifies in some respects. In particular, collisional effects are much less dominant, because the fusion products lose most of their energy to electrons before they begin to scatter significantly off of ions--at which time their radial random walk due to pitch-angle scattering begins. This is especially true for the 14.7 MeV D-^{3}He protons, which lose over 95% of their energy before pitch-angle scattering begins to compete with electron drag. Thus, the problem becomes one of orbit following. For 3-D, rippled tokamaks, either numerical codes must be used or simplifications must be invoked. At present, unfortunately, two of the main computer codes used for modelling fusion product loss in rippled tokamaks (Tani et al. 1983, Hively 1984) differ in their predictions by a large amount (Hively 1987a) and there are supporting analyses on both sides of the question (Zajtsev et al. 1986, Hitchon and Hastie 1983). Another computer code, recently written by Bittoni and Haegi (1987) has not yet been benchmarked against these codes. All of these are large codes which consume considerable computer resources for each run. We have been closely monitoring the work on resolving this question, and had a two-day working meeting with Drs. Hively and Tani on August 18-19, 1987. Substantial effort appears to remain before these codes can be used with complete confidence (Hively 1987b, Tani 1987).

Although detailed orbit-following for D-^{3}He fusion products is not feasible at present, some of the more important effects lend themselves to analytic analysis. Prompt loss may be accurately assessed, because an elegant theory exists for axisymmetric tokamaks (Rome and Peng 1979) and ripple will only slightly modify the first-orbit loss of fusion products. Collisionless ripple-loss may be estimated by the analytic map of Goldston et al. (1981) or the two-step mapping formalism of White et al. (1982), which has been verified approximately by Hitchon and Hastie (1983). Although most of the fusion-product loss effort has concentrated on prompt loss and ripple loss, there are other effects which may be important but which are more difficult to treat theoretically. For example, the magnetic field seen by the fusion products due to their finite gyroradii

varies by about 4%, as opposed to the 2% due to toroidal ripple, while the relativistic mass correction for a 14.7 MeV proton is about 1%. These effects will be neglected for the present analysis.

5.2 Prompt Loss of Fast Ions

Prompt loss is defined here as loss of fusion products because their orbits intersect the first wall, limiter, or divertor within a few bounce times of their birth. Part of the ripple-induced loss is prompt in this sense, but it will be called ripple loss in this paper. The theory of Rome and Peng (1979) for prompt loss in an axisymmetric tokamak applies reasonably well to rippled tokamaks, because ripple will only slightly perturb most prompt-loss orbits. Hively and Miley (1977) used a different formalism, and they appear to be the only reference also treating the D-^{3}He protons. The Rome and Peng theory allows treatment of non-circular, high-beta tokamaks ($\beta \leq 10\%$), although up/down symmetry and a monotonic poloidal flux function are assumed. This theory is based on the constants of the motion v, $\zeta_m \equiv \frac{v_\parallel}{v}\Big|_{\Psi_m}$ and Ψ_m where v is the total velocity, $v_\parallel$ is the velocity parallel to the plasma current, and $\Psi_m \equiv -RA_\phi$ is the maximum poloidal flux function along the ion's orbit (occurring in the equatorial plane due to the assumption that Ψ is monotonic). It is, however, necessary to modify the Rome and Peng formalism in order to estimate the first wall surface heat load instead of only the total particle and power loss. In place of the variable ζ_m (which they call ζ), the variable $\zeta \equiv v_\parallel/v$ defined locally will be used here. This allows the orbit equation to be cast in terms of the physical position of the wall and the local, fusion-product source term.

The analysis begins with the conservation of energy, the conservation of magnetic moment $\mu = v_\perp^2/2B$, and the conservation of toroidal canonical angular momentum

$$p_\phi = \gamma m R v_\parallel \frac{B_\phi}{B} - ze\Psi \tag{5-1}$$

where R is the major radius, z is the ion's charge, m is the ion's mass, $\gamma = 1/(1-v^2/c^2)^{1/2}$ and c is the speed of light. From here on, relativistic effects will be assumed to be sufficiently small so that $\gamma = 1$. Using the conservation of μ,

$$\zeta_w = \pm \left[1 - (1-\zeta^2)\frac{B_w}{B}\right]^{1/2} \tag{5-2}$$

where the subscript w indicates the point along an ion's orbit at which it hits the first wall. Evaluating Eq. (5-1) at the first wall and at a point along the orbit, and using Eq. (5-2) gives the general orbit equation

$$\frac{B_w}{B} = \frac{-(1-\zeta^2) + \{(1+\zeta^2)^2 + 4[\zeta + \frac{\omega_{ci}}{R_o B_o v}(\Psi_w - \Psi)^2\}^{1/2}}{2[\zeta + \frac{\omega_{ci}}{R_o B_o v}(\psi_w - \psi)]^2} \qquad (5\text{-}3)$$

where $RB_\phi = R_o B_o$ has been assumed. Note that Eq. (5-3) differs from the Rome and Peng formulation in that ζ, not ζ_w is used. The importance of this equation is that it is still very general, and the values for B(R,z) and Ψ(R,z) for a high-beta, non-circular equilibrium can be extracted from a sophisticated computer code and used to calculate whether a fusion product born at (R,z) with v and ζ will hit the first wall (at Ψ_w and B_w). At this point, in general, numerical methods will be needed to insert the NET equilibrium values for B, Ψ, j, n, and T into these formulas and to calculate the first wall surface heat load.

To estimate fusion-product production, the plasma density n and ion temperature T_i profiles assumed for the power balance studies can be used. These are

$$n(r) = n_o[1 - (\frac{r}{a})^2] \qquad (5\text{-}4)$$

and

$$T_i(r) = T_{io}[1 - (\frac{r}{a})^2]^{3/2} \qquad (5\text{-}5)$$

where the subscript "o" indicates an on-axis value and a is the plasma minor radius. With the assumption that the plasma density and temperature are constant on a flux surface, the local fusion-product production density, $S_{fus}(R,z)$, is equal to

$$S_{fus}(R,z) = n_D(R,z)\, n_{He}(R,z) \langle\sigma v\rangle_{DHe} \qquad (5\text{-}6)$$

where $n_D(R,z)$ is the deuterium density, $n_{He}(R,z)$ is the ^{3}He density, and $\langle\sigma v\rangle_{DHe}$ is the D-^{3}He fusion reaction rate. Simplifying the flux surfaces to concentric circles, the magnetic field and q(r) profile can be modelled by

$$\vec{B}_\theta(r) = \frac{r}{R}\frac{B_\phi}{q(r)}\hat{\theta} \tag{5-7}$$

and

$$q(r) = 1 + \frac{r^2}{a^2}(q_a - 1) \ . \tag{5-8}$$

This lead to

$$\Psi(r) = \frac{a^2 B_o}{(q_a-1) + \frac{a^2}{R_o^2}}\left\{\ln\left(\frac{R_o}{R_o + r}\right) + \frac{1}{2}\ln\left[1 + (q_a-1)\frac{r^2}{a^2}\right]\right.$$
$$\left. + \frac{a}{R_o(q_a-1)^{1/2}}\arctan\left[(q_a-1)^{1/2}\frac{r}{a}\right]\right\} \tag{5-9}$$

for $r \le a$. Also, $\Psi_w \equiv \Psi(r_{wall})$ is

$$\Psi_w = \Psi(a) + \frac{a^2 B_o}{q_a(1 + \frac{a}{R_o})}\ln\left(\frac{r}{a}\right) \ . \tag{5-10}$$

The orbit equation, Eq. (5-3) can now be used to calculate where a particle born at (B,Ψ) with velocity v and pitch angle ζ will hit the first wall, if at all. The simplest means of numerically solving the problem is to use a Monte Carlo method to generate source particles and to count the resulting impacts on regions of the first wall. This technique will work both for the simple model given here and for more realistic equilibria.

5.3 Ripple Loss of Fast Ions

Although substantial discrepancies remain between the results from the large computer codes used to address the rippled tokamak particle loss problem (Hively 1987b, Tani 1987), a large fraction of the ion loss occurs during the first few hundred ion orbits as shown in Figures 5-1a (Tani et al. 1983) and 5-1b (Hively 1984). Since the mechanism for this loss depends only very weakly on collisions (Goldston and Towner 1981), some analytical progress can be made.

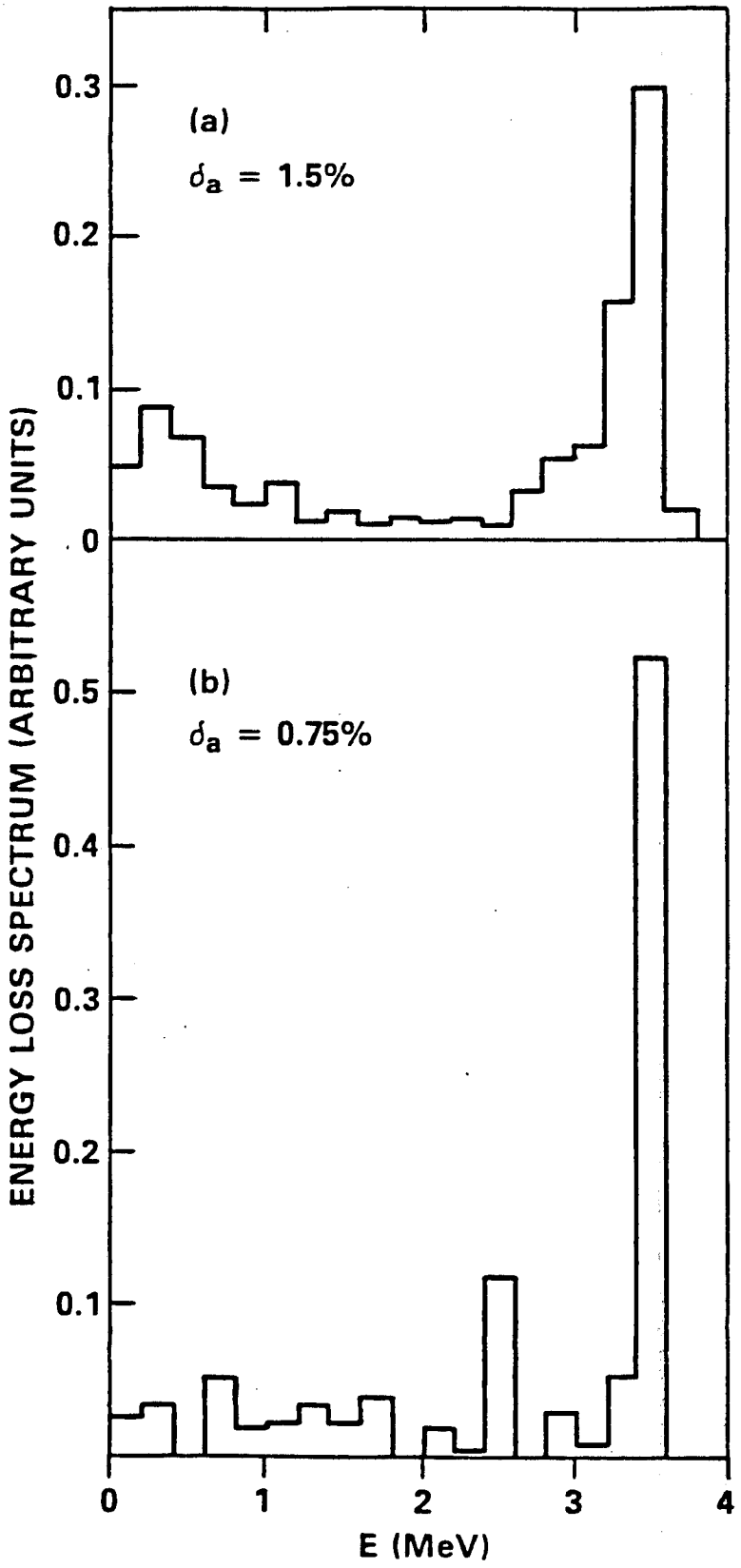

Fig. 5-1. Energy loss spectrum for alpha particles in a D-T tokamak from a) Tani et al. (1983) and b) Hively (1984).

The chief mechanism causing fast ion loss seems to be ripple-induced stochasticity of banana orbits due to radial drift at the turning points. Using an analytic mapping, Goldston et al. (1981) found a limit on the ripple at the banana-orbit turning point of

$$\delta \lesssim \left[\left(\frac{\pi N q}{\varepsilon}\right)^{3/2} \rho \frac{dq}{dr}\right]^{-1} \tag{5-10}$$

where δ is the local ripple, N is the number of magnetic field coils, q is the safety factor, $\varepsilon \equiv r/R$, and ρ is the gyroradius in the toroidal field. This limit applies to particles with large banana orbits, that is

$$\rho_p \gtrsim \frac{r}{\pi^{3/2}\, \varepsilon^{1/2}\, (Nq)^{1/2}} \tag{5-11}$$

where ρ_p is the gyroradius in the poloidal field. Almost all banana-orbit fusion products in both the D-T and D-^{3}He cases will satisfy Eq. (5-11). These formulas impose a constraint on the ripple magnitude at $\theta \simeq \pi/2$ on the order of 0.3% for INTOR alpha particles. The more sophisticated two-step mapping of White et al. (1982) and the guiding-center, orbit-following code of Hitchon and Hastie (1983) lead to somewhat more pessimistic values. However, as shown in Figure 5-2, taken from Hitchon and Hastie (1983), the analytic criterion of Goldston et al. (1981) is fairly good at the low ripple values under consideration here. The analyses indicate that stochastic ripple diffusion of alpha particles will occur only at the outer edge of the INTOR plasma for a δ_0 (peak to average) of 1.2%, which is also the NET-DN ripple value. Since the allowed ripple in Eq. (5-10) is directly proportional to ρ^{-1}, the criterion for avoiding stochastic ripple diffusion of D-^{3}He protons will be approximately twice as stringent as that for INTOR alpha particles. A preliminary plot of the ripple in NET is shown in Figure 5-3 (Bittoni and Haegi 1987). This plot indicates that the present NET design will be operating very close to the proton stochastic ripple diffusion limit of 0.15% at $\theta \simeq \pi/2$, and a more sophisticated analysis will be required. Because the banana orbits extend a considerable distance in the toroidal direction, most of the energy from this loss channel should end up on the divertor plates rather than on the first wall. Nevertheless, since the fraction of trapped fusion products for NET will be approximately 62%, only a small portion of them may be allowed to be lost due to ripple.

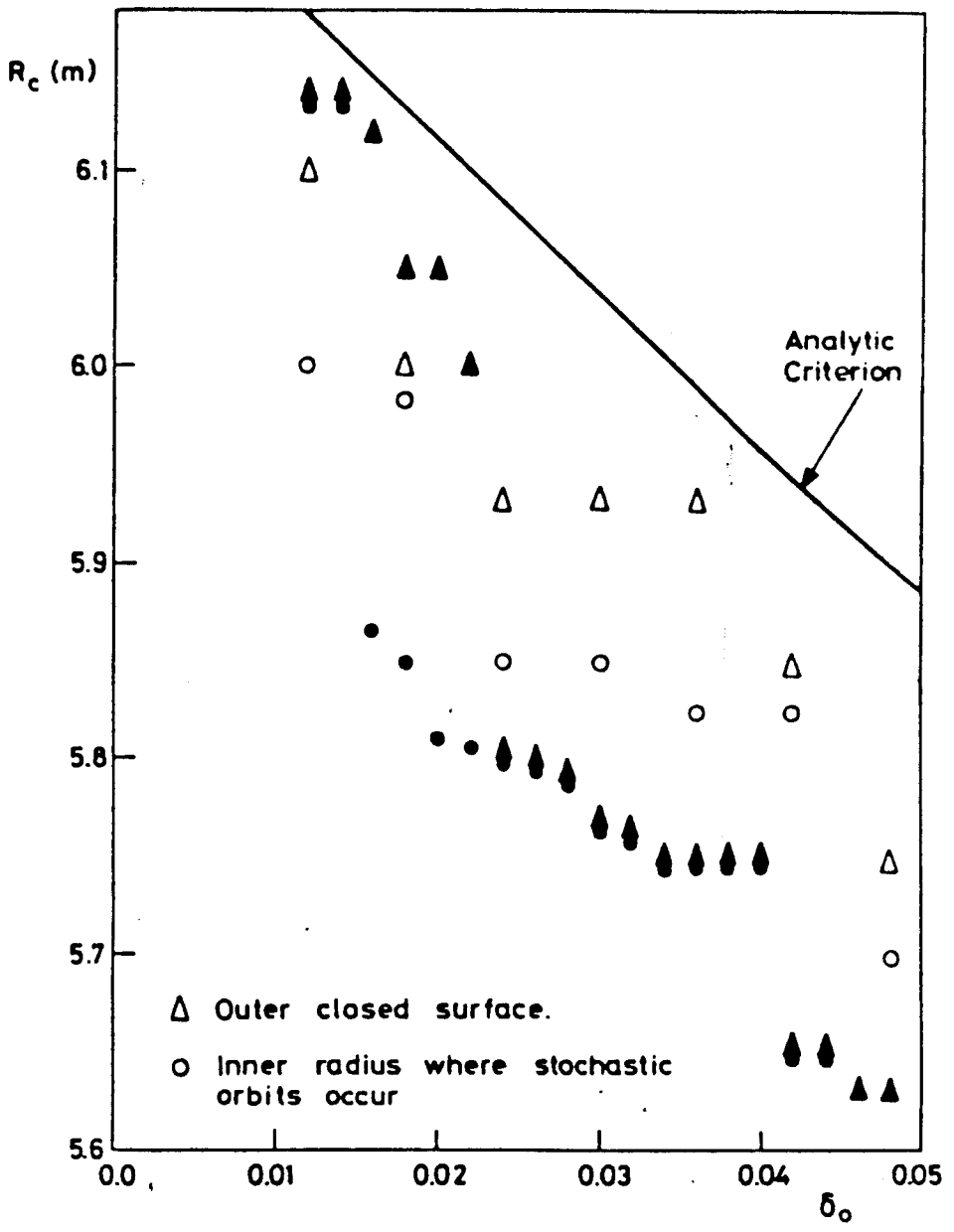

Fig. 5-2. Radius of onset of stochasticity versus ripple amplitude δ_o. Solid symbols refer to the analysis of White et al. (1982), hollow symbols to Hitchon and Hastig (1983), and the solid line to Goldston et al. (1981). The figure is from Hitchon and Hastig (1983).

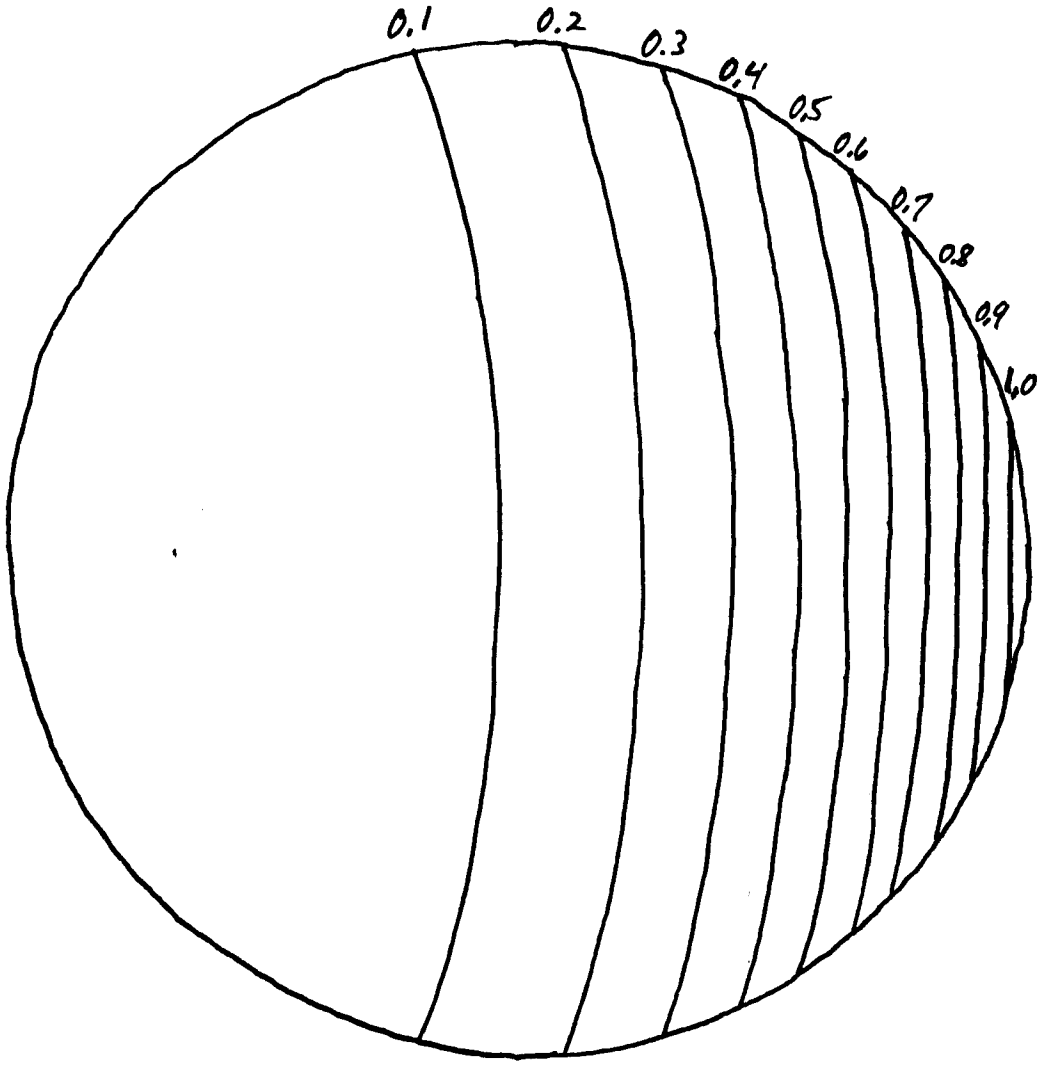

Fig. 5-3. Ripple controus in NET from Bittoni and Haegi (1987).

A mechanism which may lead to a localized surface heat load is fast ion loss due to the birth of fusion products in the ripple-trapped region. These ions quickly drift out of the device vertically along the ripple well. The direct ripple-loss region is proportional to $(2\delta)^{1/2} \simeq 0.15$ and this energy will be localized near the ripple minimum. The distribution of surface heat will depend on the detailed toroidal variation of the ripple, and will be weighted along the poloidal direction of the wall by the angle of the wall and by the fusion source term as given in Eq. (5-6). This loss region in velocity space is small compared to the prompt (first-orbit) loss discussed in Section 5-2, as shown in Figure 5-4 (Tani et al. 1983), but may lead to localization of the surface heat at different areas of the first wall.

5.4 Summary

The loss of fast fusion produced ions due to magnetic ripple has been considered in comparison to the corresponding loss in a D-T plasma. Unfortunately, there is major disagreement in the field concerning ripple losses in D-T plasmas; this makes it impossible to provide with reasonable certainty any estimates of the ripple loss in a D-^{3}He plasma. Clearly, further work in this area is required, but this is beyond the scope of the present study.

References for Chapter 5

Z. Bittoni and M. Haegi (1987) "Alpha Loss Calculation (NET)," Workshop on Alpha Particle Effects in ETR, June 15, U.S. Department of Energy Headquarters, Germantown, MD.

R.J. Goldston, R.B. White, and A.H. Boozer (1981) "Confinement of High-Energy Trapped Particles in Tokamaks," Phys. Rev. Lett. 47, 647.

R.J. Goldston and H.H. Towner (1981) "Effects of Toroidal Field Ripple on Suprathermal Ions in Tokamak Plasmas," J. of Plasma Phys. 26, 283.

F.L. Hinton and R.D. Hazeltine (1976) "Theory of Plasma Transport in Toroidal Confinement Systems," Rev. Mod. Phys. 48, 239.

W.N.G. Hitchon and R.J. Hastie (1983) "The Confinement of Alpha Particles in a Slightly Asymmetric Tokamak Reactor," Nucl. Fusion 23, 533.

L.M. Hively and G.H. Miley (1980) "Prompt and Non-Prompt contributions to Fusion Product Bombardment of a Tokamak First Wall," Nucl. Fusion 20, 969.

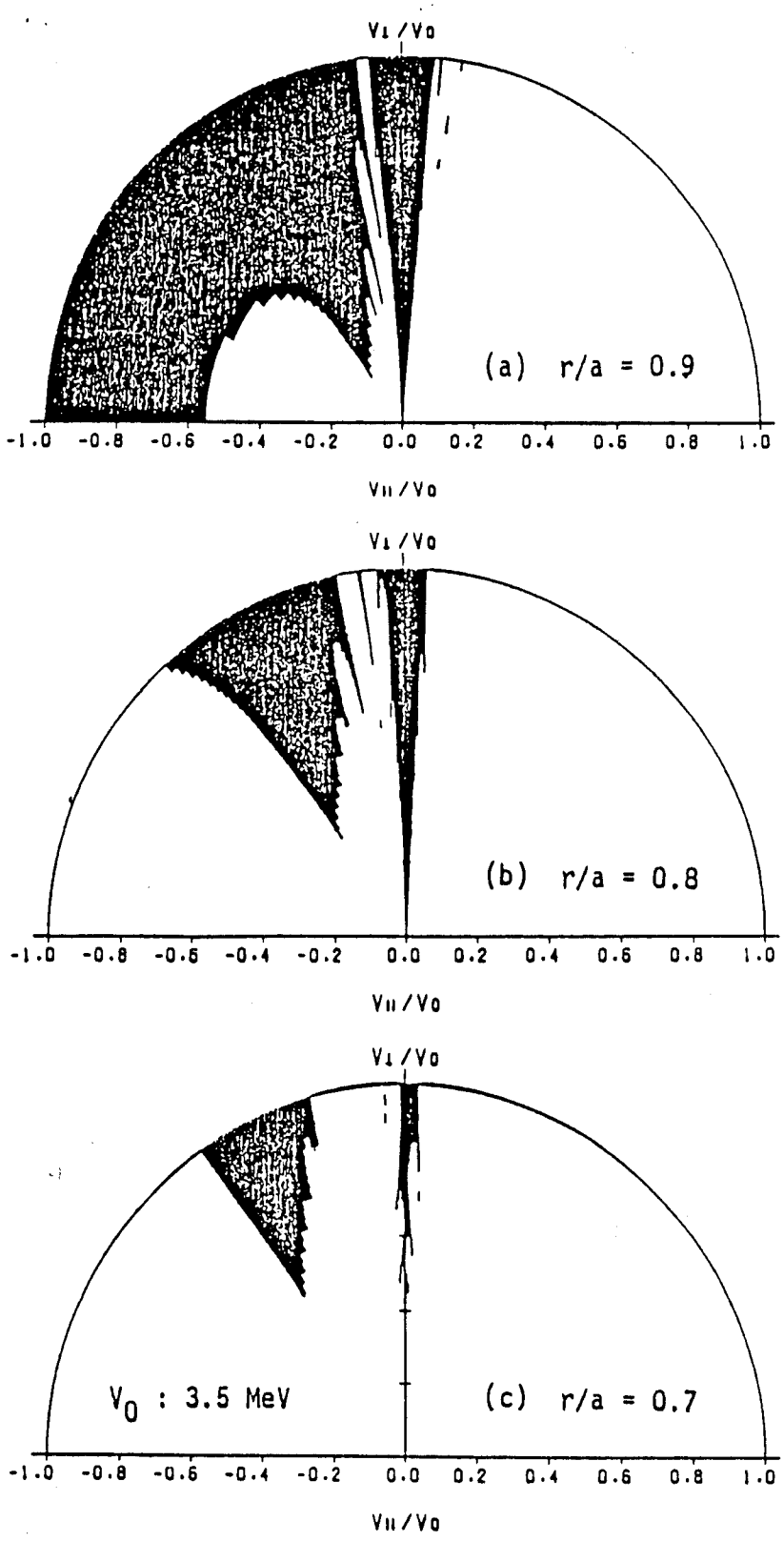

Fig. 5-4. Prompt (first-orbit) loss and ripple loss regions for INTOR with δ_0 = 0.75% from Tani et al. (1983).

L.M. Hively, G.H. Miley, and J.A. Rome (1981) "Fast-Ion Thermalization in Non-Circular tokamaks with Large-Banana-Width Effects," Nucl. Fusion \21\, 1431.

M. Hively (1984) "TF-Ripple Losses from a Non-Circular Tokamak," Nucl. Fusion 24, 779.

M. Hively (1987a) "Problems in Modeling TF Ripple Loss of Fast Alphas from a Tokamak Reactor, "Workshop on Alpha Particle Effects in ETR, June 15, U.S. Department of Energy Headquarters, Germantown, MD.

L.M. Hively (1987b) Private communication.

James A. Rome and Y-K.M. Peng (1979) "The Topology of Tokamak Orbits," Nucl. Fusion 19, 1193.

James A. Rome, J.F. Lyon, and R.H. Fowler (1981) "Using a Constants-of-Motion Space to Clarify Measurements Involving Energetic Ion Orbits in Tokamaks," Oak Ridge National Laboratory Report ORNL/TM-7913.

Tani, T. Takizuka, M. Azumi, and H. Kishimoto (1983) "Ripple Loss of Suprathermal Alpha Particles During Slowing-Down in a Tokamak Reactor," Nucl. Fusion 23, 657.

K. Tani (1987) Private communication.

R.B. White, A.H. Boozer, R. Goldston, R. Hay, J. Albert, and C.F.F. Karney, (1982) "Confinement in Toroidal Systems with Partially Destroyed Magnetic Surfaces," 9th IAEA, Baltimore, Vol III, IAEA-CN-41/T-3.

F.S. Zajtsev, A.P. Smirnov, and P.N. Yushmanov (1986) "Integral Stochastic Alpha Particle Losses in a Tokamak Reactor," Nucl. Fusion 26, 1311.

6. OTHER RELATED ISSUES

6.1 MHD Equilibrium Studies

The increased plasma size and total current required for D-^{3}He operation raise questions about increased volt-second requirements and changes in poloidal coil currents. To at least partly answer these questions, a series of MHD equilibrium calculations was performed. Since it was not feasible within the scope of the present study to duplicate the complicated PF coil optimization study described in Section II. 3.3 of the 1985 NET Report, or the complicated time-dependence of the currents during startup (e.g. Fig. III. 4-12 of the 1985 NET report), simplified configurations based on the coil locations and dimensions of Fig. III. 4-1 (NET-DN) of the 1985 report were used. In the calculations, the central cell solenoid elements P1D and P1C (using the notation and sign conventions of Fig. III. 4-2) were given negative currents; the element P1B was given a positive current (i.e. the same direction as the plasma). The calculations were done using the MHD equilibrium code NEQ0259 by Dennis Strickler of the Oak Ridge National Laboratory Fusion Energy Design Center. A flux surface map for the 20 MA plasma current reference D-^{3}He case is shown in Fig. 6.1-1. The average plasma beta for this case is 6.1%, compared to a Troyon limit of 6.4%.

As can be seen from Table 6.1-1, although the plasma current has increased from 14.8 MA for the NET DN enhanced physics case to 20 MA for the present study, the flux swing required to establish the plasma current has not increased proportionately, because the plasma inductance is smaller. The required volt-seconds are only slightly greater than the enhanced physics case and should be achievable with the present design.

In Table 6.1-2, poloidal field coil currents used in the present MHD calculations are given along with end-of-burn values from Fig. III. 4-12. It should be noted that the magnitudes of the currents in the various coils vary considerably with time and in some cases attain values larger than those given in Table 6.1-2. The PF coil currents required to maintain plasma equilibrium are within the range of values shown in Fig. III. 4-12, with the exception of coil P4, which has almost twice the current. With the winding pack envelope of Fig. III. 4-1, the required current density is 3500 A/cm^2 and the peak field 7.2 T. These values should be achievable with existing NbTi superconducting magnet technology. Another important difference is the reversed current in coil P1C; the magnitude, however, is within the value shown in Fig. III. 4-12 for earlier times in the burn. One can conclude tentatively, then, that the existing PF coil system should be able

Table 6.1-1. Plasma Parameters

	NET-EP	Present Study
Major Radius, m	5.41	4.64
Minor Radius, m	1.68	1.67 m
Elongation	2.17	2.0
Triangularity	0.61	0.42
Magnetic Field at Plasma Center, T	4.8	5.8
Plasma Current, MA	14.8	20
Beta (average), %	6.4	6.1
Plasma Self-Inductance, H	11.3×10^{-6}	8.6×10^{-6}
Plasma Magnetic Flux, wb	168	172
q at Plasma Edge	2.2	2.2

Table 6.1-2. PF Coil Currents

Coil	NET DN	Present Study
P1A	0	0.
P1B	+ 12 MA	+ 13.6 MA
P1C	+ 2 MA	-13.6 MA
P1D	-22 MA	-23 MA
P2	+ 5 MA	+ 3.6 MA
P3	0 MA	+3.8 MA
P4	-5 MA	-11.1 MA

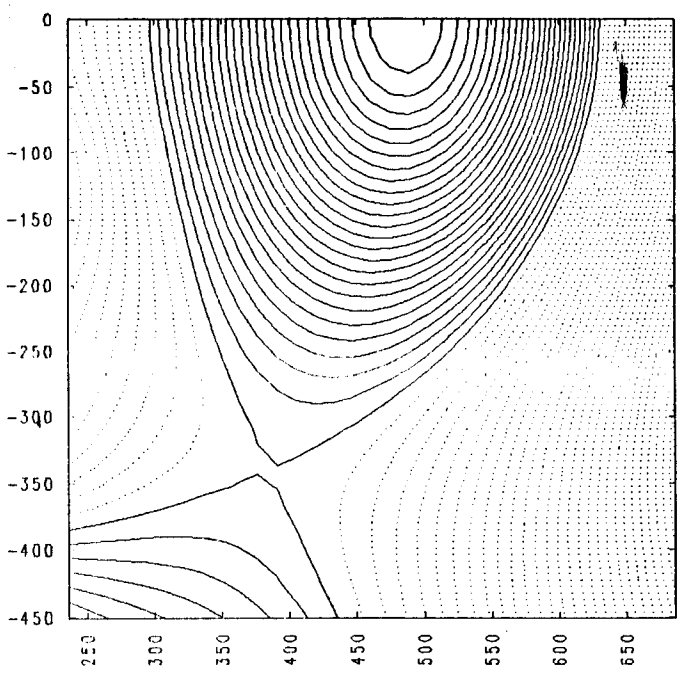

Fig. 6.1-1 Magnetic flux surfaces for the 20 MA case.

the different magnetic loads, especially the overturning moments on the TF coils. Final answers to the above questions will require a complete startup and burn analysis and a new stress analysis of the intercoil support structure.

6.2 Fuelling

6.2.1 Introduction

The fuelling of a large, high temperature plasma, such as proposed for NET, represents a formidable task, as summarized by Lengyel.[1] This task is difficult because the plasma temperature in NET fuelled with DT is much higher than in any existing plasma experiment in which pellet fuelling has been attempted. Also, no experience is available on actual DT fuelling in which the effect of the energetic α-particles has been observed. Operational models have been developed to simulate the mechanisms involved in plasma fuelling but these models have not been tested at high plasma temperatures or in the presence of fusion reaction products. Consequently, suggesting a fuelling scheme for a D/^{3}He plasma is difficult at this time because the plasma temperature in this case will be ~ 3 times higher than for a D/T device and the reaction products will include not only a 3.5 MeV α-particle but also a 15 MeV proton.

The experimental techniques presently demonstrated for plasma fuelling are gas puffing and pellet injection using frozen particles of H_2 or D_2. For larger, high temperature plasmas visualized for power reactor stations, it has been suggested that advanced fuelling techniques may need to be developed, such as plasma guns[2] or accelerated plasmas from compact toroids.[3] In the meantime, several plasma experiments have demonstrated that pellet injection is a viable fuelling technique and superior to gas puffing because it delivers fuel into the center of the plasma much faster than the time required for a gaseous fuel to diffuse into the plasma. Such fuelling results in increased density limits and energy confinement in the plasma. Multiple fuel injections into TFTR[4] have demonstrated ($n\tau$) values of 1.4×10^{20} m^{-3} at central electron temperatures of 1.4 keV. Because of this success with pellet fuelling, the concept of D/^{3}He fuel pellets is considered in this study for fuelling the early experiments in NET. We also include some remarks on plasma injection.

6.2.2 Fabrication of D/^{3}He Fuel Pellets

The fabrication of a fuel pellet containing ^{3}He is extremely difficult because the critical temperature (3.2 K) is the lowest of any substance. As the temperature is

decreased further it remains a liquid, requiring a pressure of ~ 3 MPa to cause solidification. Because a fuel pellet could not be delivered into the plasma at such a high pressure, the fuel pellet must contain liquid ^{3}He. An exposed liquid droplet could neither be accelerated nor remain intact during its penetration of the plasma; therefore, the liquid must be encapsulated. Any encapsulating material will contaminate the plasma. We are suggesting, therefore, that the liquid ^{3}He be encased in a thin-walled polymer sphere which is coated with D_2 ice.

The fabrication of the fuel pellet would begin with the production of hollow, thin-walled spheres. The mass-production of high-quality, hollow glass and polymer membrane spheres has been extensively studied for the ICF program[5] and this technology will be utilized for our study. The wall thickness of the spheres will need to be < 2.5 μm in order to minimize the carbon contamination of the plasma. These hollow spheres will be loaded into a pressure vessel at 300 K to which ^{3}He will be added. This gas, which diffuses into the spheres, will be slowly increased in pressure to ~ 45 MPa at which temperature and pressure the gas density will equal the density of ^{3}He liquid at 3 K. The entire pressure vessel containing the spheres and the ^{3}He gas will be cooled to ~ 16 K. During the cooling process the helium permeability of the spherical membrane approaches zero, so that the ^{3}He is trapped in the sphere. At 16 K D_2 gas is mixed with the ^{3}He in the pressure vessel and a coating of D_2 ice is formed on the spheres using fluidized-bed technology. Following the coating process, the entire apparatus is cooled to 3 K and the excess ^{3}He removed from the vessel. The ^{3}He pressure in the spheres is, now, only 0.11 MPa (1 atm) and the strength of the spheres are calculated to retain this pressure.

The spheres must be kept at 3 K and transported to the pneumatic injector device.

6.2.3 Ablation of Fuel Pellet in the Plasma

The models[6] proposed for the ablation of the pellet in the plasma suggest that the pellet is rapidly bombarded by the plasma electrons which heat the surface of the pellet and vaporize fuel material. The fuel molecules released from the surface rapidly accelerate and form a vapor cloud surrounding the pellet. This vapor cloud begins to attenuate incoming electrons, forming a shield. At steady-state the electron energy deposited in the cloud is ~ 10^3 times greater than the energy deposited on the pellet. The ablation of the pellet due to the heating caused by energetic particles in the plasma have been modelled in a similar manner.[7] The results of such calculations indicate that 40 keV

protons, supplied by neutral beam injectors, contribute approximately the same heating energy to the pellet as the electrons when the electron density is high; therefore, the combined effects of electrons and energetic particles have been simply added, in the absence of any experimental verification.

Based upon a simplified relationship by Milora and Foster[6] for electron heating, the velocity of a D-^{3}He pellet required to penetrate the plasma has been calculated for several different input parameters and is given in Table 6.2.-1. For the ignition case, in which the central electron temperature is 60 keV, the velocity required of a pellet to approach the center of the plasma would be too high (> 100 km/s) for any pellet launching system; therefore, this case was set-aside pending further experimental data, and the fuelling required to achieve energy-breakeven (Q = 1) was considered with the results given in Table 6.2.-1. For Case A, with T_e = 30 keV, the velocity is excessively large, 370 km/s. We can introduce, however, the technique of multiple pellet fuelling as demonstrated in TFTR in which the electron temperature decreased significantly for pellet penetration of only 50% of the plasma radius. This technique could be used with D-^{3}He plasma because ICRF heating would keep the central ^{3}He ions hot and their heating of the electrons at the periphery would be low. On the assumption that T_e could be reduced by 75%, Case B, the velocity required is reduced to 36 km/s, which is still excessive. Up to this point, we have considered pellets which contain only 10% of the mass of fuel in the plasma. Now, we consider fuel pellets which contain 40%, Case C, of the ions in the plasma. The density fluctuation associated with this large pellet is a concern, although larger pellets have been injected successfully in some experiments. For Case C, the velocity is reduced to 16 km/s. Finally, we consider pellet penetration to only 30% of the distance into the plasma, Case D. For Case D, the velocity required is only 3.5 km/s which is a reasonable extrapolation from presently available pneumatic pellet accelerators.[8]

The examples given in Table 6.2-1 illustrate some of the choices which may be possible for the design of fuel pellets and the requirements for the design and mode of operation for the pellet accelerators. The conclusion of the brief study is that fabrication of D-^{3}He pellets can be developed and that these pellets could probably be used to fuel plasmas at low Q values. Much more experimental work is needed however regarding the pellet fueling of high temperature plasmas before our conclusions can be evaluated.

Table 6.2-1. Velocity Requirements for Fuel Pellets Injected into the NET Reactor Operating on D-^{3}He Fuel at Low Q Values

Case #	Pellets Injected	T_e (a) keV	f (b)	r/a (c)	Velocity Required km/s
A	single	30	0.1	0.5	370
B	multiple	7.5	0.1	0.5	36
C	multiple	7.5	0.4	0.5	16
D	Multiple	7.5	0.4	0.7	3.5

(a) $n_e = 9 \times 10^{19}$ m^{-3} for all cases

(b) fraction of the total fuel in the plasma continued in one fuel pellet.

(c) r = radius of the plasma at which the pellet disappears
a = distance from the plasma core to the outside edge of the plasma (1.6 m for all cases)

6.2.4 Plasma Injection

An alternative fuelling technique is plasma injection. This has been demonstrated[2] in the Tokapole-II tokamak using plasma from a Marshall gun. The plasma density was approximately doubled during the tokamak discharge by the injection from a single firing of the Marshall gun. The injected plasma penetrated to the center of the discharge. The injection mechanism appears to be polarization of the incident plasma beam and penetration by $\vec{E} \times \vec{B}$ drift until electron flow parallel to the magnetic field causes depolarization.

This fuelling technique appears to be applicable to larger tokamaks and is not dependent on the plasma species. Consequently, it can be used with D-^{3}He plasmas as well as with hydrogen isotopes. Introduction of impurities by the Marshall gun is a concern, but no noticeable increase in the impurity level was observed in the experiment. Electrodeless plasma guns, such as conical theta pinch guns, could be used to minimize contamination with impurities.

It is premature to choose this form of plasma fuelling, although it is an interesting possibility. Experimental tests with larger tokamaks are needed to better establish the scaling of the injection efficiency with size, density, and temperature. Preliminary theoretical modelling indicates the scaling is favorable for its use in larger tokamaks.

References for Section 6.2

1. L.L. Lengyel, "Assessment of Pellet Injection for NET (Summary and Conclusions)," EUR-FU/XII-80/86/53, December 1985.

2. A.W. Leonard, R.N. Dexter and J.C. Sprott, "Trapping of Gun-Injected Plasma by a Tokamak," Phys. Rev. Letters, 57, 333 (1986).

3. L.J. Perkins, S.K. Ho and J.H. Hammer, "Deep Penetration Fueling of Reactor-Grade Plasmas with Accelerated Compact Toroids," UCRL-96894 (Preprint) June 23, 1987.

4. G.L. Schmidt, et al., "Pellet Injection Results During TFTR Ohmic and Neutral Beam Heating Experiments," Paper CN-47/A-III-4, Eleventh Intnl. Conf. on Plasma Phys. Controlled Nucl. Fusion Res., Kyoto, Japan, Nov,. 13-20, 1986.

5. R. Crawley, "A Hollow Droplet Generator for Polymer Shell Production," J. Vac. Sci. Technol., A4, 1138 (1986).

6. S.L. Milora and C.A. Foster, "ORNL Neutral Gas Shielding Model for Pellet-Plasma Interactions," ORNL/TM-5776, May 1977.

7. Y. Nakamura, H. Nishihara and M. Wakatani, "An Analysis of the Ablation Rate for Solid Pellets Injected into Neutral Beam Heated Toroidal Plasmas," Nucl. Fusion, 28, 907, (1986).

8. S.K. Combs, S.L. Milora, C.R. Foust, G.L. Schmidt and T.P. McBride, "Operation of a Repeating Pneumatic Hydrogen Pellet Injector on TFTR," J. Vac. Sci. Technol., A4, 1113 (1986).

6.3 Heat Loads on the First Wall and Divertor

6.3.1 Heat Load on the First Wall

In this section we consider the heat load on the first wall in NET with D-^{3}He operation. The heat load on the first wall is composed primarily of three parts. First, there is the load from synchrotron and bremsstrahlung radiation emitted by the plasma. Next, there will be a neutral particle flux incident on the first wall. Finally, there will be energetic ions striking the wall because of trapping in the magnetic field ripple. The ripple loss is discussed in Chap. 5.

Bremsstrahlung is radiation emitted during Coulomb collisions of the electrons with ions; the photons emitted have a broad energy spectrum extending up to about 2 or 3 times the mean electron energy. For a D-^{3}He plasma the electron temperature is generally about 30 - 60 keV in the center of the discharge, so one can expect the spectrum to extend up to about 200 keV. The photons don't penetrate far into the walls so this appears primarily as a surface heat load. There will be a poloidal variation of the heat load with a profile similar to the poloidal variation of the neutron wall loading (see Chapter 4), since for both forms of radiation, the plasma acts like a volume emitter. Consequently, the ratio of the peak to average bremsstrahlung heat load will be about 2.

Synchrotron radiation is microwave radiation emitted at harmonics of the electron cyclotron frequency. Because of relativistic and doppler broadening and the variation of the magnetic field strength in the plasma, the frequency spectrum becomes smeared out. The poloidal variation is a little harder to deduce since the plasma is optically thick for synchrotron radiation. Consequently, one expects the escaping photons to have come from near the surface of the plasma. Due to the variation of the magnetic field strength, one might expect the radiation to be stronger on the inboard side where B is higher. Since the emission is proportional to $B^{2.5}$, a peak to average ratio of 2 can be expected. The peak surface heat load for both bremsstrahlung and synchrotron radiation will be on the inboard side at the midplane.

For D-^{3}He operation in NET, the average surface heat load due to radiation is not large. For NET-DT and NET-EP the average heat load is about 5 W/cm^2. The Q = 2.5 - 3 cases have an average surface heat load of about 15 w/cm^2, and the ignition cases have an average surface heat load of 30-50 w/cm^2, depending on the plasma elongation.

The neutral particle flux emitted from a D-^{3}He plasma has not been analyzed in detail, but some conclusions based on atomic processes and cross-sections can be made. The charge exchange processes leading to escaping neutral atoms are present in a D-^{3}He plasma, but will be reduced in magnitude in comparison to a D-T plasma since helium does not charge exchange well with hydrogen isotopes. Helium can undergo resonant charge exchange with itself, but the cross-sections are smaller since a two-electron transfer is required to produce a neutral helium atom. It is difficult to be quantitative about the expected power loss due to charge exchange but the problem should be less severe than it is in a D-T plasma. Generally, the overall power loss due to charge exchange is small, but localized peaking near the divertor where the recycling occurs can be a problem as in D-T plasmas.

6.3.2 Heat Load on the Divertor

An upper limit to the heat load to the divertor is the total fusion power plus the injected power minus the power carried to the first wall by synchrotron and bremsstrahlung radiation. For the NET-DT and NET-EP cases with D-^{3}He, this power is about 55-60 MW. For the Q = 2.5 - 3 cases, this power is about 75 MW, and for ignition it is about 95 - 100 MW. This number should be compared to the alpha heating power of 120 MW in NET using D-T. Consequently, one can expect the power to the divertor with D-^{3}He to be less than, or comparable to that with D-T. The NET divertor is designed for 80 MW using the assumption that the remaining 40 MW is radiated from the scrape-off layer plasma and is distributed over a larger area than the target plates. Plasma transport and recycling in the scrape-off layer and divertor has not been analyzed with D-^{3}He operation, but there is no reason to expect that the plasma scrape-off layer will be thinner with D-^{3}He than it is with D-T. Consequently, the power density on the divertor target plates will be similar to, or less than, that already designed for in the D-T version of NET. (Note: values in Table 3.3-2 are maximum heat fluxes to the divertor with no allowances for charge exchange.)

7. Q ENHANCEMENT BY ICRF HEATING

7.1 Introduction

The concept of ICRF enhanced fusion Q = (fusion power out/auxiliary power in) was first examined by Scharer, Jacquinot, Lallia and Sand[1] for a modest ICRF power level near breakeven for D-T operation in JET. It was found that minority deuterium fundamental ion resonance non-Maxwellian tail heating produced fusion Q enhancements of factors of two compared to a Maxwellian equivalent. Majority deuterium second harmonic heating was also found to produce Q enhancements for D-T reactors by the same order of magnitude by Harvey, Kerbel and McCoy.[2] We feel that ICRF induced tail formations should produce even larger Q enhancements for the high energy reactivity peak E ≈ 300 keV in D-^{3}He fusion scenarios. In recent JET[3] and earlier PLT[4] D-^{3}He ICRF ^{3}He minority ion heating experiments 3-5 keV majority deuterium ion temperatures have been achieved with strong tail formation. The γ-ray detection measurements on JET[5] have inferred 9 kW of D-^{3}He fusion power and a $Q = P_{FUSION}/P_{RF} = 2 \times 10^{-3}$. Current experiments underway planned for up to 20 MW of ICRF power anticipate a good fraction of a megawatt of D-^{3}He fusion power and a fusion Q of several percent.

We will examine ICRF D-^{3}He heating and fusion scenarios for the NET Enhanced Physics (NET-EP) regime. Issues include: 1) Review of previous ICRF D-^{3}He experiments, 2) the single pass NET-EP minority ^{3}He and second harmonic absorption at concentrations ranging from 2-35%, 3) control and confinement of the heated ion tails, 4) deuterium and fusion proton ICRF absorption in the machine and 5) the fusion Q enhancement in the sub-ignited state when compared to the Maxwellian equivalent energy content. Only the first two issues are addressed in this Phase I part of this research and the later subjects will be treated in Phase II of the program.

7.2 JET D-^{3}He ICRF Fusion Results

The ICRF heating and confinement program on JET has concentrated recently on ^{3}He minority fundamental cyclotron resonant heating with a concentration of 2-5% averaged over the cross section. The remainder is majority deuterium with a typical Z_{eff} of 4 and a dominant carbon impurity. These experiments are similar to previous PLT experiments[4] in which comparable coupled power yielded a somewhat cooler majority temperature. The experiments have concentrated on this regime to examine the confinement of high energy fusion products without the use of tritium and neutron activation of the vessel. The proton is born at 14.7 MeV with the alpha particle at 3.6 MeV. These species do not resonate at the position corresponding to the ^{3}He

cyclotron resonance unless the Doppler shift corresponding to their high energies causes a sufficient overlap. This is a potential advantage over D-T ICRF heating scenarios in which the unhifted deuterium and alpha particle cyclotron resonances occur at the same position.

The best JET experimental results have been done at 5.5 MW of radiofrequency power coupled at a frequency of 33 MHz and several magamp discharges at electron densities of $3 \times 10^{13}/cm^3$. The deuterium ion temperatures are heated to the neighborhood of 4 keV with hotter electron sawteeth phenomena with average central temperatures of 5-6 keV. The diagnostic of the ^3He tail temperature is difficult to measure and Sadler et al.[5] have used gamma ray detection coming from a separate branch of the fusion reaction and helium reactions with carbon have been used to determine the fusion production and tail temperature of the minority helium tail temperature. They find that the spectral shape of the gamma rays corresponds to a fusion power output of 9 kW and that the energy of typical helium ions in the tail of the distribution corresponds to 200 keV. The coupled ICRF power of 5.5 MW corresponds to a fusion Q of 2×10^{-3}.

Hellsten[6] has used an isotropic steady state solution Fokker-Planck code to estimate the fusion Q that is achievable on JET. The case of ^3He-D fusions is compared to second harmonic deuterium radiofrequency waves interacting with 80 keV deuterium beam ions with a 50/50 mix of helium and deuterium background and to a second harmonic heating of helium with a 50/50 mix of helium and deuterium with beams. The background temperature and density is an input to the code and no accounting for losses or synchrotron radiation is considered in the code. The results are plotted versus the absorbed radiofrequency power in the core region in MW/m^3 and the results are shown in Fig. 7.2-1. The maximum fusion Q of 0.05 for occurs for the minority helium case with the minimum RF absorbed power density corresponding to about 0.25 MW/m^3. These curves should be taken as an estimate and a more detailed calculation taking into account the self-consistent equilibration between the tail formation and the electron and background ion temperatures as well as energy and confinement losses should be taken into account. Yet for these cases factors of 10-100 times the Q value for an equivalent Maxwellian tail temperature is obtained with large thermal anisotropies in the heated ion velocity distribution. For purposes of NET-EP it would be interesting to carry these calculations out for Q values near and above breakeven to see if the expected substantial Q enhancement can be obtained.

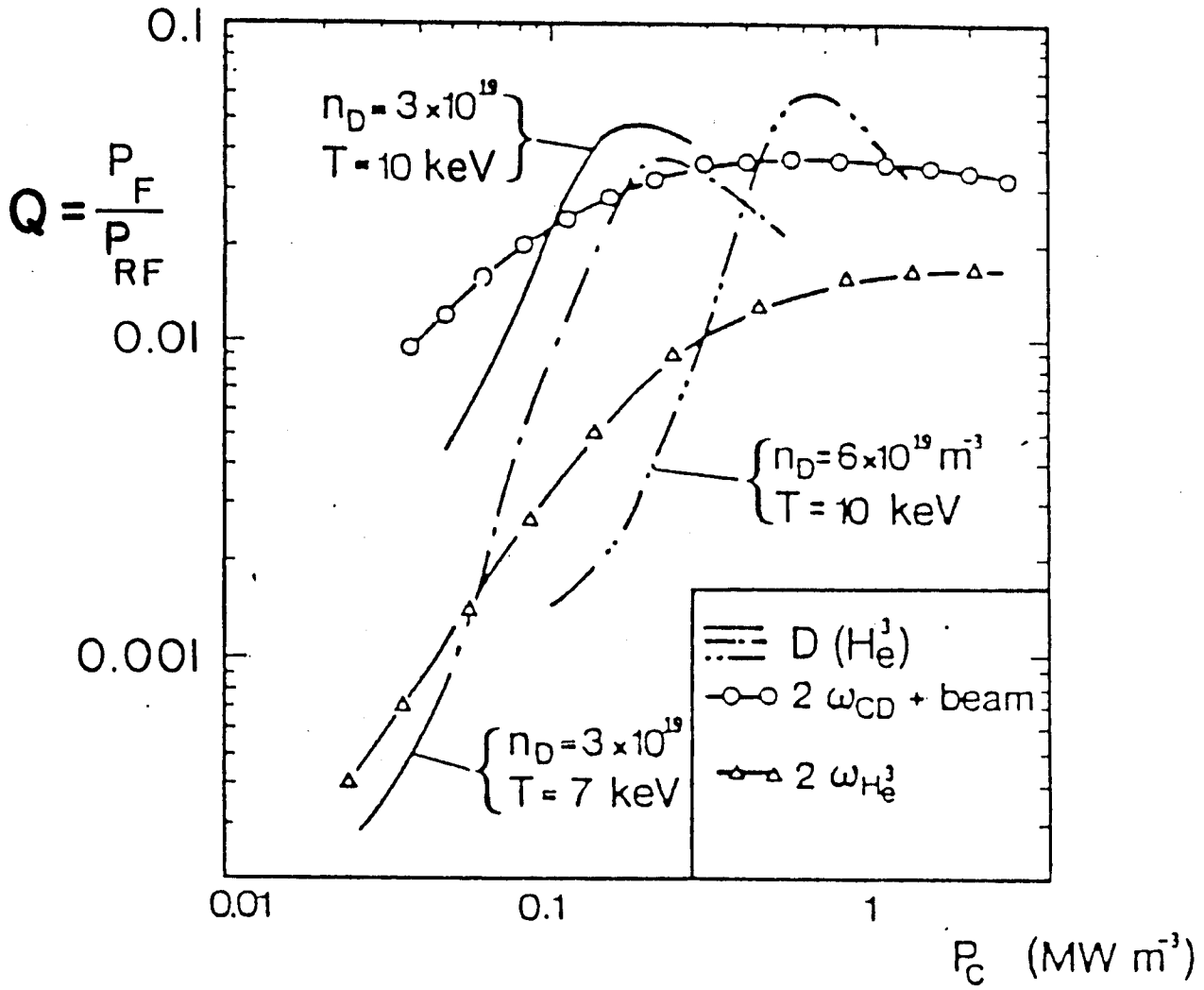

Fig. 7-1. From invited paper by J. Jacquinot et al., ICRF Heating on JET, presented at Radiofrequency Heating of Plasmas Conference at Kissiminee, FL, May 1987. Fusion amplification factor for D-^{3}He reaction versus the power damped in the resonating species. Three scenarios are considered (i) D(^{3}He), ^{3}He resonating minority with $n_{He}/n_D = 0.02$, (ii) $2\omega_{CD}$, harmonic resonance with deterium beam ions, $E_{inj} = 80$ keV, $n_{He}/n_D = 1$, (iii) $2\omega_{C\ He}$, harmonic resonance with Helium-3, $n_{He}/n_D = 0.5$. In all cases $Z_{eff} = 1$.

7.3 Single Pass Fast Wave Absorption for NET-EP ^{3}He-D Plasmas

To examine the efficiency of absorption for NET-EP parameters we use a computer code corresponding to a definition power absorption and the associated conservation relation for inhomogeneous plasmas developed by McVey, Sund and Scharer.[7] The code correctly solves the propagation and coupling of incident fast magnetosonic waves from the low field side of the machine to ion Bernstein waves in the resonant core region. It has also been checked with good agreement with a PLT data set and range of parallel wavelengths with other groups at Princeton, ORNL and NYU.

We take parameters corresponding to NET-EP startup of a 7 keV temperature for all species with an electron density of $1.78 \times 10^{14}/cm^3$, a toroidal field on axis of 5.6 T and a minor radius of 1.7 m. The helium fraction is taken to be 2% initially to achieve an optimum single pass absorption at lower temperatures. Figure 7.3-2 shows the dispersion relation near the core helium resonance for the incident and reflected fast wave (F) at a frequency of 115 MHz and incoming and outgoing Bernstein (B) wave, which is a backward wave in a tokamak. The solid lines correspond to the real part of the wavenumber and the imaginary parts correspond to the dashed lines which indicate absorption or mode conversion.

The real and imaginary parts of the left hand polarization of the composite field solution is show on Fig. 7.3-3. Note the peaking of this heating component on the high fields side near resonance at $x = 0$. Finally, the local absorbed power and Poynting and kinetic flux for the incoming wave is shown on Figs. 7.3-4a and 7.3-4b. The electron absorption is a small part of the heating (7%) corresponding to the cross-hatched region with the majority of the 65% single pass total absorption done by the helium species. The production of ion tails should broaden this absorption curve and increase the single pass absorption values.

The previous case, which has a very low helium concentration of 2%, achieves good single pass absorption at lower startup temperatures. As the plasma heats up, the helium concentration can be raised to 35% although an absorption description at elevated temperatures $T_{eff} \simeq 50$ keV at this high density is more complex. An alternative heating scenario is to use second harmonic helium absorption at a frequency of 230 MHz. This would make the single pass absorption less sensitive to the helium concentration but would yield a lower single pass absorption and reactivity enhancement during startup.

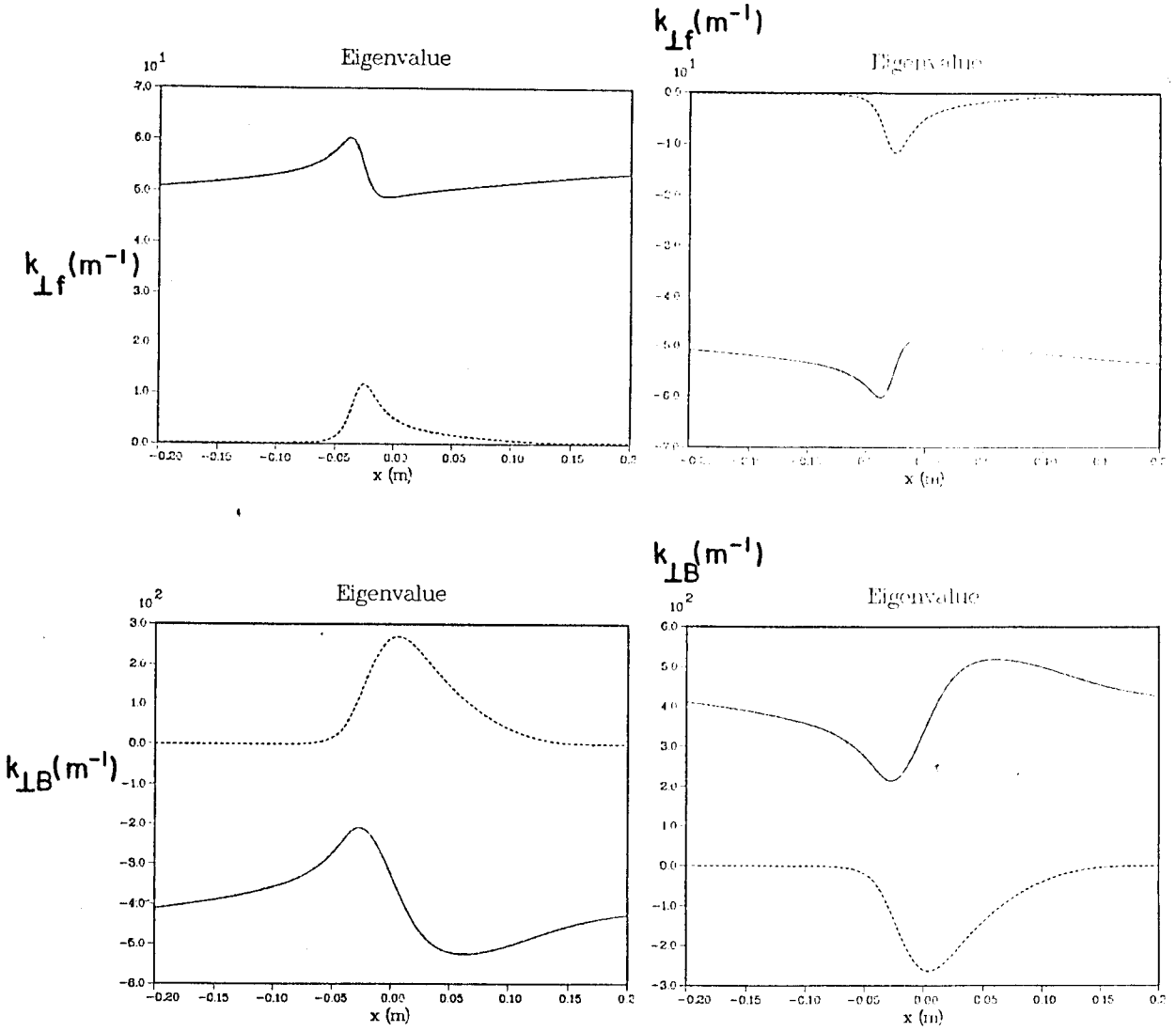

Fig. 7-2. Fast (F) and ion Bernstein wave (P) dispersion for fundamental ^{3}He heating in NET-EP.

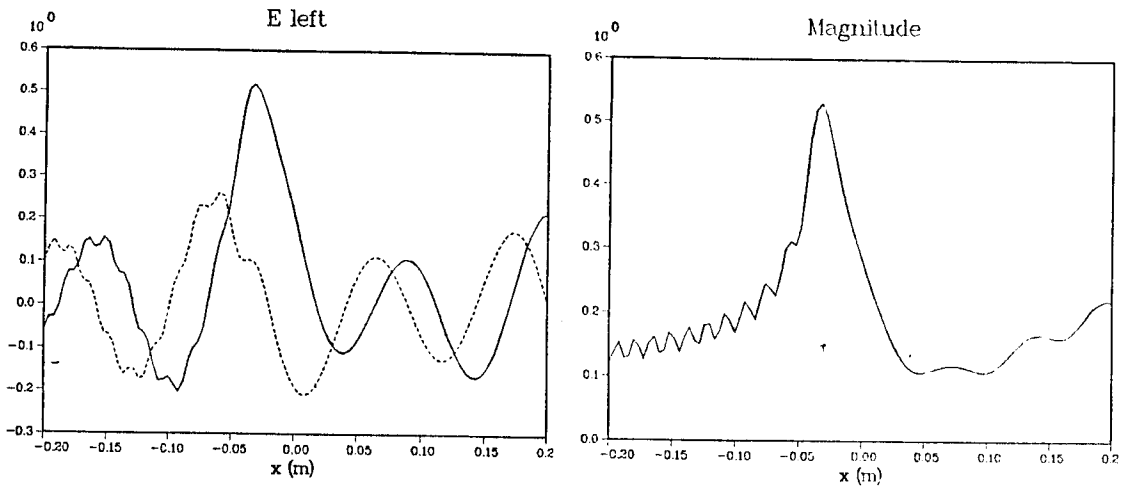

Fig. 7-3. Lefthand wave polarization for NET-EP parameters.

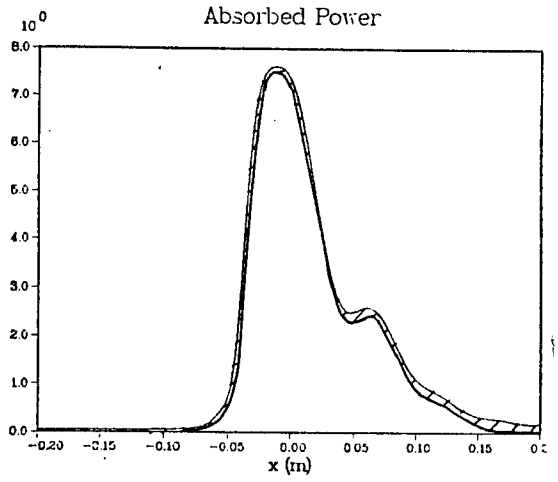

Fig. 7-4a. Helium and electron (hatched) fast wave absorption for NET-EP parameters.

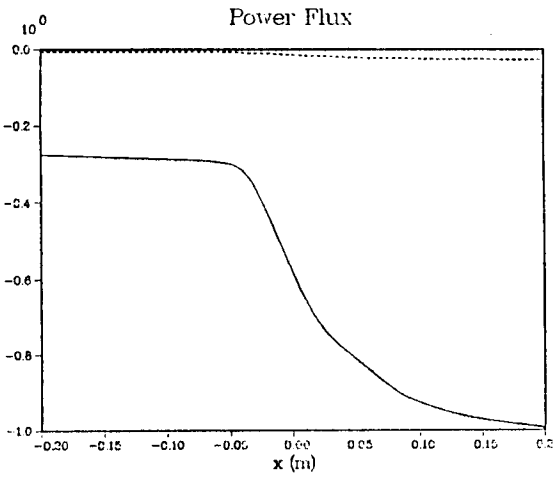

Fig. 7-4b. Poynting (solid) and kinetic flux for a fast wave incident from the right for NET-EP parameters.

The self-consistent non-Maxwellian helium tail formation and fusion Q calculation requires the solution of a Fokker-Planck code with ^{3}He-D non-Maxwellian anisotropic cross sections included. In Phase II we will evaluate the Q enhancement corresponding to helium tail formation and compare with the Maxwellian fusion Q for NET-EP parameters. These scenarios appear attractive for NET-EP reactivity enhancement and ignition operation.

References for Chapter 7

1. J. Scharer, J. Jacquinot, P. Lallia and F. Sand, "Fokker-Planck Calculations for JET ICRF Heating Scenarios," Nuclear Fusion 25, 435 (1985).

2. Harvey, Kerbel, McCoy, and Chiu, "ICRF Fusion Reactivity Enhancement in Tokamaks," Nuclear Fusion 26, 43 (1986).

3. JET Team, "RF Heating on JET," International Conference on Plasma Physics and Controlled Fusion Research, IAEA-CN-47/F-I-1 (1986) Kyoto, Japan.

4. Hosea, J. et al., 12th European Conference on Controlled Fusion and Plasma Physics, 9F Part II, 120 (1985) Budapest, Hungary.

5. G. Sadler, O. Jarvis, P. Belle, N. Hawkes and B. Syrne, "Observation of Fusion Reaction γ-Rays in JET," Proc. of European Conference on Plasma Physics and Controlled Fusion, 1232 (1987) Madrid.

6. Hellsten, part of invited paper presented by J. Jacquinot, "Results of RF Heating on JET and Future Prospects," Seventh APS Topical Conference on Applications of Radiofrequency Power to Plasmas, Kissemmee, FL (May 1987) to be published.

7. B. McVey, R. Sund and J. Scharer, "Local Power Conservation for Linear Wave Propagation in an Inhomogeneous Plasma," Phys. Review Letters July 29, 507 (1985).

8. SUMMARY AND CONCLUSIONS

A preliminary study of the feasibility of achieving significant energy multiplication, Q, with D-^{3}He fuel in NET, and variations of it, has been performed. The starting point for this study is the reference NET design for D-T operation,[1] referred to here as NET-DT, and an enhanced plasma case,[2] NET-EP, also developed by the NET team for D-T operation.

A physics model based on a power balance of the plasma, with consideration of MHD equilibrium and stability, fusion product charged particle heating, fast ion pressure, bremsstrahlung and synchrotron radiation losses, and energy transport across the magnetic field has been developed and used for a parametric study of the energy multiplication and ignition margin expected with D-^{3}He operation. Neutronics calculations to estimate the thinnest possible shield for the neutron spectrum expected with D-^{3}He fuel have been performed; the reduced shield thickness allows a much better utilization of the magnetic field generated by the toroidal field magnets. Shield thicknesses of about 25-30 cm, depending on the neutron power level, are feasible.

Using the above physics model and neutronics results, a parametric study of D-^{3}He operation in NET-DT, NET-EP, and possible modifications to NET-EP to improve the energy multiplication and/or achieve ignition has been performed. From this parametric survey the following general conclusions may be drawn.

Breakeven (Q = 1) may be obtained in the present NET-DT design if ASDEX H-mode scaling is applicable. In addition, the required injection power is less than that planned for startup in NET-DT. If Kaye-Goldston scaling continues to plague tokamaks, then the Q-values obtained are much lower (Q = .4) and the injection power is much higher (P_{inj} = 120 MW). The enhanced plasma size NET case (NET-EP) can achieve a Q-value of about 1.4 using ASDEX H-mode scaling with no changes in the machine parameters except for the fuel and the operating temperature.

The Q-value can be increased in many ways in NET because of the low neutron production with D-^{3}He fuel. Reduction of the major plasma radius to 4.61 m increases the Q-value to about 3. This improvement in Q is due to the increase in magnetic field at the plasma and to the reduced aspect ratio which leads to higher plasma current, energy confinement times, and beta. The reduction in major radius can be achieved by removing the inboard blanket designed for DT operation and using much thinner shield designed for the low DD and DT neutron exposure.

An alternative approach is to increase the magnetic field at the toroidal field magnets without changing the plasma dimensions from the NET-EP case. Q values of about 2.5 - 3 can be obtained by a 20% increase in the magnetic field strength at the TF coil.

Ignition with D-^{3}He in NET is feasible if the plasma major radius is reduced in conjunction with an increase in the toroidal field and in the plasma elongation. The required elongation for ignition is about 2.4 at B_c = 13 T and 2.7 at B_c = 10.5 T. (B_c is the toroidal field at the TF magnet.)

The above predictions are obtained using the ASDEX H-mode scaling law. Break-even in NET is possible with the Kaye-Goldston scaling law for an H-mode factor of about 2.5, but the required injection power is about 120 MW. This assumes the major radius of the plasma has been reduced to 4.61 m and the toroidal field at the magnet remains at the NET value of 10.4 T.

This work assumes all the ions have a Maxwellian distribution at the same temperature. By judicious use of RF it is possible to improve the energy multiplication, for sub-ignited operation, by driving an enhanced tail in the ^{3}He distribution and thereby enhancing the fusion reaction rate. This has been considered briefly and appears attractive, but specific results are left for later study.

Using parameters developed by the parametric survey, we have considered briefly the poloidal field implications of reducing the plasma major radius to 4.6 m and increasing the plasma current to 20 MA. Because of the reduced major radius, the coupling of the plasma to the OH system is improved. Consequently, there is no significant increase in the volt-sec of the OH system required to establish the plasma current. The higher plasma current increases somewhat the current required in the poloidal field magnets; this may be relaxed by further optimization of the PF system.

The D-^{3}He fusion reaction produces all its energy in the form of charged particles; this could lead, potentially, to larger surface heat loads than is experienced in D-T fusion where 80% of the fusion energy is in the form of neutrons which heat the blanket and shield volumetrically. It turns out that, because of the lower fusion power density with D-^{3}He, the surface heat loads on the first wall due to bremmstrahlung and synchrotron radiation are similar to, or less than those encountered in the D-T version of NET. The power density on the divertor neutralizer plates due to charged particle impact are also similar to those designed for in the D-T version of NET.

The loss of fast fusion produced ions due to magnetic ripple has been considered in comparison to the corresponding loss in a D-T plasma. Unfortunately, there is major disagreement in the field concerning ripple losses in D-T plasmas; this makes it impossible to provide with reasonable certainty any estimates of the ripple loss in a D-^{3}He plasma. Clearly, further work in this area is required, but this is beyond the scope of this study.

From these results we see that significant energy multiplication in a mildly revised form of NET can be obtained if nature is not too perverse. Significant energy multiplication means that the fusion reactions are as important as the external heating power in determining the power balance of the plasma. Consequently, important questions regarding burn physics and the effects of a significant number of fast fusion produced ions in the plasma can be studied with such a machine. In addition, the much reduced neutron production makes the environment more hospitable to performing physics experiments on burning plasmas than is the case with DT fuel.

References for Chapter 8

1. The NET team, NET Status Report 1985, NET report 51, Commission of the European Communities, (1985).

2. F. Engelmann, Concept and Parameters of NET, NET Report 64, EUR-FU/XII-80/86/64, Commission of the European Communities, (1986).